EIDESSTATTLICHE ERKLÄRUNG

Ich erkläre an Eides statt, dass ich die vorliegende Arbeit selbstständig verfasst, andere als die angegebenen Quellen/Hilfsmittel nicht benutzt, und die den benutzten Quellen wörtlich und inhaltlich entnommenen Stellen als solche kenntlich gemacht habe.

Graz, am …………………………   …………………………………………………..
                                                                                        (Unterschrift)

Englische Fassung:

STATUTORY DECLARATION

I declare that I have authored this thesis independently, that I have not used other than the declared sources / resources, and that I have explicitly marked all material which has been quoted either literally or by content from the used sources.

……………………………   …………………………………………………..
            date   (signature)

Denis Schütz

The Development of High Strain Actuator Materials

DISSERTATION

zur Erlangung des akademischen Grades eines Doktors der Naturwissenschaften

erreicht an der

Technischen Universität Graz

Betreut von:

Klaus Reichmann

Institut für Chemische Technologie von Materialien

2012

Dear reader;

At this point I have much to be thankful for, first I would like to thank my advisor Dr. Reichmann who deserves much thanks and respect for creating an environment where this was all possible in the first place. I really cannot thank him enough for the chance he gave me and through advice, critique, nourishment and pressure molded me into a scientist, technician and a better man.

I would like to thank the good people at EPC-TDK Deutschlandsberg especially Dr. Michael Schossmann and Dr. Wolfgang Athenstaedt. Their help and advice was invaluable and showed me fundamental insights that a purely academic context often misses.

Thanks are in order to all colleagues and coauthors. Science is teamwork, a fact I will never forget.

I would like to thank all those that believed in me and all those that did not-you helped me most of all.

I would like to thank my family and loved ones as well as all those partners in crime, aiders and abettors and general scoundrels that I call my friends. I would not want you any other way.

Lastly I would like to thank the often mentioned giants on which shoulders I had the fortune to stand.

Denis Schütz

Table of contents

1 Introduction

1.1   Preface

The subject of this thesis is the development of high strain piezoelectric actuators. Being cumulative in nature these introductionary words and the subsequent chapters provide a primer and an introduction to facilitate reading of the five peer reviewed publications included. It is by no means a complete collection but will provide the reader with the means and the literature to understand the processes, methods and techniques for synthesis, fabrication and analysis of the piezoelectric materials studied herein. The five publications are:

1. Schütz, D.; Deluca, M.; Krauss, W.; Feteira, A.; Jackson, T. Reichmann K.: Lone-Pair-Induced Covalency as the Cause of Temperature- and Field-Induced Instabilities in Bismuth Sodium Titanate. - in: **Advanced functional materials** (2012) 22 2285–2294
2. Naderer, M.; Schütz, D.; Kainz, T.; Mittermayr, F.; Reichmann, K.: The formation of secondary phases in Bi0.5Na0.375K0.125TiO3 ceramics. - in: **Journal of the European Ceramic Society** 32 (2012) , S. 2399 - 2404
3. Krauss, W.; Schütz, D.; Naderer, M.; Orosel, D.; Reichmann, K.: BNT-based multilayer device with large and temperature independent strain made by a water-based preparation process. - in: **Journal of the European Ceramic Society** 31 (2011), S. 1857 - 1860
4. Krauss, W.; Schütz, D.; Mautner, F.-A.; Feteira, A.; Reichmann, K.: Piezoelectric properties and phase transition temperatures of the solid solution of (1-x)(Bi0,5Na0,5)TiO3 - xSrTiO3. - in: **Journal of the European Ceramic Society** 30 (2010) , S. 1827 - 1832
5. Schütz, D.; Krauss, W.; Albering, J.; Kurta, C.; Reichmann, K.: The Chemical Interaction of Silver–Palladium Alloy Electrodes with Bismuth-Based Piezomaterials. - in: **Journal of the American Ceramic Society** 93 (2010) 4, S. 1142 - 1147

All of these deal with either the development of materials for high strain applications or the development and testing of prototypes of said actuator devices. They can broadly be divided into two categories: Primary authorship and secondary authorship.

In the publications 1 and 5, the papers, the primary authorship was entrusted to me. I have written the whole of the article, headed the direction of research and am responsible for final wording and the shape of the publication. In the secondary authorship papers I assisted with the more theoretical part: Materials selection, composition selection, burnout and sintering curves but most importantly the interpretation and (in all papers) some of the measurements. In all publications I aided in the final wording and figures.

As a short summary of the novelties and important points provided by each paper:

- Clarification of a phase transition (at T_d) and the mechanism of extended strain (arising from factors other than the inverse piezoelectric effect) in a BNT derived material (paper 1)

- Demonstartion of the breaking of a covalent bond as the cause and mechanism of both the above mentioned phase transition at T_d and the extended strain.

- First in situ measurement of a solid under high fields (7kV/mm) in a Raman spectrometer (paper 1)

- First accurate tracking of A-site-Oxygen modes in a perovskite material under applied temperature and field (paper 1)

- First measurement of a piezoelectric stack under Raman spectroscopy (paper 1)

- Clarification of the formation of secondary phases in a BNT/BKT ceramic (paper 5)

- First demonstration of a near temperature independent strain in a bismuth based material (paper 3)

- First demonstration of a prototype actuator using said materials (paper 3)

- Application of a novel water based production route for said actuator (paper 3)

- Completing the quasi-binary phase diagram of BismuthSodium Titanate and Strontium Titanate and thereby establishing strontium as a doping agent in Bismuth Sodium Titanate (paper 4)

- Clarification and verification of the compatibility of Bismuth based piezomaterials with the industry standard Ag/Pd electrodes for multilayer fabrication (paper 5)

Relevance of the Studied Phenomena:

The relevance of piezoelectric ceramics lies naturally in their application, such as actuators, transducers, sensors and generators. Primary applications of actuator will be discussed in the following chapter. The special significance of lead-free piezoelectric materials will be discussed in Chapter 1.4 (Lead free Ceramics). Special technical and scientific problems solved by our work will be discussed in the section following page 19. In general piezoelectric actuators, while proving a solution to a variety of technical problems, are not the only technically feasible solution. The only application where piezoelectric actuators are the sole solution to a problem is very accurate micropositioning, which is used in the photolithography of semiconductors and the positioning in Electron microscopy techniques. As such without a piezoelectric actuator there is no semiconductor industry.

1.2 Actuators

"An actuator is a type of motor for moving or controlling a mechanism or system. It is operated by a source of energy, usually in the form of an electric current, hydraulic fluid pressure or pneumatic pressure, and converts that energy into some kind of motion. An actuator is the mechanism by which an agent acts upon an environment." [1]

So the first thing to do is to be precise in which type of actuator this introduction deals with. The first distinction would be that the actuators in question are used for very precise, fast, high force movement on small length scales. To be more precise we will deal with actuators based upon the indirect piezoelectric effect.

Piezoelectric micro-actuators are almost exclusively built in the multilayer geometry. Types of multilayers include a Stack, a Bender. Other geometries include Actuator-tubes, linear motors, rotary motors and stepper motors.
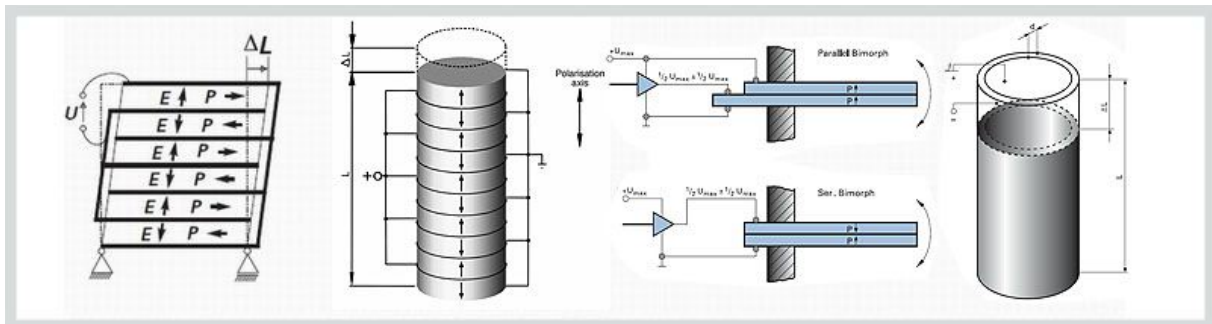

Figure 1: Geometries of piezoelectric actuators (multilayer, bender/bimorph, tubular actuator) [from PI Gmbh [2]]

The application of these devices is manifold[3,4,5,6,7]. Any precise movement on a small length scale can be done by a piezoelectric actuator. The most common would be a fuel injection valves in common rail or unit injector combustion engines. It is also used in auto focus cameras and photo shutters and the reading heads of Magnetic recording equipment (hard disk drives. The ultra precise actuation necessary for sample movement in various analytic equipment (light Microscopy, SEM, AFM, direct metrology nano indentation, PFM) rely exclusively on piezoelectric actuators. Contemporary semiconductor technology would not be possible without the precision and speed offered by these devices for the positioning of wafers e.g. in lithography processes[3]. Although other technological solutions exist for less precise applications like fuel injection valves (where the solenoid motor is the chief rival[3]) the primary advantage of the piezoelectric actuator is the fast response to the control signal.
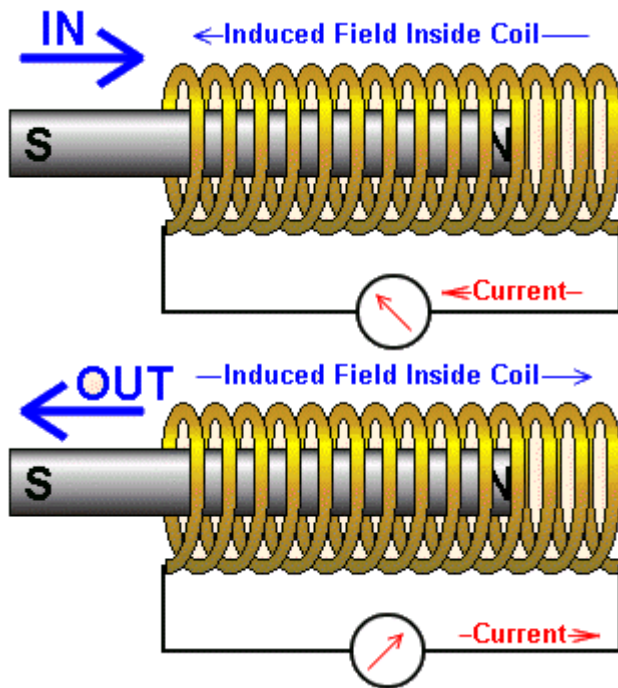
Figure 2: Solonoid actuators operate on the same basic principles as a DC motor. The difference between a solenoid and a motor is that a solenoid is spring loaded and cannot rotate. [Copyright: Society of Robots]

That being said, the development of an application of a piezoelectric actuator, especially one of a novel composition, is far from unproblematic. In this collection we will present some common problems and the solutions we have found (e.g. see 1.4.2 for the complete description) aiding in the development of next generation the development of high performance lead free piezoelectric actuators.

1.3   Piezoelectric Effect

1.3.1 Timeline of Discovery

Table I.   Notable Events in the History of
Ferroelectric Materials

Timeline	Event[†]
1824	Pyroelectricity discovered in Rochelle salt
1880	Piezoelectricity discovered in Rochelle salt, quartz, and other minerals
1912	Ferroelectricity first proposed as property of solids
1921	Ferroelectricity discovered in Rochelle salt
1935	Ferroelectricity discovered in KH_2PO_4
1941	$BaTiO_3$ high-K ($>$1200) capacitors developed
1944	Ferroelectricity discovered in ABO_3-type perovskite $BaTiO_3$
1945	$BaTiO_3$ reported as useful piezo transducer, Pat. No. 2 486 560
1949	Phenomenological theory of $BaTiO_3$ introduced
1949	$LiNbO_3$ and $LiTaO_3$ reported as FE
1951	Concept of antiferroelectricity introduced
1952	PZT reported as FE solid-solution system, phase diagram established
1953	$PbNb_2O_6$ reported as FE
1954	PZT reported as useful piezo transducer, Pat. No. 2 708 244
1955	PTC effect in $BaTiO_3$ reported
1955	Chemical coprecipitation of FE materials introduced
1955	Alkali niobates reported as FE
1957	$BaTiO_3$ barrier layer capacitors developed
1959	PZT 5A and 5H MPB-type piezo compositions, Pat. No. 2 911 370
1961	Lattice dynamics theory for FE materials, soft modes introduced
1961	PMN relaxor materials reported
1964	Oxygen/atmosphere sintering for FEs developed
1964	FE semiconductor (PTC) devices developed
1967	Optical and E/O properties of hot-pressed FE ceramics reported
1969	Terms "ferroic" and "ferroelasticity" introduced
1969	Optical transparency achieved in hot-pressed PLZT ceramics
1970	PLZT compositional phase diagram established, Pat. No. 3 666 666
1971	Useful E/O properties reported for PLZT, Pat. No. 3 737 211
1973	Oxygen/atmosphere sintering of PLZT to full transparency
1977	FE thin films developed
1978	Engineered (connectivity designed) FE composites developed
1980	Electrostrictive relaxor PMN devices developed, Pat. No. 5 345 139
1981	Sol–gel techniques developed for the preparation of FE films
1983	Photostrictive effects reported in PZT and PLZT
1991	Moonie piezo flextensional devices developed, Pat. No. 4 999 819
1992	RAINBOW piezo bending actuators developed, Pat. No. 5 471 721
1993	Integration of FE films to silicon technology, Pat. No. 5 038 323
1997	Relaxor single-crystal materials developed for piezo transducers

[†]FE is ferroelectric, K is relative dielectric constant, PZT is lead zirconate titanate, MPB is morphotropic phase boundary, PLZT is lead lanthanum zirconate titanate, PMN is lead magnesium niobate, PTC is positive temperature coefficient, E/O is electrooptic, RAINBOW is reduced and internally biased oxide wafer.

Figure 3: Timeline of discovery of piezoelectric materials and devices[from [3]]

The most important addition to this timeline would be the first commercial use of PZT based multilayer actuators in fuel injection valves in 2000, the Reach(2007) and RoHS(2006) acts of legislation which restricts the use of lead in electronic devices and (of special relevance to my work) the rediscovery of

9

BNT derived materials by S.T. Zhang 2008 as well as the patent application for a piezoelectric fuel injection valve by Kabushiki Kaisha in 1994.

1.3.2 Standard Model

Piezoelectricity, the most direct energy transformation between kinetic energy and electrical energy, can be summed up into two distinct phenomena: The direct- and the indirect piezoelectric effect. The direct effect is a charge generation by applying stress to the material. The indirect is the generation of strain by the application of an electric field. In theory any non ferroelectric ideal solid, which exhibits no center of symmetry will have the ability to do both to an equal amount in a linear fashion, described in Equation 1.

Equation 1: $S_{pz} = d \cdot E$

With S_{pz} is the deformation, d is the piezoelectric coefficient and E is the applied field intensity

It is however best illustrated using the perovskite crystal structure.
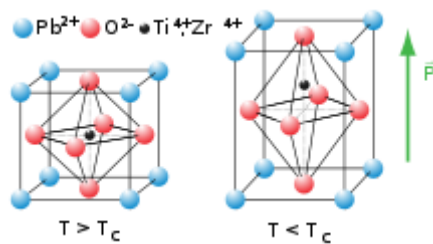

Figure 4: Perovskite structure illustrated as PZT in cubic and tetragonal conformation [CC]

The Standard model of piezoelectric solids is based upon the theory of point groups. Any material who's repeating crystal structure lacks a center of inversion will develope piezoelectric characteristics.

Of the 32 classes of crystal systems 21 have no center of inversion, the cubic group 432 does not exhibit piezoelectricity due to the high symmetry, prohibiting charge separation even when under the influence of mechanical strain[8,9]. These 20 crystal classes encompass nearly all types of materials the only other prerequisite is that they are not electrically conductive. As such it is widespread and common in any class of material (biological, inorganic, polymer) with the sole exception of metals whose definition includes the ability to conduct electricity and as such cannot be piezoelectric by default. Indeed all highly conducting materials are unable to extend in the manner of a piezoelectric material.
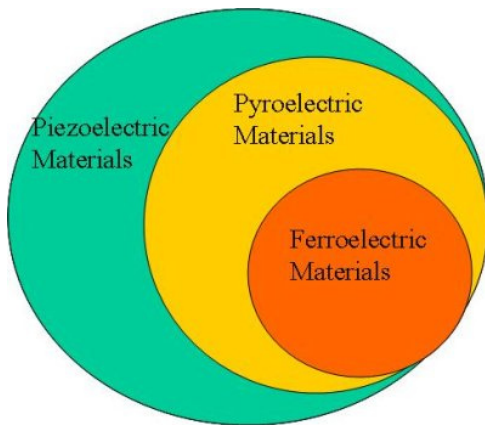
10

Figure 5: Hierarchy of piezoelectric materials.[CC]

Of the 20 non-centrosymmetric crystal classes 10 are polar (exhibit a permanent polar axis), all polar crystals are pyroelectric. The name is derived from the greek *pyr* meaning fire. In contrast to pure piezoelectrics the polarization is permanent (spontaneous). As such they have the ability to separate charge (and therefore introduce an electric potential) with the application of temperature. Mechanistically, this is the result of the change of atomic distances within the whole crystal due to thermal expansion and should not be confused with thermoelectricity which is the result of a temperature gradient. Pyroelectric materials that are not ferroelectrics show this behavior all through their stable solid states.

Ferroelectrics are therefore a subgroup of pyroelectrics they are distinct in two primary properties.

- The spontaneous polarization has an upper temperature boundary →the Curie Temperature (T_c) at which the spontaneous polarization is lost.
- The possibility that the direction of the spontaneous polarization can be reversed by the application of an electric field

The directionality of the polarization gives these materials their characteristic properties. It also allows the materials to be poled, a technique used to align most of the dipoles in the virgin material along the desired axis/direction. This is best illustrated using the common plot of polarization P vs. electric field (E) called hysteresis.
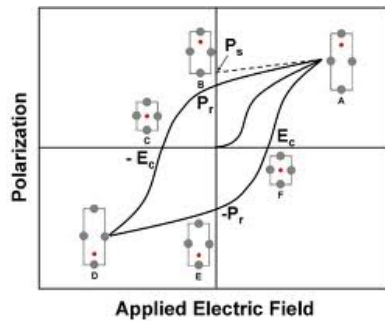
Figure 6: Hysteresis of a ferroelectric material(PZT) from [8]

Primarily the term Hysteresis illustrates the dependence of a system not only upon its current but also its past state. The phenomenon of remanence is the most direct effect of this, meaning that the past state does influence the position of the curve. In Ferroelectrics this is caused by the inertia of the crystals redirecting themselves to the new field only if sufficient field intensity is applied in the opposite direction. This is called the coercitive field intensity (E_c) and can be read from the graph as it intersects with the abscissa. At this point the individual dipoles start to align themselves with the applied field. The second is the remanent polarization (P_r) where the curve intersects with the ordinate (0-field) it is the net polarization in the material after having been fully polarized. The third is the point of saturation, the point where an increase in field does not yield a substantial increase in polarization. As such it is visible as a flat section in the curve and it is necessary for it to be reached for the first two points to be reliably measured. A piezoelectric with a high E_c and low P_r is termed a "hard" ferroelectric. The opposite is termed a "soft" ferroelectric[8]. These terms were taken from ferromagnetic materials which were discovered and named earlier than ferroelectrics.

The other characteristic plot is the so called butterfly curve (Fig ?). It is a plot of strain (elongation) (dx/x vs E). it shows the dependence of achievable strain versus the intensity of the field. In canonical ferroelectrics they are shaped like a butterfly, hence the name. As with the P-E loops the butterfly curve shows hysteretic characteristics. As a measure of the true ability of the material to extend, only the intersection of the positive and negative field interaction can be taken as the 0-point, previously unpoled material is exhibiting considerably more strain, but only for the first poling loop.
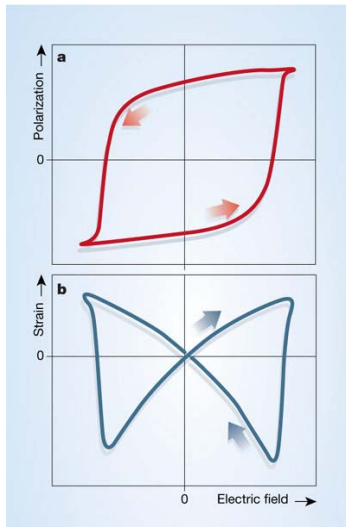
Figure 7: Butterfly strain curve of PZT and the corresponding polarization curve [from [10]]

These phenomena lead directly to one of the more fascinating properties of piezoelectric materials – the development of domains. Domains are regions of the crystal that are identical in all respect except the direction of the spontaneous dipole. These can develop in any ferroelectric, even single crystals. Upon cooling from the Curie temperature (above which no polarization persists) the direction of the domains is random and consequently the net polarization of the whole sample will always be zero. Domains are regions that have aligned themselves to a common direction for reasons of an enthalpic but also entropic nature [11,12,13]. Under field this dipoles switch to align with the field and net polarization increases. This produces polarization in the material. The necessary energy to overcome the inherent resistance of the dipoles to switch is reached at the coercitve field intensity(E_c). Since the polarisation tends to switch as an ensemble, the movement of the polarity can be visualized and is called a domain wall movement. Although it might appear this way, no atoms are moved by this process, instead the polarization just changes direction.[12]

Figure 8: Ferroelectric domains in PZT made visible through channeling contrast imaging

It is important to note that unlike ferromagnetic materials[8] (where polarization is localized in elemental poles; meaning the spin state of the baryon) the polarization of ferroelectrics is distributed as a function of e^- density and cannot be fully localized. One unit cell alone would not exhibit ferroelectricity, it only works within a continuum[14].

1.3.3 Perovskites

The most common crystal system used in ferroelectrics is perowskites. The name derives from the mineral Perovskite ($CaTiO_3$) discovered by Gustav Rose in 1839 (Ural Mountains) and named after the interior minister of Nicholas I (and crystallographer) Lev Perovski[3]. Most perovskites follow the primary scheme of A B X_3: A usually being of valence 2+ B of 4+ and X to be occupied by oxygen. This is however not set in stone with 3-3 or even defect perovskites being observed. As long as electric neutrality is observed the compound can be stable. X can also be occupied by any non-metal with sufficient electronegativity (e.g. $KMgF_3$). The most important structural element of any Oxygen perovskite is the oxygen octahedra surrounding the B-site, with the A-site occupying the octahedral open spaces De:*Oktaederlücken*)[8]. The octahedra play the most important role in the polarization of the material, with the direction of polarization directly following the elongation of the octahedra. They also facilitate the particularly adaptive chemical bond inherent in this type of crystal. Similar in structure and bonding to an

octahedrally coordinated complex, Jahn Teller distortions (1st and 2nd order) are observed[15,16], enhancing the polarizability of the crystal. It also serves as a focal point of the distributed covalent bond facilitated by A-site lone pairs discussed in later sections.

The range and combination of ions able to form a perovskite were first established by Victor Goldschmidt in 1928 using simple geometrical considerations[17,18]. With the update of the ionic radii by Shannon, it remains valid and relevant to this day.

$$t = \frac{r_A + r_0}{\sqrt{2}(r_B + r_0)}$$

Formula 2: Goldschmidt factor

Ra Ionic radius of the A site

Rb Ionic radius of the B site

Rx Ionic radius of the X site

A t > 1 means that the A ion is too big or the B ion too small forcing a rhombohedral or hexagonal structure

A t ~0,9-1 means ideal size and consequently forms a cubic structure

A t < 0,7 means A ions are too small to fit into the octahedral interstices generating a variety of structures

Note that the tolerance factor does not take anything beside ionic radius into account, therefore influence such as Jahn Teller distortions[15], covalence or disorder phenomena are not applied.

1.3.4 Expanded Model

The expanded model for the actuation of ferroelectrics culminates mostly around domains and their behavior under an applied field. As previously mentioned domains are regions within a single- or poly-crystal that share a common direction. Since the crystal system is elongated in the direction of the polar axis (distorted) the switching of the direction can lead to extension. In principle the literature differentiates between 90° and 180° domains in respect to the direction of the field.
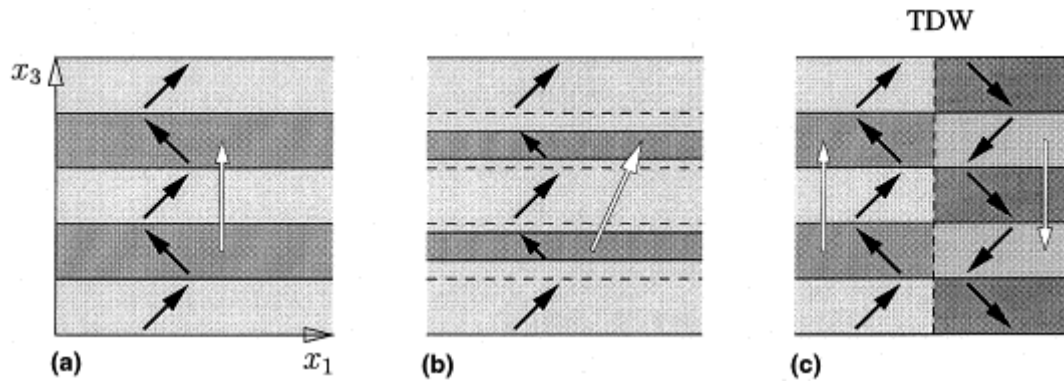
Figure 8: Simplified domain configuration in tetragonal ferroelectric ceramics and resulting domain reorientation mechanisms according to Arlt[13] (a) laminar domain stack consisting of 90° domains; (b) rotation of the effective polarization of the grain by domain wall displacement; (c) switching of the domain orientation by generating a new domain wall (transient domain wall)[from[12]].

However, 90° domains mean any direction not in the immediate opposite direction of the applied field (46°-135°) these are the domains that interact in domain wall movement[13]. 180° domains do not contribute to extension despite the fact that they are influenced by the applied field. Merely their direction changes, therefore there is no macroscopic elongation associated with the switching.

Despite decades of study, the magnitude of the influence of domain wall movement on the process of extension of piezoelectric materials has been difficult to establish. Most studies focused on separating the reversible (indirect piezoelectric effect) and the irreversible contributions (DWM is partly irreversible through the inclusion of defects in the ceramic similar to bloch defects [13] [] in ferromagnetic materials) through the application of sub-coercive loops (Raileigh loops). In one of the most important publication of the field Trolliard-McKinstry combined the sub-coercive loops with High resolution neutron scattering under field. This allowed for the first time to directly measure the extension of the crystal system itself and relating the irreversible part of the extension with the role of DWM. The indirect piezoelectric effect was determined to contribute only approximately 10 percent to the strain of the material. This explains the superiority of tetragonal crystal systems to rhombohedrally based piezoceramics. Also the superiority of electrically soft materials was explained, through the fact that the domain walls moved like a membrane, unlike hard materials that move along a jagged edge. Although methods to utilize this phenomenon were known through purely empirical studies and industry work, the result still have wide ranging consequences for the developing of actuators.

16

1.3.5 Lead Zirconium Titanate

Lead zirconium titanate is the most standard material for piezoelectric elements. Compromised of a single A-site (Pb) and a mixture of two atoms at the B side it exhibits an interesting phase diagram.
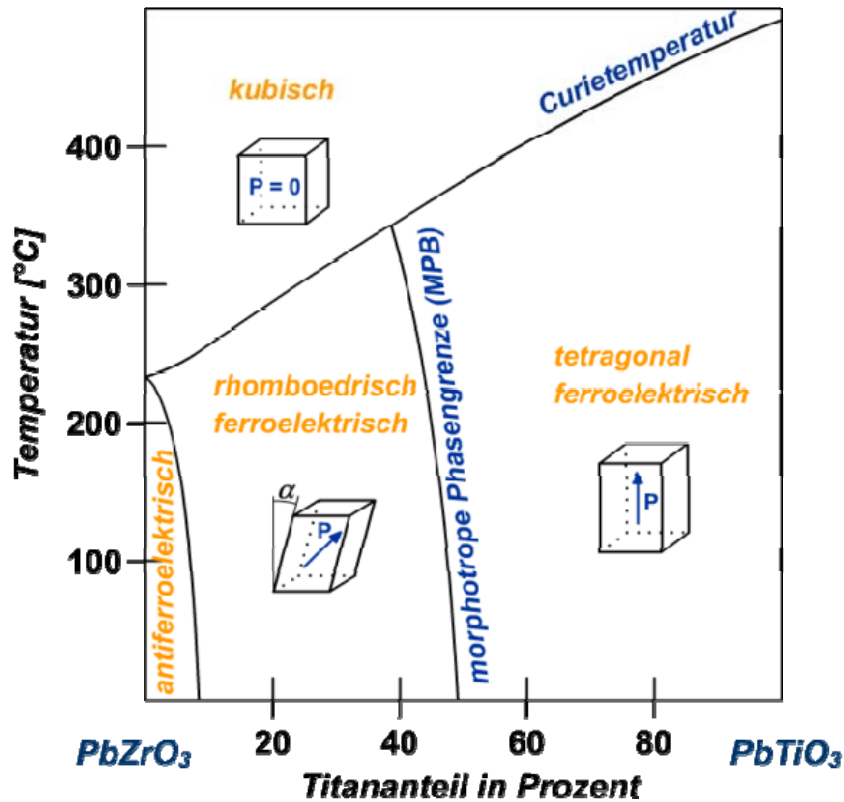

Figure 9: PZT phase diagram [CC]

The most distinctive feature of the phase diagram is the existence of a morphotropic phase boundary (MPB). The MPB was subject of considerable debate (and to a certain extent still is)[19] within the literature. Unquestionable is the fact that the MPB exhibits the best properties in regard to actuation (extension), generation (indirect piezo effect) and capacity[8]. Consequently most devices are close to the MPB in compostion. The simplest explanation is a thermodynamic one. The addition of further degrees of freedom leads to a better response within the confined system of a solid. This explanation is however incomplete. A long standing debate within the scientific community is about the exact nature of the MPB. This is mostly due to the inability to measure all relevant parameters locally and within the same area. The theories are: A coexistence of two or more crystal systems without chemical separation, two or more structures through chemical separation and a very small region of a monoclinic phase. The difficulty to establish an exact answer has to do with the inability of most macroscopic scattering methods to measure

17

anything beside an average of a symmetry e.g. that of a mixture of rhombohedral and tetragonal symmetries within the same sample would lead to a monoclinic symmetry being calculated from the diffractograms (note that being of lower symmetry than either rhombohedral or tetragonal phases means that either symmetry by itself could be refined to monoclinic). The MPB itself is poorly defined either structurally or chemically, but for the fact that within this region of the phase diagram the electrical properties are enhanced. Recent Raman studies have pointed into the direction of a mixture of phases with a monoclinic structure being present and enhanced at lower temperature(<100K)[20]. Also relaxor phenomena are reported at the MPB.

What the attentive reader will no doubt immediately notice is the fact that the diagram itself is "merely" a technical phase diagram violating the phase rule according to Gibbs. The calculated phase diagram for the system is substantially different. However the necessary activation energies correspond to temperatures above the stable range of PZT. This leads to the situation that while technically the phase diagram does not correspond to the equilibrium state (and therefore is not a phase diagram proper), the calculated phase diagram is not reachable experimentally, and the region around the MPB is (chemically speaking) a meta-stable state. This has been remarked upon on as one of the reasons for the high degree of disorder and the subsequent phenomena associated with the diverging regions between experimental and "true" (equilibrium) phase diagram. The debate is not likely to end until true single crystals of usable size have been procured, which due to the strong inherent disorder present within the system is still a tremendous challenge, the biggest single crystals grown measuring in the sub millimeter range[21,22,23,24,25].

PZT can be modified by doping to include most desired properties in ferroelectrics and as such it is by far the most used ferroelectric material. However concerns over its toxicity (Pb mainly)[10,26,27] have been raised and its used has been subsequently outlawed within the European Union. However since no usable material to replace it in the vital application is market ready the ban is still suspended.

The distinction between hard and soft ferroelectric material is mostly shown with PZT. [11,28,29,30,31] Generally Donor dopant (dopants that introduce electrons into the compound in excess) lead to fewer Oxygen vacancies in the material by forcing the chemical pressure (LeChatelier principle) into the direction of the solid. Acceptor dopants naturally do the opposite. The most common donor dopants are Nd, Nb, the most common acceptor dopants are Fe, Mn and Ni.
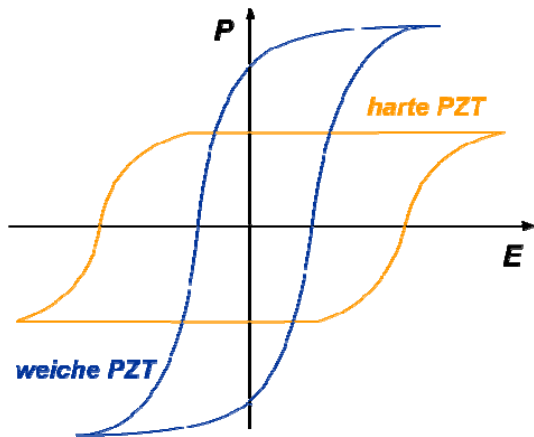
Figure 10: The distinction between "hard and soft" style ferroelectricity in PZT [CC]

Generally donor doped and therefore soft PZT is preferred when manufacturing actuators, because donor doping eases the processes aligned with DWM. Hard applications forego the need for extensions primarily focusing on a high quality factor (reciprocal loss factor), so ultrasound emitters sensors or Transformers prefer this type of material.[16]

1.4   Lead Free Piezomaterials

1.4.1 Why Lead is so hard to replace

The Primary question regarding lead free materials is why lead is so hard to replace, to which there is no easy answer. Primarily the properties for an A-Site ion are:

- Ionic radius: best illustrated by the tolerance factor (see there)

- High polarizability: Is a function of ionic radius and the electronic configuration [8]

- Valence: an A site has ideally a 2+ valence although other configurations are possible, they need compensation to achieve charge neutrality

- Lone pairs: Ideally the A-site exhibits an distorted (non symmetric) s^2 lone pair[24]

When taking all these factors into account, of all 120+ elements only lead has this desirable combination of properties. Although to preserve the properties a mixture of Bi and Tl is thinkable thallium would however completely defeat the purpose of non-toxicity. Generally due to the high toxicity and high volatility (which would contaminate any furnace used)[32] it has not even been tried to be included in any high temperature ceramic process.

Disregarding valence the closest nontoxic material to this "ideal" set of properties is bismuth. bismuth itself is rather unique within heavy metals in its non-toxicity, prompting fears that it is not as harmless as it is initially believed, which would have wide reaching consequences since many cosmetic products and pigments contain it instead of the lead that was traditionally used. Interestingly enough Bi has no known isotopes and is actually radioactive, however it´s recorded half life is longer than the existence of the universe and therefore highly unlikely to have health hazards associated with this. In fact it´s radioactivity was first proven as late as 2010 despite theoretical calculations pointing into this direction for 60 years. Despite these concerns no conclusive evidence for any health hazards are to be found so far. [32]

1.4.2 Types of Lead free materials

The most important lead free ferroelectric so far is Barium Titanate, mostly used for capacitator applications. Although it can be used as an actuator or sensor the miniscule piezoresponse and the neglegabele DWM make it an unlikely candidate for the replacement of actuators. The other materials have to be classified as emerging materials with varied strengths and weaknesses. Generally it is highly unlikely that there will be a single material to replace PZT in the wide range of applications that it occupies due to its unique versatility. For "hard" applications potassium Sodium niobate is a strong contender, showing nearly no deviation from the ideal piezoelectric behavior (unlike PZT f.i.). This makes it ideal for ultrasound emitters or transducers since a high quality factor is the most desired property for this type of application[20]. Bismuth Sodium Titanate based materials are forerunners to replace lead in actuator and capacitator applications.

BNT:

Bismuth sodium titanate (BNT) was first synthesized by Smolensky[33] in 1960. As it necessitated an inconvenient Ethanol based processing route and exhibited no significant strain under low fields, it remained nothing more than a curiosity within the class of lead free piezoelectric ceramic materials and was studied only by an exclusive group of scientists. Most notable among these is Tadashi Takenaka´s group[5,34,35,36], who subjected the material to extensive modification that remains relevant to this day. This trend changed in 2008 when Zhang *et.al.* [37,38,39] discovered a slightly modified solid solution of the material that could reach strains up to 0, 45 % under high fields (7kV/mm) surpassing the properties of the state of the art PZT (lead zirconium titanate) actuator materials. Combined with new legislation necessitating a move away from lead in electronic components (REACH,2007; RoHS 2005), currently unenforced due to lack of alternatives, but expected to be enforced in the future, this has provided sufficient incentive to cause a surge of research interest towards lead free materials in general but also into BNT derived materials specifically.

Chemically all BNT derivates are solid solutions of either Bismuth sodium titanate or Bismuth potassium titanate and therefore conform to the perovskite structure. Despite having a tolerance factor between 0,97 to 0.99, at room temperature all studied compositions have been refined as non-cubic, either of rhombohedral tetragonal or monoclinic symmetry. The most common inclusions are: solid solution with BT and other alkaline earth titanates, KNN or A site substitution with rare earth ions . These additions show various structural differences to the unmodified ceramic, mostly changing the position of the MPB between rhombohedral and tetragonal phases. Structurally the solid solution and the pure

21

compound show remarkable properties. It has been shown that any single grain of the material can exhibit up to three symmetries side by side without macroscopic or chemical separation[40,41,42].

Generally BNT-BKT (and BNT-BT) solid solutions exhibit a compositional phase transition between macroscopically rhombohedral and tetragonal symmetry. This phase transition is very diffuse and strongly dependent on temperature, unlike PZT where this transition is (nearly) temperature invariant. While the diffuse nature of this compositional phase transition [41] is subject to considerable investigation, the thermally induced phase transition T_d, usually measured either by thermally resolved electric (d_{33}, or loss factor[20]) measurements is much more important.

This is a phase transition from a macroscopic ferroelectric to an antiferroelectric (in other readings non-polar) phase. It can be considered the key to understanding the material. In any BNT-derived ceramics that shows this transition, the piezoelectric and dielectric properties under high electric fields are tremendously enhanced. Above (and especially close to) T_d, such compounds exhibit pinched polarization loops that have become a hallmark of the material.
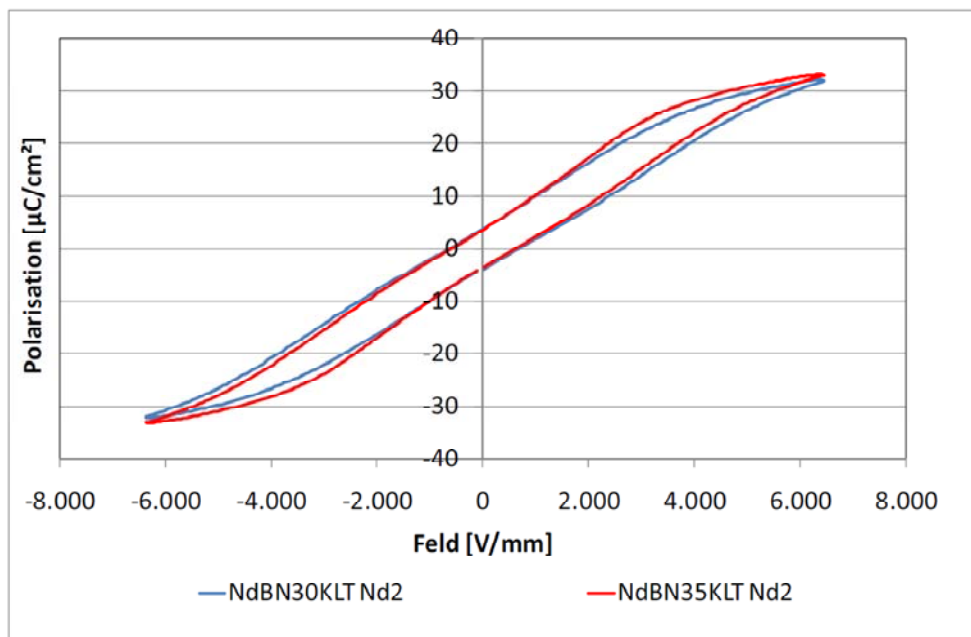

Figure 11: Pinched polarization loops of two compositions of BNT/BKT (doped with Li and Nd)

Conversely, if (for any reason) the (BNT-derived) material lacks this phase transition, it becomes a canonical soft ferroelectric. In a recent paper we have shown that the phase transition is caused by the loss of hybridization of the Bi-lone pair with the surrounding oxygen, thereby releasing the constraint that it puts on the crystal system, which can be regarded as a corner-sharing network of oxygen octahedra

containing the B-site cations (in this case Ti^{4+}). This resets the material to the structural phase that is predicted by the ionic radii (via the tolerance factor t of the Goldsmith rule). This covalence- based mechanism is usually called the *lone pair effect* [24,40,43,44] in literature concerned with ferroelectric materials. It is caused by the electron pull of the overlap of orbitals from the B-site cation (in ferroelectric perovskites almost exclusively d_0 transition metals). This causes a decrease in electron density on the outside of the oxygen octahedra[45,46,47,48] (in the direction of the A-site cation) and thereby facilitates the formation of bonding by the lone pairs of the A-site cations. In PZT this bond is very stable and contributes to the temperature stability of this material (exceptionally high Curie temperature[15,43,47] compared to alkaline earth titanates). In BNT-derived materials, only half the A-site is occupied by a lone pair carrying ion, and this is the reason why the loss of hybridization is not coinciding with the transition to para-electric behavior at elevated temperatures; instead forming an intermediate temperature dependent phase transition. We could show this effect by deconvoluting the temperature dependent Raman spectra of our prototype actuator and plotting the modes indicative of A-site-oxygen vibrations. At T_d, the inter-atomic spring constant responsible for the total energy of the mode was lowered abruptly, accompanied by a rapid change in symmetry of the whole crystal system[40]. This is a hallmark of the breaking of a covalent bond.

However despite the extension under field being superior to PZT there are still several obstacles for market readiness. Some of them we have been able to lay to rest, some of them will be subject of further attention of the scientific community. The most important obstacles are:

Incompatibility to industry standard inner electrodes:

One of the main constituent of the ceramic Bi_2O_3 was previously reported to be incompatible with the industry standard Ag/Pd alloy used in electroceramic multilayer devices, we were able to lay this fears to rest, first through preliminary studies then by manufacturing a functioning prototype. The reason why in contrast to the primary compound BNT ceramics are compatible is that after the initial calcination no free Bi_2O_3 is present throughout the sintering. Therefore unlike the prior applications of Bi_2O_3 as a flux (sintering aid) there is no evidence of Bismuth Palladate being procured. Therefore the associated problems of lack of conduction and the development of micro cracks were unfounded.

Ethanol based process:

Primarily the necessity to use organic solvent in the process of synthesizing BNT is complex. For one it is simply the desire of the associated scientist not to change the process too much for fear of losing comparability with the literature. Since the influences on properties of electroceramics are manifold, it is a general tendency of the field to keep within very narrow specifications, and with good reason. The original reason for the organic solvent process was most likely the sensitivity of Alkaline carbonates to Water. For one, the problem of adsorbed water, which makes it hard to keep stochiometry makes even the primary weighing in a challenge on an experimental level. But also the tendency of the alkaline carbonates to partially dissolve in water has a great influence on the microstructure. If no precautions are taken the partially dissolved carbonates crystallize after the first milling step and do not readily react with the rest of the educt leading to an inhomogeneous ceramic. Our research shows that after the calcination step (which produces the compound necessary, sintering is a purely physical process) the perovskite is completely stable forgoing the necessity of using organic solvents after calcination. In the interest of making our process compatible with industrial equipment we [] developed a process whereby the educts are spray dried after the first milling so the recrystallization does not lead to bigger aggregates and is therefore not detrimental to the solid state reaction as well as the microstructure.

High excitation Voltage necessary:

One of the fascinating properties that set BNT derived materials apart from conventional piezoelectric ceramics is the necessary high excitation field of 6-8 kV/mm necessary for the full stretch of the material to manifest itself. This is one of the reasons why the excellent properties of BNT derived compound have been obscured for so long after their initial discovery. Usually, following the standard model the piezoresponse is linearly correlated with the field applied (Equ.1). Consequently the usual way to determine the magnitude of a piezoresponse until Zhangs seminal paper, were to measure the piezoresponse under low field amplitudes. The necessary voltage using the same sample geometry as in PZT (70-100µm layer thickness), which operates under 2 kV/mm usually would be over 600V which would make it unusable in most applications. Fortunately both the material properties (tougher than PZT) as well as the high strain reachable under high fields but especially the exceptional dielectric breakdown strength allowed us to reduce the thickness of the active layers to 30 µm while preserving the same number of active layers and reaching more strain than a comparable PZT actuator.

Secondary phases:

Another difficulty for the development of BNT as a viable alternative was the propensity of the material to form secondary phases. Both Bi-rich phases as well as polytitanates are reported. Concern

about secondary phases in perovskites are however solely based on the experience with PZT where (due to the lack of propensity for secondary phases) a secondary phase is usually a sign of a botched processing run indicating decomposition of the material or failure of proper homogenization of the educts, in any case being detrimental to piezoelectric properties. In fact the secondary phases are a result of improper stochiometry, however since Alkaline metals as well as bismuth are volatile compared to other metals it is nearly impossible to be fully stochiometric. In fact the problem of volatilization exists in lead based materials as well, only that the non-inclusion of alkalines does no yield such significant alkaline polytitanate secondary phases. Our research shows that we can manufacture BNT (and it´s derivates) without secondary phases only when a sufficient deficiency of Ti is introduced, thereby offsetting the loss of the volatile elements. This however ruins the ceramic for the purpose of electric actuation. We judged that the inclusion of a Ti rich secondary phase is not harmful; in some cases (dielectric breakdown strength) a secondary phase filling the inevitable pores of the material is actually preferable to a single phase composition. The Bi rich phases on the other hand are usually a result of an alkaline deficiency. Such can be illustrated by the work of König *et. al.* where a multistage process designed to minimize Bi loss lead to a development of a secondary phase in the ceramic rich in bismuth. Again the inclusion of a secondary phase seems to be actually beneficial for capacitor applications.

Despite the existence of a usable actuator, no long term tests have been done on the material in a realistic setting so any data on the problems that might develop when the material is used in production run products (under hostile conditions such as moisture) is available. These conditions might still have some surprises for scientists and engineers in store. So far only the non existence of dielectric fatigue has been shown by Matt Hoffmans group in Sidney. But whatever the challenges I personally remain confident that the material will be used in commercial devices within the decade.

2. Practical Part

2.1 Synthesis and fabrication

2.1.1 Lab Scale

On the industrial scale as well as in laboratory the most important route for the synthesis of ferroelectric ceramics is the mixed metal oxide route (MMO). The MMO route was initially developed for use with PZT and BT. Other routes include solution deposition, and templating methods. Templating methods deserve a special mention since by using partly organic precursors, the direction of polarization and structure is not dictated by sintering (and therefore random) but by molecular self assembly mechanisms aided by the partly organic precursors. Also due to much smaller particle sizes a lower sintering temperature is possible (and usually the only step). The only electroceramic where this has any importance is KNN where it is used to offset the miniscule piezoelectric properties.
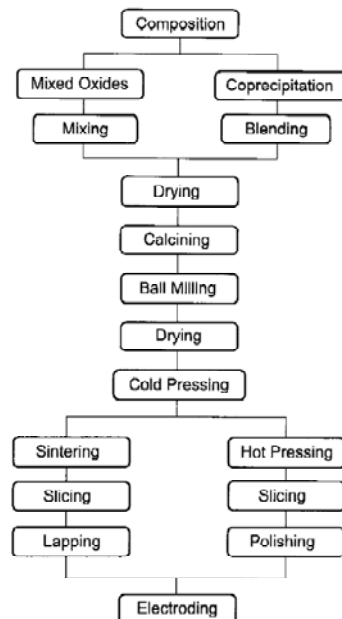
Figure 12: Mixed Metal Oxide(MMO) route including further processing step of a multilayer [from [3]]

After weighing to the desired stoichiometry the educts usually carbonates or oxides (although nitrates and sulfates are possible as well) of the desired constituents of the ceramic, a homogenization step is necessary. The homogenization step is both for the benefit of gaining a uniform powder as well as a method to break down the raw materials into small particles to facilitate the solid state reaction. Larger aggregates would inhibit the solid state reaction through the development of layers of reacted material

acting as a diffusion barrier. A poor homogenization would lead to a local non-stochiometry of the constituents. While unavoidable to a certain extent it has to be minimized otherwise the following sintering step would be inhibited. Also, a local excess of certain constituents would lead to the development of secondary phases as well as educts being left over and interfering with further processing. This is usually carried out either in a high energy ball mill or a low energy roller mill (for a longer time). Due to the high brittleness of oxides and carbonates no cooling is necessary to facilitate the breaking apart of the initial educts. After homogenization the mixture is usually dried and submitted to the calcination step. Usually a detergent is necessary to keep the educts from reagglomeration. One thing to look out for in the first milling stage is the ionic potential of the constituents since the oxides or carbonates involved are lewis acids/bases they will change the pH-Value of the suspension and therefore may be coming dangerously close to the iso-electric point of one or more of the constituents. Since at the isoelectric point the re-aggregation of particles is maximized due to the repulsive forces in suspension being minimized [49]this is of tremendous value. In fact the whole process of milling on a µm scale depends more on the prevention of re-agglomeration than the breaking down (milling) of the educts. Typically if one or more of the educt are close to their isoelectric point this will be visible as a clear tailing of the log-normal curve of a dynamic light scattering particle-sizer pattern (which is also good practice to use in every new process). Once a uniform compound has been achieved (i.e. after calcination) this problem is much less imminent due to only a single compound being present. Other common problems of the milling stages are : contamination, zirconia abrasion (from the milling containers and /or media) loss of the dispergent to excessive heating of the container (avoided by introducing breaks within the milling program).

The calcination step of the process is named after the Latin *calcinare* [32](to burn lime) due to its earliest/most common application. It is a heat treatment of the educt usually carried out in a laboratory kiln or furnace. The most common container are round oblong jar of either Aluminum oxide or zirconia. Aluminum oxide is preferred for its favorable ratio between thermal conductivity (high) and thermal capacity (low). This minimizes the inertia introduced into the kiln and allows for more finely tuned control of the kiln. The calcination step is where the actual solid state reaction to aquire the compound desired takes place. It is good practice to check every calcination by XRD to make sure that the reaction has been complete. Typical calcination temperatures are (800°C-950°C) The choice of calcination temperature is usually one of weighting the benefits of a quicker and more complete reaction with the detriments of evaporation of volatile elements. After calcination the samples are usually milled again this time to prime the mass for sintering.

After the second milling a forming process is employed. Generally on a lab scale, uniaxial pressing of pellets is employed. The milled and dried calcined powder is mixed with up to 10 % of an organic

binder (f.i. PEG 20000) its function and properties have to be chosen along two lines, first to facilitate the binding, but also to be burned out (pyrolized) without detrimental effects to the sintering. Also no residue organic or inorganic should be left within the ceramic after pyrolysis. To this effect a differential calorimetric analysis (DTA) of the binder is usually done beforehand, and a separate burning out step is introduced before sintering immediately above the peak of pyrolysis determined by the DTA. For PEG 20k the burn out temperature is c.a. 300°C. Depending on the speed of sintering and the amount of introduced binder the separate burn out stge can be omitted, For instance barium titanate has a very late onset of sintering (defined as the temperature at which rapid densification starts and as such the burn out can be included within the sintering curve.

Sintering is a complex process, however an entirely physical one. It is however similarly to a chemical reaction a thermodynamic process to find a minimum energy state. This process is however not driven by a change in compound but is a process to find the lowest possible surface area.
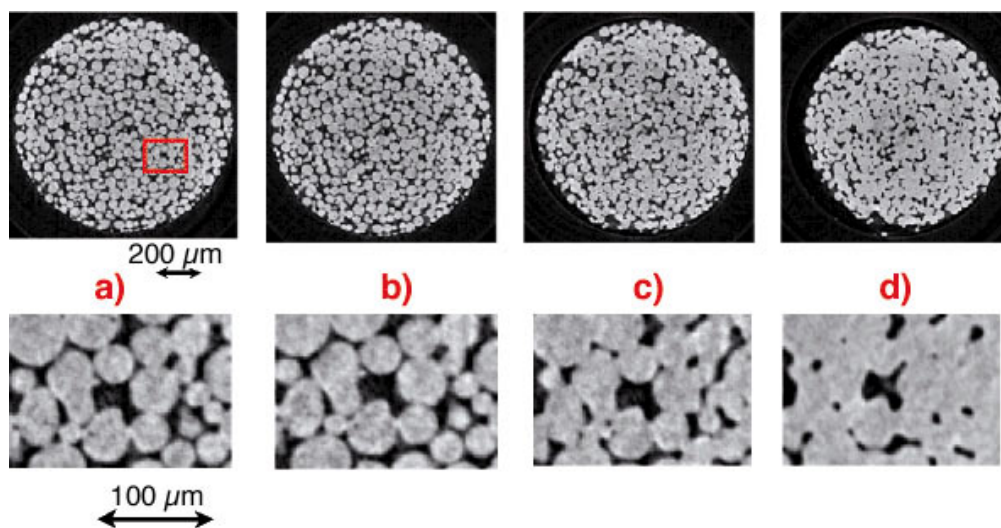
Figure 13 : Distinct stages of growth in sintering [from [50]]

Sintering is a complex and often arcane process since anything that can influence the diffusion during the distinct stages of growth will influence the microstructure of the material. As an example a sintering aid that promotes the formulation of a partial liquid phase between the growing grains (e.g. Bi_2O_3) lead to a much greater exchange of particles than the usual pathway that are involved in a non-liquid phase sintering process. As such the density is increased but at the cost of grain size[50]. This can be best explained by the stage in sintering where growing grain grow at the expense of other grains, if some grains have access to ideal growing conditions and other do not they cannibalize. So if ideal diffusive conditions persist the material will be dense with uniform but small grains. If diffusion is minimized, the opposite will happen: Large and small grains with large pores and a wide distribution of grain sizes, but

28

bigger grains in general. In principle any route to minimize maximize diffusion during the sintering will yield this result.
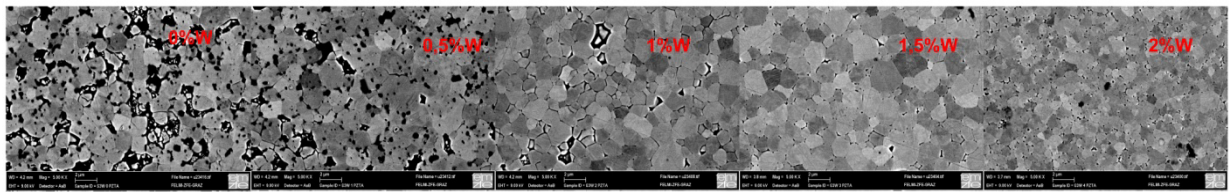

Figure 14: Overviev of PZT with various additions of a liquid phase sintering aid (W). The size bars below are 2µm in size.

One common problem of sintering is again the loss of volatile elements. To counteract this there are usually one of two strategies involved, either to introduce an excess of the volatile elements, or to bury the samples within a similar powder to keep a high partial pressure of the volatile elements and therefore minimize evaporation.

2.1.1 Industrial Scale

The prime difference between lab scale and industrial scale when processing ferroelectrics is in forming stage. The disc shaped pellets usually used on the laboratory scale are not very common in industrial products. The most common geometry is the rectangular multilayer. A Multilayer is a device consisting of alternating layer of ceramic and electrode:
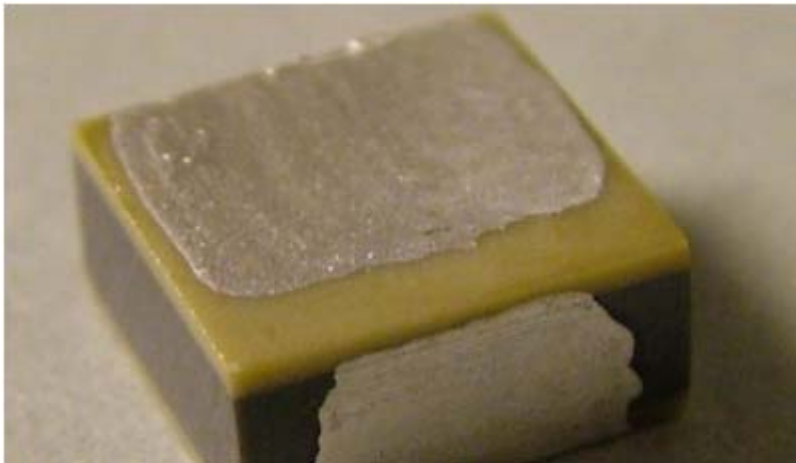
Figure 15: Prototype BNT multilayer(50 layers a 30 µm)

The main benefit of a multilayer is to forego the requirement for a high voltage to reach the field intensities necessary for actuation. A perfect example would be a PZT actuator. In order to extend for the same length (typically a few micrometers) a solid block of 1mm with a single electrode pair would take 2500V a comparable multilayer with 10 layers â 100µm only 250V. This is an enormous advantage in usability but also in safety.

Multilayers are usually fabricated by Tape casting followed by screen printing of the electrode and subsequent stacking. The green multilayer is cut and sintered together with the electrode in a process called co-firing.
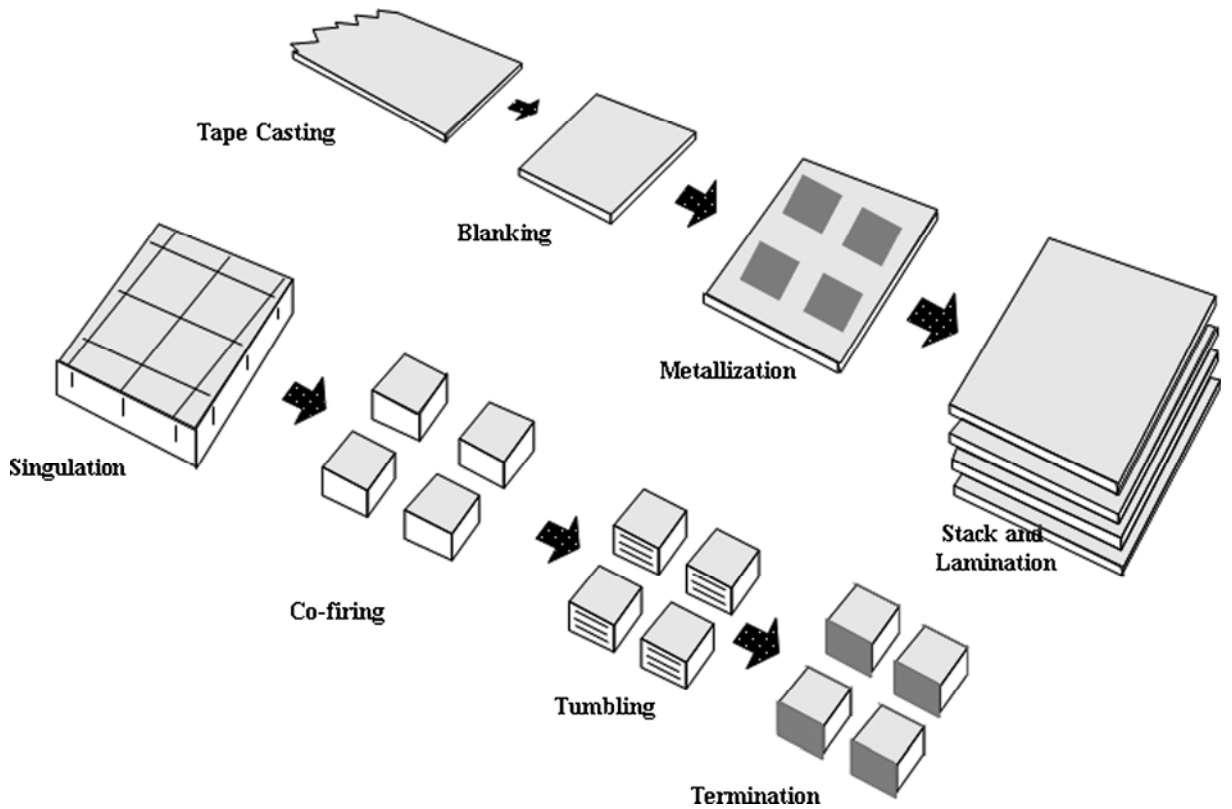
Figures 16: Schematic of the tape casting and subsequent assembly process as applied for multilayer ceramics [from[6]]

Naturally co-firing ceramics with an electrode introduces enormous problems[6,18,31,51,52,53,54,55], that have to be considered. The first would be the question of chemical compatibility. If the electrode layer forms an intermediate phase with the ceramic a number of processing problems will occur. Chief among these would be the loss of conduction. Micro-cracks and loss of bonding would be a close second.

Another problem immediately apparent is the problem of interdiffusion. Most constituents of ferroelectric ceramics are not soluble in the metals employed in a ceramic layer. Quite the opposite is true for the metals employed as electrode layers. Both the noble metals Pd or Ag/Pd alloys common to ambient air processes as well as Copper (PZT) or Nickel(BT) used in base metal processes that have to use reducing atmospheres show clear signs of interdiffusion. This however can topple the delicate donor acceptor balance inherent to ferroelectric ceramics. Also both Ag (the more diffusive of the two constituents of an Ag/Pd alloy) as well as Cu have been shown to influence sintering and change the conductive behavior of ferroelectrics.
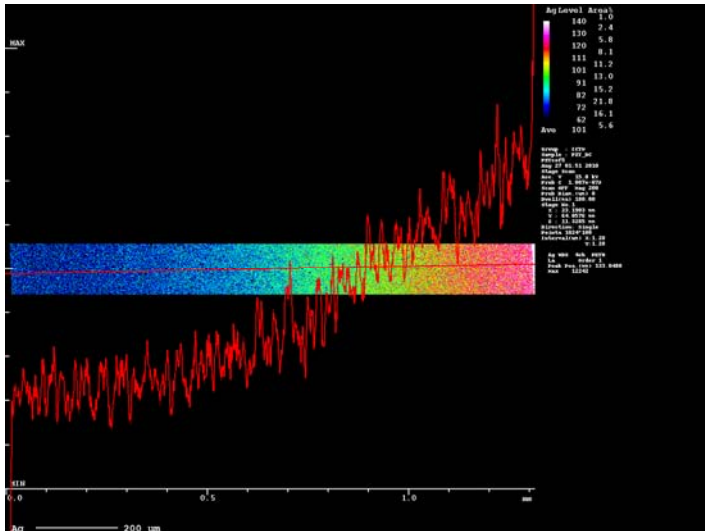
Figure 17: Diffusive curve taken from a PZT Ag/Pd diffusion couple sintered for 1h measured by an Electron Micro Probe (EMPA)
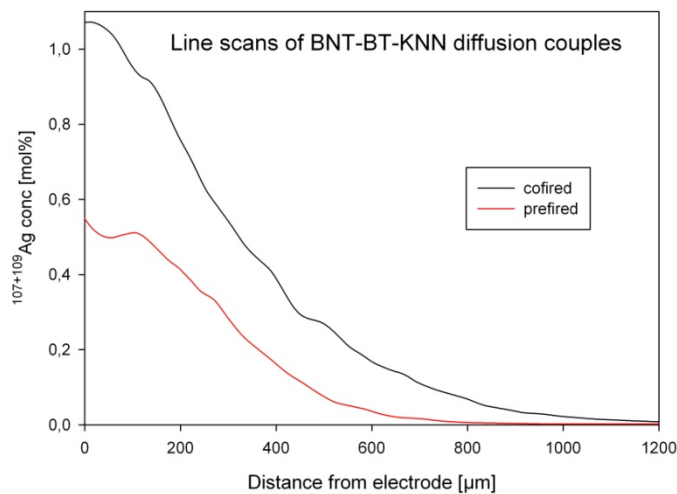

Figure 18: Diffusive curves acquired by LA- ICPMS

Of particular complexity is the metallurgy of the Ag/Pd alloy, that has to be taken into account for the temperature curve of sintering. Between 245-935°C Pd forms an Oxide, enriching the alloy of Ag which in turn leads to a much higher Ag partial pressure. This is usually combated by increasing the ramp of the sintering curve between 350-1000°C (it is common to double the heating rate) to take advantage of the slow oxidation of Palladium and thereby prevent the vapor pressure to rise and preserving the ratio within the alloy.
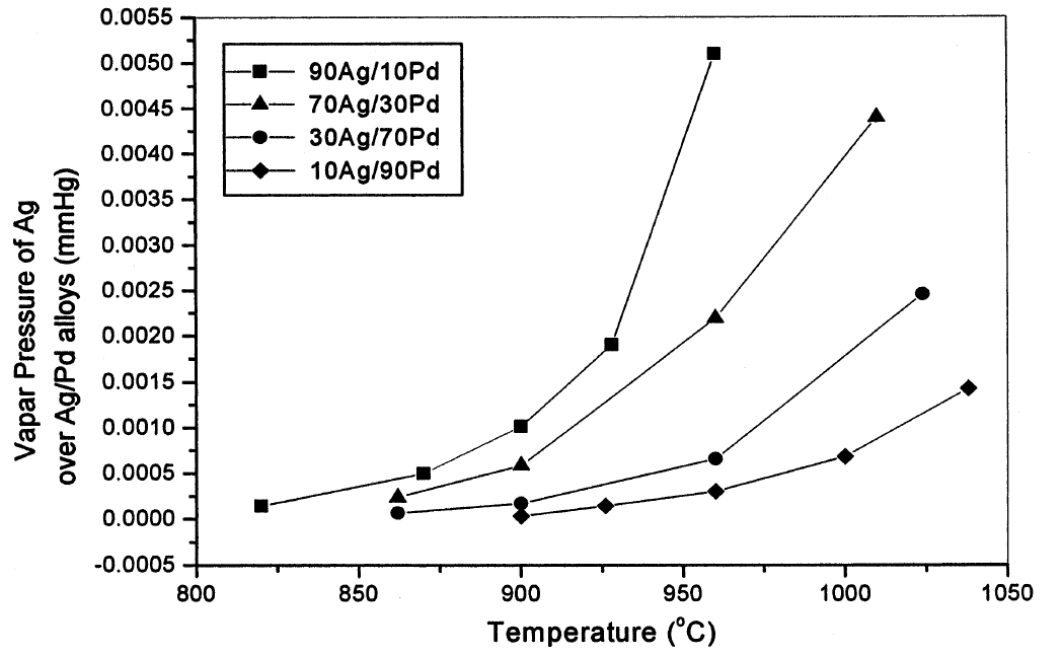
Figure 19: Ag vapor pressure vs temperature and for different Ag/Pd alloys [from 52]

Tape casting also employs a much higher content of binder within the forming slurry making complex burnout steps necessary. Failure to do so will result in a destruction of the device or the forming of intergranular graphite, being conductive this renders any electroceramic inoperable.

Apart forming the chief difference between lab and industrial scale is the magnitude of material processed. This usually means that instead of batch mills being used, continuous mills are employed.
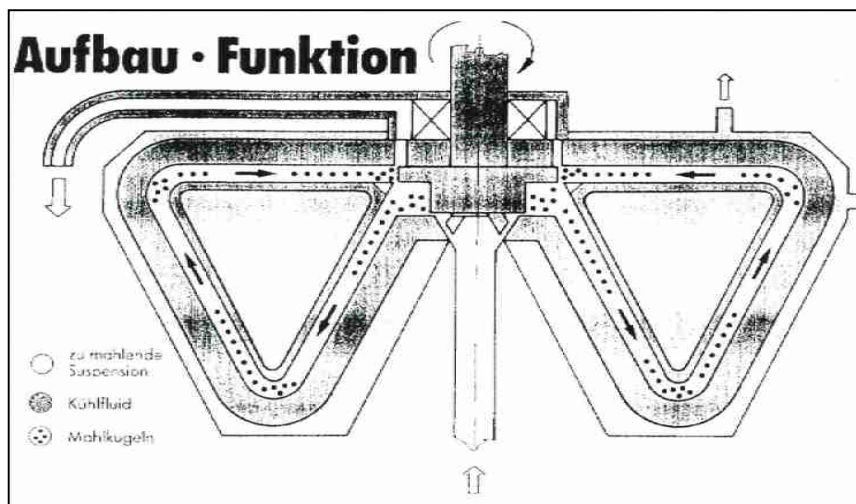
Figure 20: Schematic and explanation of the components of a continuous mill [from3]

This leads to a high degree of overlap between lab scale processing and industrial fabrication which makes the turnover rate in electroceramics a rather high one. This is one of the aspects that make this field really exciting.

33

2.2 Analysis

2.2.1 Image based techniques

The most important imaging technique for the development of ceramics is Scanning Electron Microscopy. It is used for checking the homogenity of a material, the phase content, microstructure (shape, size and grain size distribution), and a brief overview over the elemental content. The most common imaging method utilizes low-energy secondary electrons that are excited from the K-orbitals of the specimen atoms by inelastic scattering of the primary electron beam. In addition to topographic information secondary electrons offer information about the elementary composition and homogeneity of the sample. Generally and increase in proton count of the interacting atoms increases brightness of the area. A good example would be the alkaline-polytitanate secondary phases of a BNT ceramic. Being of lower proton count than Bismuth and having the same amount of oxygen per volume they are visible as dark areas in a micrograph.

Most research devices employ an Energy-dispersive X-ray spectrometer (EDX) to offer more specific information over smaller sections of the sample. The capabilities of this method will be discussed in the appropriate section.
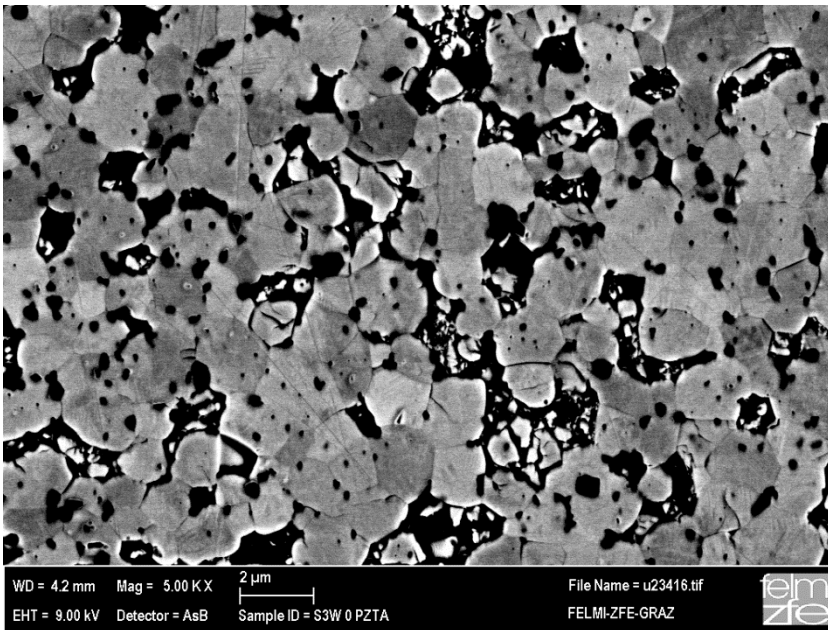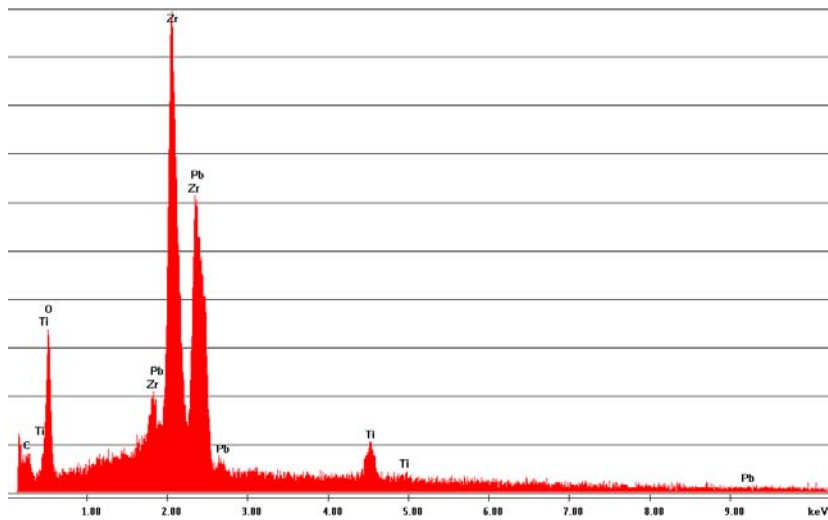
Figure 21a,b,: Undoped PZT ceramic(a) and the corresponding EDX Spectrum(b)

Together these two methods offer a very good preliminary overview over phases and composition of the sample but fall short in several areas and have to be complimented with other methods. One particular area is the microstructure of the ceramic which (due to the uniformity of a polished sample) needs to either pre-etch the ceramic to dissolve the intergranular material or employ backscatter methods capable of resolving the crystallographic direction(discussed below). However etching destroys a lot of usable information (secondary phases, intergranular material) and is therefore limiting.

Electron backscatter diffraction (EBSD), also known as backscatter Kikuchi diffraction (BKD) is a microstructural-crystallographic technique used to examine the crystallographic orientation of many materials. It enjoys a particular advantage in ferroelectrics because of the ability to resolve individual grains

35

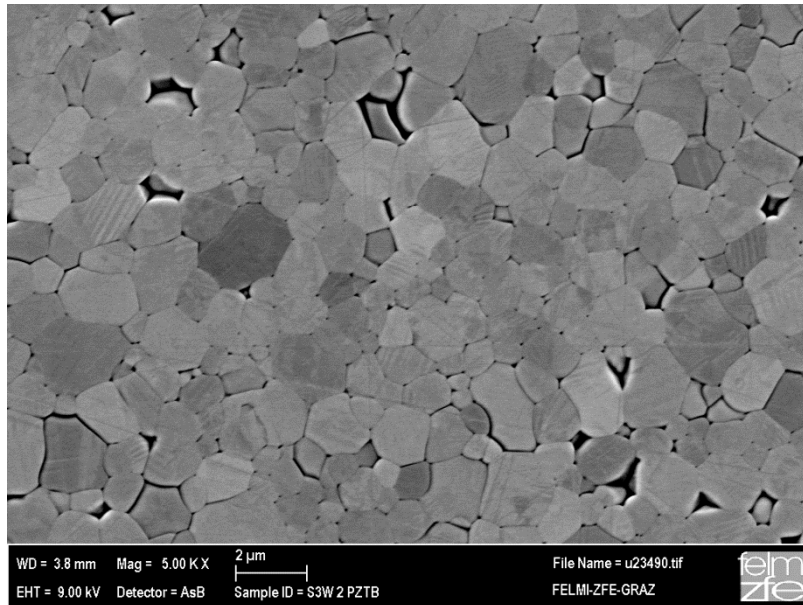without the need to pre-etch the material. An easily employed variant of this principle is channeling contrast.

Figure 22: Channeling contrast image of Sr and W doped PZT

2.2.2 Symmetry sensitive techniques

XRD (X-Ray Diffraction) is a family of techniques that offer information about the crystal structure of a material. All XRD Techniques utilize inelastic scattering of X-Rays along the crystal system utilizing Bragg´s Law. As such any amorphous material will not offer any information. Primarily the distinction is between powder and single crystal scattering. In powder scattering the sample is finely ground and the distribution of orientation is assumed to be stochastic. In materials that are susceptible to templating such as mineral slate this assumption is incorrect. It is also one of the chief limitations of powder diffractometry, that the diffractogramm is a representation of the average of all crystal structures and orientations over the whole incident beam. Also, materials that show a mixture of similar phases are extremely difficult to analyze. This problem is especially pronounced in BNT based compositions usually averaging as a pseudocubic structure[42,56,57,58,59]. All of this could be bypassed by utilizing single crystals.

Single crystal X-Ray diffractometry is much more accurate and able to resolve the crystal structure, including its component parts (e.g. individual molecular structures of sugars). It is however dependent on the manufacture of single crystals of sufficient size which is quite a challenge in materials as disordered as PZT. Also an additional factor is the absorption of the crystals involved. Heavy ions such as bismuth and

lead absorb a lot of intensity from the incident beam and therefore need specialized equipment with high incident intensities.

Raman spectroscopy (named after Chandrasekhar V. Raman) is a spectroscopic technique used to study low-frequency modes of a vibrational, rotational or other nature in a sample. It relies on inelastic scattering, or Raman scattering, of monochromatic light supplied by a laser.
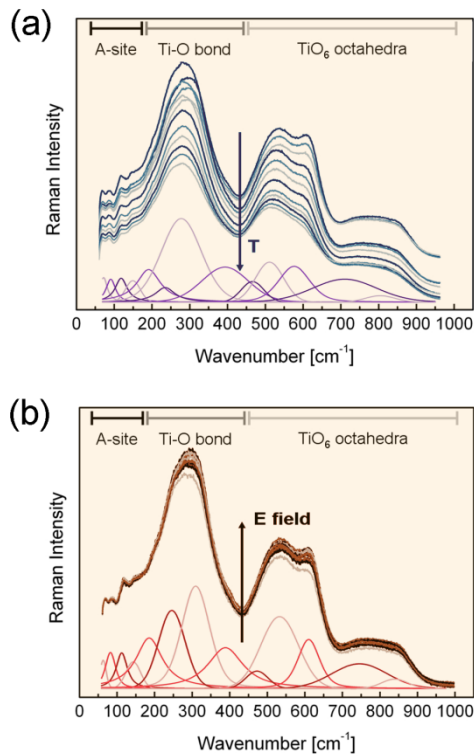

Figure 23: Raman modes of our BNT based actuator (a) denotes the spectra under the influence of increasing temperature (b) under increasing electric field

Its unique advantage is to detect local structure (versus the long range structure gained from diffraction methods) and the ability of refinement through multiple stages of Fourier Transform to resolve individual modes (deconvolution). Since a crystal structure, much like a molecule is not a discret entity but an integral of permittable modes at the time (mostly as a function of temperature but other surrounding parameter influence the permittable modes as well). For example the transition to a cubic state over the T_c observed in ferroelectrics is simply a "white light" of multiple modes interacting and therefore showing higher symmetry (cubic). We took advantage of this to plot the individual modes of a perovskite type Bismuth-Alkali-Titanate (Fig. 24) with a special emphasis on A- Site-Oxygen modes. This allowed us to track the thermal evolution of the individual modes and support and prove our theory of a fragile A- Site to oxygen orbital overlap as the mechanism responsible for the T_d.
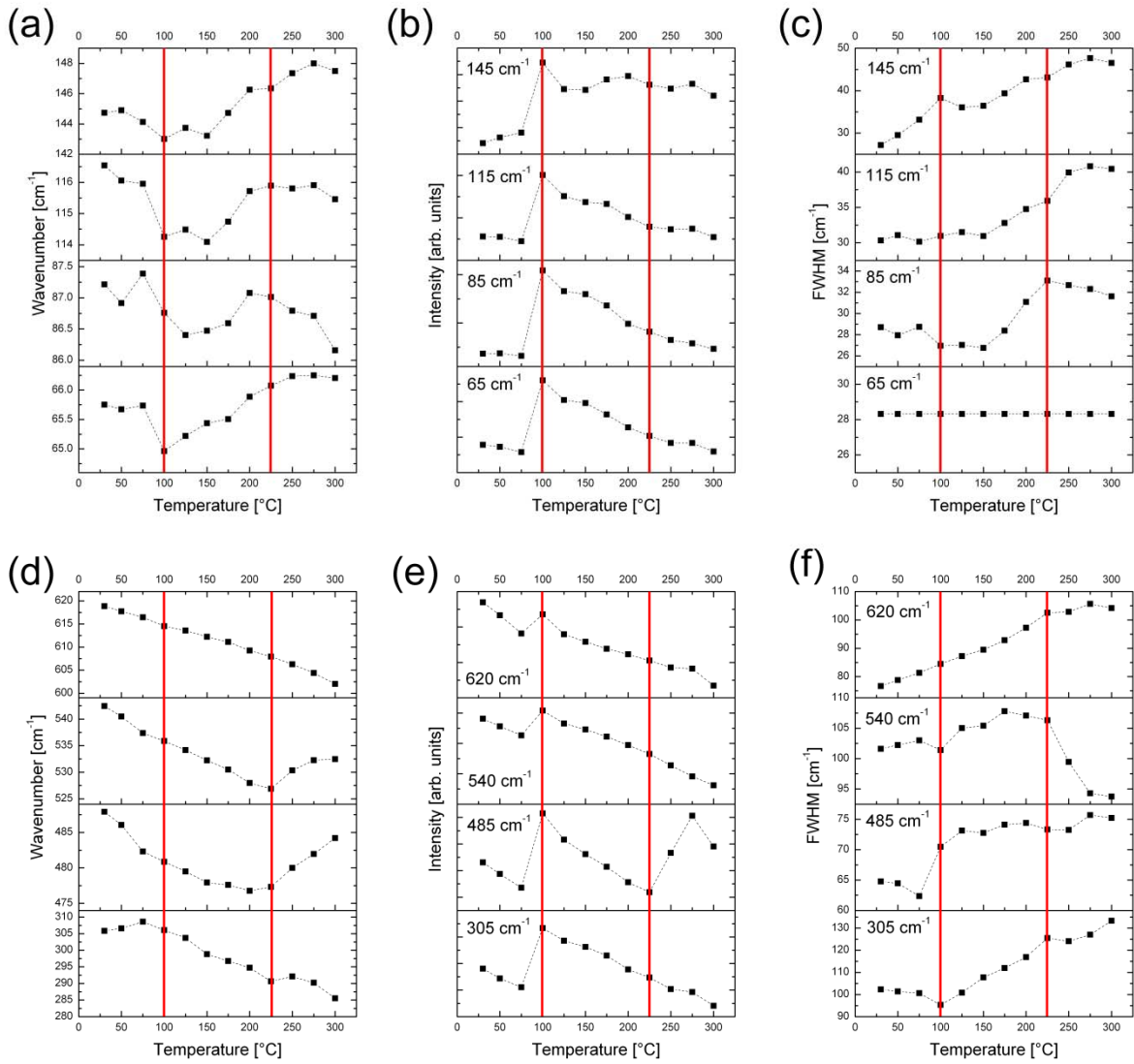
Figure 24: Refined and deconvoluted individual raman active modes in a BNT material under applied temperature

2.2.3 Microanalysis

Energy-dispersive X-ray spectroscopy (EDS or EDX) is an analytical technique used for the elemental analysis. It is mostly used in tandem with SEM. Like secondary electron imaging it uses the K-shells of atoms to determine elemental compositions. While being very accurate and showing a low limit of detection when detecting heavy elements in a light elemental matrix)[60] its chief limitation is the interference generated by the k shells of a matrix containing heavy elements. A good rule of thumb is that for qualitative analysis in such matrices the detection limit is around 1 mole%. Since the incident beam is interacting with the material in a pear shaped manner, also its lateral resolution is limited to 1-2μm. It

provides however a quick and moderately accurate qualitative representation of most elements within an analyte and serves as a good companion for SEM for initial analysis of an unknown sample.

Mechanistically it is dependent on the emission of characteristic X-rays from a specimen which is only semi-characteristic. A significant overlap exists especially when dealing with multiple heavy elements.

EDX is often contrasted with its counterpart WDX (wavelength dispersive X-ray spectroscopy; WDS). WDX can be thought of as reverse single crystal diffractometry. While diffractometry is gathering the scattering pattern from a known wavelength and determining the crystal parameters this way, WDX is scattering an unknown wavelength along a known single crystal, therefore in WDX, only one element can be analyzed at a time, while EDS gathers a spectrum of all interacting elements. It is for this reason that multiple detectors are combined to form an electron microprobe (along with the excitation happening through a filament instead of field emission). Correspondingly a microprobe is a much more accurate analytical instrument than the normal EDX-SEM combination, capable of resolving trace elements on a micrometer scale.

Table 1: Fully quantitative Electron microprobe analysis of BNT-BKT solid solutions and secondary phases sintered at different temperatures.

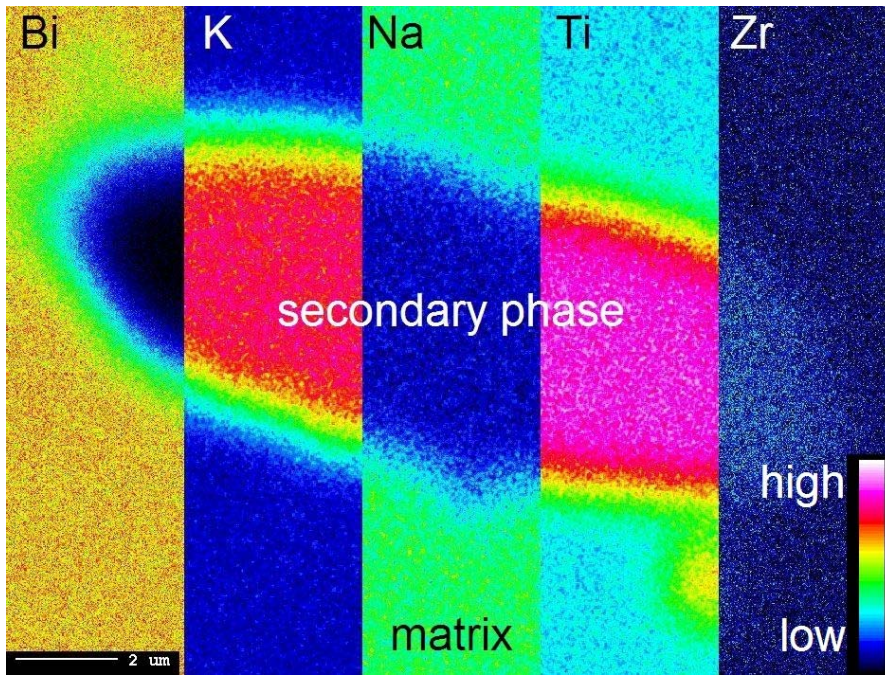| Temperature	Matrix					Secondary phase				
	Bi	Na	K	Ti	Zr	Bi	Na	K	Ti	Zr
1000 °C	0,495	0,401	0,115	0,979	0,021	0,917	0,592	1,263	5,234	0,113
1050 °C	0,498	0,398	0,111	0,978	0,021	0,356	0,335	1,503	5,598	0,174
1100 °C	0,493	0,403	0,110	0,987	0,015	0,046	0,253	1,693	5,876	0,103
1150 °C	0,499	0,408	0,085	0,989	0,013	0,013	0,311	1,637	5,849	0,156

Figure 25: EMPA (Electron MicroProbe Analysis) Mapping of the common polytitanate secondary phase in BNT-BKT

3 Literature

1   http://en.wikipedia.org/wiki/Actuator. (retrieved 23.12.2012).

2   PI GmbH, P. C. http://www.piceramic.com/piezo_actuator.php. (retrieved 23.12.2012).

3   Haertling, G. H. Ferroelectric ceramics: History and technology. *Journal of the American Ceramic Society* 82, 797-818 (1999).

4   Takenaka, T., Nagata, H. & Hiruma, Y. Current Developments and Prospective of Lead-Free Piezoelectric Ceramics. *Japanese Journal of Applied Physics* 47, 3787-3801, doi:10.1143/jjap.47.3787 (2008).

5   Takenaka, T. & Nagata, H. Current status and prospects of lead-free piezoelectric ceramics. *Journal of the European Ceramic Society* 25, 2693-2700, doi:10.1016/j.jeurceramsoc.2005.03.125 (2005).

6   Randall, C. A., Kelnberger, A., Yang, G. Y., Eitel, R. E. & Shrout, T. R. High strain piezoelectric multilayer actuators - A material science and engineering challenge. *Journal of Electroceramics* 14, 177-191 (2005).

7   Shrout, T. R. & Zhang, S. J. Lead-free piezoelectric ceramics: Alternatives for PZT? *Journal of Electroceramics* 19, 113-126 (2007).

8   Jaffe, B., Cook, W. R. & Jaffe, H. L. C. *Piezoelectric ceramics / by Bernard Jaffe and William R. Cook Jr. and Hans Jaffe*. (Academic Press, 1971).

9   Newnham, R. E. *Properties of Materials*. Vol. 1 (Oxford university Press, 2005).

10   Cross, E. Materials science - Lead-free at last. *Nature* 432, 24-25, doi:10.1038/nature03142 (2004).

11   Ravez , J. Ferroelectricity in solid state chemistry. *Comptes Rendus de l'Académie des Sciences - Series IIC - Chemistry* 3, 267-283 (2000).

12   Rodel, J. Modelling linear and nonlinear behavior of polycrystalline ferroelectric ceramics. *Journal of the European Ceramic Society* 23, 2297-2306, doi:10.1016/S0955-2219(03)00084-0 (2003).

[13]   Arlt, G. Switching and dielectric non-linearity of ferroelectric ceramics. *Ferroelectrics* 189 (1998).

[14]   Dorcet, V., Trolliard, G. & Boullay, P. The structural origin of the antiferroelectric properties and relaxor behavior of Na0.5Bi0.5TiO3. *Journal of Magnetism and Magnetic Materials*, 1758-1761, doi:10.1016/j.jmmm.2009.02.013 (2009).

[15]   Garcia-Fernandez, P., Aramburu, J. a., Barriuso, M. T. & Moreno, M. Key Role of Covalent Bonding in Octahedral Tilting in Perovskites. *The Journal of Physical Chemistry Letters* 1, 647-651, doi:10.1021/jz900399m (2010).

[16]   Albareda, a. *et al.* Influence of donor and acceptor substitutions on the extrinsic behaviour of PZT piezoceramics. *Journal of the European Ceramic Society* 27, 4025-4028, doi:10.1016/j.jeurceramsoc.2007.02.087 (2007).

[17]   Goldschmidt, V. M. Die Gesetze der Krystallochemie. *Naturwissenschaften* 14, 477-485-485, doi:10.1007/bf01507527 (1926).

[18]   Troccaz, M., Gonnard, P., Fetiveau, Y., Eyraud, L. & Grange, G. Goldschmidt factor and phase diagrams of doped titanate zirconates. *Ferroelectrics* 14, 679-681, doi:10.1080/00150197608236699 (1976).

[19]   Damjanovic, D. Comments on Origins of Enhanced Piezoelectric Properties in Ferroelectrics. *Ultrasonics, Ferroelectrics and Frequency Control, IEEE Transactions on* 56, 1574-1585 (2009).

[20]   Aksel E., F., Kowalski B., Deluca M. , Damjanovic D. , and Jones J. Structure and properties of Fe-modified $Na_{0.5}Bi_{0.5}TiO_{3}$ at ambient and elevated temperature,. *Physical Review B*. 85, 21-24 (2012).

[21]   Dmowski, W. *et al.* Local Lattice Dynamics and the Origin of the Relaxor Ferroelectric Behavior. *Physical Review Letters* 100, 137602 137601-137604, doi:10.1103/PhysRevLett.100.137602 (2008).

[22]   Tan, X. *et al.* Electric-field-induced antiferroelectric to ferroelectric phase transition in mechanically confined $Pb_{0.99}Nb_{0.02}[(Zr_{0.57}Sn_{0.43})_{0.94}Ti_{0.06}]_{0.98}O_{3}$. *Physical Review B* 81, 014103 014101-014105, doi:10.1103/PhysRevB.81.014103 (2011).

23   Tan, X., Frederick, J., Ma, C., Jo, W. & Rödel, J. Can an Electric Field Induce an Antiferroelectric Phase Out of a Ferroelectric Phase? *Physical Review Letters* 105, 2-5, doi:10.1103/PhysRevLett.105.255702 (2011).

24   Warren, W. *et al.* Pb displacements in Pb(Zr,Ti)O3 perovskites. *Physical review. B, Condensed matter* 53, 3080-3087 (1996).

25   Wylie-van Eerd, B., Damjanovic, D., Klein, N., Setter, N. & Trodahl, J. Structural complexity of (Na_ {0.5} Bi_ {0.5}) TiO_ {3}-BaTiO_ {3} as revealed by Raman spectroscopy. *Physical Review B* 82, 104112 (2010).

26   Baettig, P., Schelle, C. F., LeSar, R., Waghmare, U. V. & Spaldin, N. a. Theoretical Prediction of New High-Performance Lead-Free Piezoelectrics. *Chemistry of Materials* 17, 1376-1380, doi:10.1021/cm0480418 (2005).

27   Daniels, J. E., Jo, W., Rödel, J. & Jones, J. L. Electric-field-induced phase transformation at a lead-free morphotropic piezoelectric ceramic. *APPLIED PHYSICS LETTERS* 95, 032904-032904, doi:10.1063/1.3182679 (2009).

28   Takenaka, T. & Nagata, H. Current status and prospects of lead-free piezoelectric ceramics. *Journal of the European Ceramic Society* 25, 2693-2700, doi:10.1016/j.jeurceramsoc.2005.03.125 (2005).

29   Zhang, S., Lim, J. B., Lee, H. J. & Shrout, T. R. Characterization of Hard Piezoelectric Lead-Free Ceramics. *Ultrasonics, Ferroelectrics and Frequency Control, IEEE Transactions on* 56, 1523-1527 (2009).

30   Zhang, S. T., Kounga, A. B., Aulbach, E. & Deng, Y. Temperature-Dependent Electrical Properties of 0.94Bi0.5Na0.5TiO3-0.06BaTiO3 Ceramics. *Journal of the American Ceramic Society* 91, 3950-3954, doi:10.1111/j.1551-2916.2008.02778.x (2008).

31   Zhu, M. K., Hu, H. C., Lei, N., Hou, Y. D. & Yan, H. Dependence of depolarization temperature on cation vacancies and lattice distortion for lead-free 74(Bi1/2Na1/2)TiO3-20.8(Bi1/2K1/2)TiO3-5.2BaTiO3 ferroelectric ceramics. *Applied Physics Letters* 94, doi:10.1063/1.3130736 (2009).

32   Holleman, A. F. & Wiberg, N. *Inorganic Chemistry*. 101st (German) edn, Vol. 1 (Walter de Gruyter, 2001).

33   Smolenskii, G., Isupov, V., Agranivyskaya , A. & Krainik , N. New ferroelectrics of complex composition. *Soviet Physics Solid State IV* 2, 2651–2654 (1960).

34   Takenaka, T., Maruyama, K. & Sakata, K. $(Bi_{1/2}Na_{1/2})TiO_3$-$BaTiO_3$ System for Lead-Free Piezoelectric Ceramics. *Japanese Journal of Applied Physics, Part 1: Regular Papers, Short Notes & Review Papers* 30, 2236-2239 (1991).

35   Takenaka, T., Nagata, H. & Hiruma, Y. Current Developments and Prospective of Lead-Free Piezoelectric Ceramics. *Japanese Journal of Applied Physics, Part 1: Regular Papers, Short Notes & Review Papers* 47, 3787-3801, doi:10.1143/jjap.47.3787 (2008).

36   Shujun, Z., Shrout, T. R., Nagata, H., Hiruma, Y. & Takenaka, T. Piezoelectric properties in (K0.5Bi0.5)TiO 3-(Na0.5B0.5)TiO3-BaTiO 3 lead-free ceramics. *Ultrasonics, Ferroelectrics and Frequency Control, IEEE Transactions on* 54, 910-917 (2007).

37   Zhang, S. T., Kounga, A. B., Aulbach, E., Ehrenberg, H. & Rodel, J. Giant strain in lead-free piezoceramics $Bi_{0.5}Na_{0.5}TiO_3$-$BaTiO_3$-$K_{0.5}Na_{0.5}NbO_3$ system. *Applied Physics Letters* 91, doi:10.1063/1.2783200 (2007).

38   Zhang, S.-t. *et al.* Lead-free piezoceramics with giant strain in the system Bi0.5Na0.5TiO3"BaTiO3"K0.5Na0.5NbO3. I. Structure and room temperature properties. *Journal of Applied Physics* 103, 2-9, doi:10.1063/1.2838472 (2008).

39   Zhang, S.-t. *et al.* Lead-free piezoceramics with giant strain in the system Bi0.5Na0.5TiO3"BaTiO3"K0.5Na0.5NbO3. II. Temperature dependent properties. *Journal of Applied Physics* 103, 034108 034101-034107, doi:10.1063/1.2838476 (2008).

40   Schütz, D. *et al.* Lone-Pair-Induced Covalency as the Cause of Temperature- and Field-Induced Instabilities in Bismuth Sodium Titanate. *Advanced Functional Materials* 22, 2285-2294, doi:10.1002/adfm.201102758 (2012).

41   Schmitt, L. a. *et al.* Structural investigations on lead-free Bi1/2Na1/2TiO3-based piezoceramics. *Journal of Materials Science* 46, 4368-4376, doi:10.1007/s10853-011-5427-6 (2011).

42   Schmitt, L. A. & Kleebe, H.-J. Single Grains Hosting Two Space Groups - a Transmission Electron Microscopy Study of a Lead-Free Ferroelectric. *Functional Materials Letters* 03, 55-55, doi:10.1142/s1793604710000920 (2010).

44

43   Shirane, G., Pepinsky, R. & Frazer, B. C. X-ray and neutron diffraction study of ferroelectric PbTiO2. *Acta Crystallographica* 9, 131-140, doi:doi:10.1107/S0365110X56000309 (1956).

44   Halasyamani, P. S. Asymmetric Cation Coordination in Oxide Materials: Influence of Lone-Pair Cations on the Intra-octahedral Distortion in d 0 Transition Metals. *Chemistry of Materials* 16, 3586-3592, doi:10.1021/cm049297g (2004).

45   Zhurova, E. A. & Tsirelson, V. G. Electron density and energy density view on the atomic interactions in SrTiO3. *Acta Crystallographica Section B* B58, 567-575 (2002).

46   Villesuzanne, a., Elissalde, C., Pouchard, M. & Ravez, J. New considerations on the role of covalency in ferroelectric niobates and tantalates. *The European Physical Journal B* 6, 307-312, doi:10.1007/s100510050553 (1998).

47   Cohen, R. E. Origin of Ferroelectricity in Perovskite Oxides. *Nature* 358, 136-138 (1992).

48   Goodenough, J. B. Theory of the role of covalence in the perovskyte-type Manganites [La, M (II) MnO3. *Phys. Rev.* 100, 564-573 (1955).

49   Aktins, P. W. *Physical Chemistry*. 9th edn, (Oxford university Press, Oxford;UK, 2010 (9th)).

50   Kang, S. J. *Sintering*. (Butterworth-Heineman; London UK, 2005).

51   Zuo, R. Z., Li, L. T., Zhang, N. X. & Gui, Z. L. Interfacial reaction of Ag/Pd metals with Pb-based relaxer ferroelectrics including additives. *Ceramics International* 27, 85-89 (2001).

52   Zuo, R. Z., Li, L. T., Gui, Z. L., Ji, C. X. & Hu, X. B. Vapor diffusion of silver in cofired silver/palladium - ferroelectric ceramic multilayer. *Materials Science and Engineering B-Solid State Materials for Advanced Technology* 83, 152-157 (2001).

53   Zuo, R. Z., Li, L. T. & Gui, Z. L. Cofiring behaviors between BaTiO3-modified silver-palladium electrode and Pb-based relaxor ferroelectric ceramics. *Materials Chemistry and Physics* 70, 326-329 (2001).

54   Wang, S. F. & Huebner, W. Interaction of Silver Palladium Electrodes with Lead-Based and Bismuth-Based Electroceramics. *Journal of the American Ceramic Society* 76, 474-480 (1993).

55   Pepin, J. G. Subsolidus Phase-Relations in the System Pd-Ag-O and Application to Multilayer Ceramic Composites. *Advanced Ceramic Materials* 3, 517-519 (1988).

56   Zeng, M., Or, S. W. & Chan, H. L. W. First-principles study on the electronic and optical properties of Na[0.5]Bi[0.5]TiO[3] lead-free piezoelectric crystal. *Journal of Applied Physics* 107, 043513, doi:10.1063/1.3309407.

57   Krauss, W., Schütz, D., Naderer, M., Orosel, D. & Reichmann, K. BNT-based multilayer device with large and temperature independent strain made by a water-based preparation process. *Journal of the European Ceramic Society* 31, 1857-1860, doi:10.1016/j.jeurceramsoc.2011.02.032 (2011).

58   Hinterstein, M. *et al.* Field-induced phase transition in Bi 1/2 Na 1/2 TiO 3 -based lead-free piezoelectric ceramics. *Journal of Applied Crystallography* 43, 1314-1321, doi:10.1107/s0021889810038264 (2010).

59   Aksel, E. *et al.* Monoclinic crystal structure of polycrystalline Na[0.5]Bi[0.5]TiO[3]. *APPLIED PHYSICS LETTERS* 98, 152901-152901, doi:10.1063/1.3573826 (2011).

60   Moya, J. S., Lopez-Esteban, S. & Pecharroman, C. The challenge of ceramic/metal microcomposites and nanocomposites. *Prog. Mater. Sci.* 52, 1017-1090, doi:10.1016/j.pmatsci.2006.09.003 (2007).

4 Curriculum Vitae and Academic Record

Denis Schütz, Mag. rer.nat.
Born in Leoben (Styria), Austria. Date of birth: 5. Nov 1980
Austrian Citizen; Unmarried

CURRENT POSITION

In progress since May 2009	PhD in Chemistry, Graz University of Technology, Austria. PhD thesis:*"The development of high-strain actuator materials"* Supervisor: Prof. Dr. Klaus Reichmann (Inst. for Chemistry and Technology of Materials (**Anticipated date of graduation:** Sept-Dec 2012) Industry cooperation with EPC-TDK (no overlap with published activities)
Main Research Interests:	Ferroelectrics, Industrial manufacture of multilayer Components, Lead free piezoelectrics, ferroelectric relaxors, Diffusion in solids, Solid state trace element analysis on μm scales, Raman spectroscopy

EDUCATION AND ACADEMIC BACKGROUND

October 2002 – February 2009	Master of Science (Mag. rer. nat.) Chemistry, Karl-Franzens University, Graz, Austria. Master thesis: *"The Chemical Interaction of Bismuth based electronic materials and Ag/Pd Electrodes"*
May-December 2007	Joint-study Project at the Iowa State University (graduate lvl.) Project in the group of Prof. Bent Shanks "Synthesis of Zinc-Aluminate-Spinell catalysts for Industrial FAME production"
October 2000-2002	Studies in Physics, Graz University of Technology, Austria (first state exam); switch to chemistry

TEACHING EXPERIENCE

2011	*Teaching assistant and short lecture "Chemical Technology Lab",*
2012	*Teaching assistant and short lecture "Chemical Technology Lab" Basic course "Chemistry for Molecular Biologists"*

47

5 MOST IMPORTANT PUBLICATIONS

- Schütz, D.; Deluca, M.; Krauss, W.; Feteira, A.; Jackson, T. Reichmann K.:
Lone-Pair-Induced Covalency as the Cause of Temperature- and Field-Induced
Instabilities in Bismuth Sodium Titanate. - in: **Advanced functional materials (2012) 22
2285–2294**
- Naderer, M.; Schütz, D.; Kainz, T.; Reichmann, K.; Mittermayr, F.:
The formation of secondary phases in Bi0.5Na0.375K0.125TiO3 ceramics. - in: **Journal
of the European Ceramic Society 32 (2012) , S. 2399 - 2404**
- Krauss, W.; Schütz, D.; Naderer, M.; Orosel, D.; Reichmann, K.:
BNT-based multilayer device with large and temperature independent strain made by a
water-based preparation process. - in: **Journal of the European Ceramic Society 31
(2011), S. 1857 - 1860**
- Krauss, W.; Schütz, D.; Mautner, F.-A.; Feteira, A.; Reichmann, K.:
Piezoelectric properties and phase transition temperatures of the solid solution of (1-
x)(Bi0,5Na0,5)'TiO3 - xSrTiO3. - in: **Journal of the European Ceramic Society 30
(2010) , S. 1827 - 1832**

  Schütz, D.; Krauss, W.; Albering, J.; Kurta, C.; Reichmann, K.:
The Chemical Interaction of Silver–Palladium Alloy Electrodes with Bismuth-Based
Piezomaterials. - in: **Journal of the American Ceramic Society 93 (2010) 4, S. 1142 -
1147**

5 MOST IMPORTANT CONFERENCE PRESENTATIONS

- *Schütz, D.; Reichmann, K.; Deluca, M.; Feteira, A.; Supancic, P.:
The electromechanical Properties of BNT based actuators. - in: **Electroceramics XIII**.
Enschede am: 24.06.2012
- *Schütz, D.; Deluca, M.; Krauss, W.; Feteira, A.; Reichmann, K.:
Lone-Pair-Induced Covalency as the Cause of Temperature- and Field-Induced
Instabilities in Bismuth Sodium Titanate. - in: **Nature Conference on the Frontiers of
Electronic Materials**. Aachen am: 17.06.2012
- *Schütz, D.; Mittermayr, F.; Reichmann, K.:
Controlling Microstructure by Influencing the Diffusive Processes during Sintering:
Establishing a Tool Kit for Materials Design in PZT. - in: **MS&T; Material Science and
Technology** 2011 . Columbus, OH am: 16.10.2011
- *Schütz, D.; Reichmann, K.; Kurta, C.:
A new approach for quantifying diffusion illustrated at metal/ceramic interfaces . - in:
19th International Symposium on the Applications of Ferroelectrics - Edinburgh
10th European Conference on the Applications of Polar Dielectrics . Edinburgh am:
09.08.2010
- *Schütz, D.; Albering, J.; Frömmling, T.; Fleig, J.; Reichmann, K.:
Metal-Ceramic Interaction between Bismuth Based Lead Free Piezoelectric Ceramics and
Ag/Pd Electrodes. - in: **11th Conference and Exhibition of the European Cermic
Society**. Krakau Poland am: 21.06.2009

ACADEMIC AWARDS

November 2011   *"Inventor at the TU-Graz Award 2011"* **Graz University of
Technology**

COOPERATION PARTNERS

Antonio Feteira (Sheffield Hallam University, UK/POR)
Tim Jackson (University of Birmingham, UK)
Marco Deluca (University of Mining; Leoben, AT)
Marija Kosec (IJS Ljubljana, SLO)
Christoph Kurta (KF-University Graz, AT)

MEMBERSHIP IN PROFESSIONAL ORGANIZATIONS

GÖCH (Austrian Society of Chemists) since 2009
Austrian Ceramic Society since 2011
American Ceramic Society since 2011

PEER-REVIEW ACTIVITIES

2011   Sensors and Actuators A: Physical
                                  Materials Chemistry and Physics

2012   Chemical Engineering: Research and Design
                                  Romanian Research Council

LANGUAGES

German (native)
English (native level, as defined by TOEFL)
Italian (advanced)
Latin, French (reading knowledge)

Publication list for Denis Schütz for the last 5 years (no earlier publications):

Journal articles:

2012

- Schütz, D.; Deluca, M.; Krauss, W.; Feteira, A.; Jackson, T. Reichmann K.:
  Lone-Pair-Induced Covalency as the Cause of Temperature- and Field-Induced Instabilities in Bismuth Sodium Titanate. : Advanced functional materials (2012) 22 2285–2294; In Press
- Naderer, M.; Schütz, D.; Kainz, T.; Reichmann, K.; Mittermayr, F.:
  The formation of secondary phases in Bi0.5Na0.375K0.125TiO3 ceramics. : Journal of the European Ceramic Society 32 (2012) , S. 2399 - 2404; In press

2011

- Krauss, W.; Schütz, D.; Naderer, M.; Orosel, D.; Reichmann, K.:
  BNT-based multilayer device with large and temperature independent strain made by a water-based preparation process. : Journal of the European Ceramic Society 31 (2011) , S. 1857 - 1860

2010

- Krauss, W.; Schütz, D.; Mautner, F.-A.; Feteira, A.; Reichmann, K.:
  Piezoelectric properties and phase transition temperatures of the solid solution of (1-x)(Bi0,5Na0,5)TiO3 - xSrTiO3. : Journal of the European Ceramic Society 30 (2010) , S. 1827 - 1832
- Schütz, D.; Krauss, W.; Albering, J.; Kurta, C.; Reichmann, K.:
  The Chemical Interaction of Silver–Palladium Alloy Electrodes with Bismuth-Based Piezomaterials. : Journal of the American Ceramic Society 93 (2010) 4, S. 1142 - 1147

Oral presentations at International Scientific conferences (*Presenting)

2012

- *Schütz, D.; Deluca, M.; Feteira, A.; Reichmann, K.:
  Lone pair induced Covalency as the cause for the extended strain in BNT based solid solutions. : Electroceramics XIII. Enschede am: 24.06.2012
- *Schütz, D.; Reichmann, K.; Deluca, M.; Feteira, A.; Supancic, P.:
  The electromechanical Properties of BNT based actuaTORS. : Electroceramics XIII. Enschede am: 24.06.2012
- *Schütz, D.; Deluca, M.; Krauss, W.; Feteira, A.; Reichmann, K.:
  Lone-Pair-Induced Covalency as the Cause of Temperature- and Field-Induced Instabilities in Bismuth Sodium Titanate. : Nature Conference on the Frontiers of Electronic Materials. Aachen am: 17.06.2012

2011

- Kainz, T.; Naderer, M.; Mittermayr, F.; Schütz, D.; Reichmann, K.:
  Study of the formation reaction of lead-free (1-x) BNT- x BKT ceramic. : ECERS 9th Student Meeting on Processing and Applications of Ceramics. Novi Sad am: 15.11.2011
- *Schütz, D.; Krauss, W.; DeLuca, M.; Feteira, A.:
  Prototype BNT-based multilayer device with large and temperature independent strain. : ECERS 9th Student Meeting on Processing and Applications of Ceramics. Novi Sad am: 15.11.2011

- Kurta, C.; Schütz, D.; Mittermayr, F.; Gössler, W.:
  LA-ICPMS in Materials Research - Diffusion analysis in actuator materials. : European Winter Conference on Plasma Spectrochemistry . Zaragoza am: 01.02.2011
- *Schütz, D.; Reichmann, K.; Krauss, W.; DeLuca, M.; Feteira, A.:
  BNT-based multilayer device with large and temperature independent strain. : Material Science and Technology 2011 . Columbus, OH am: 16.10.2011
- *Schütz, D.; Mittermayr, F.; Reichmann, K.:
  Controlling Microstructure by Influencing the Diffusive Processes during Sintering: Establishing a Tool Kit for Materials Design in PZT. : Material Science and Technology 2011 . Columbus, OH am: 16.10.2011
- Naderer, M.; Reichmann, K.; Schütz, D.; Mittermayr, F.:
  Electron microprobe analysis of(1-x)BNT-xBKT. : The 20th IEEE International Symposium on Applications of Ferroelectrics International Symposium on Piezoresponse Force Microscopy & Nanoscale Phenomena in Polar Materials. Vancouver am: 24.07.2011
- Kurta, C.; Hauzenberger, C.; Mittermayr, F.; Prattes, K.; Schütz, D.; Gössler, W.:
  The right technique for the right application - elemental analysis of solid samples - a comparison. : 7. ASAC JunganalytikerInnen Forum. Linz am: 26.08.2011

2010
- *Schütz, D.; Kurta, C.; Arar, M.; Reichmann, K.:
  A novel way to measure diffusional profiles in metal-ceramic composites. : Electroceramics XII. Trondheim am: 15.06.2010
- Arar, M.; Schütz, D.; Kurta, C.; Sprengel, W.; Reichmann, K.:
  Determination and Analysis of Diffusion of Metals in PZT. : ICCPS-11 (International Conference on Ceramic Processing Science). Zürich am: 29.08.2010
- *Schütz, D.; Reichmann, K.; Kurta, C.:
  A new approach for quantifying diffusion illustrated at metal/ceramic interfaces . : 19th International Symposium on the Applications of Ferroelectrics - Edinburgh 10th European Conference on the Applications of Polar Dielectrics . Edinburgh am: 09.08.2010

2009
- *Schütz, D.; Albering, J.; Frömmling, T.; Fleig, J.; Reichmann, K.:
  Metal-Ceramic Interaction between Bismuth Based Lead Free Piezoelectric Ceramics and Ag/Pd Electrodes. : 11th Conference and Exhibition of the European Cermic Society. Krakau Poland am: 21.06.2009

Book Section:

- Schütz, D. Deluca, M.; Krauss, W.; Feteira, A.; Reichmann, K:
  Lone-Pair-Induced Covalency as the Cause of Temperature- and Field-Induced Instabilities in Bismuth Sodium Titanate. : Frontiers of Electronics Materials - Technical Digest of the Nature Conference. (2012) In Press

Posters at Scientific conferences:

- Naderer, M.; Schütz, D.; Reichmann, K.; Kainz, T.:
  The influence of Ti-nonstoichiometry on electric parameters and microstructure in BNT. : Advanced Materials Day. Graz am: 21.06.2012
- Kainz, T.; Naderer, M.; Schütz, D.; Orosel, D.; Mautner, F. A.; Reichmann, K.; Schütz, D.:
  Calcination of (100-x)BNT-xBKT System investigated by high-temperature XRD. : Electroceramics XIII. Enschede, Niederlande am: 24.06.2012
- Naderer, M.; Schütz, D.; Reichmann, K.; Kainz, T.:
  The influence of Ti-nonstoichiometry on electric parameters and microstructure in BNT. : Electroceramics XIII. Enschede, Niederlande am: 24.06.2012

- Reichmann, K.; Schütz, D.; Orosel, D.; Mittermayr, F.:
  Dopant Segregation in Bismuth-Sodium-Titanate Single Crystals Investigated by Electron Probe Microanalysis. : 10th EMAS Regional Workshop. Padua/Italien am: 17.06.2012

Misc.:

1 Article currently undergoing peer review (Journal of Material science)

3 Articles in preparation

Academic Awards:

Inventor Award of the TU-Graz (2011)

Patents:

2 Pending patents (A1) on the Manufacture of a lead-free actuator in cooperation with EPC-TDK (non-public at the moment)

5 Relevant Publications

1. Schütz, D.; Deluca, M.; Krauss, W.; Feteira, A.; Jackson, T. Reichmann K.:
   Lone-Pair-Induced Covalency as the Cause of Temperature- and Field-Induced
   Instabilities in Bismuth Sodium Titanate. - in: **Advanced functional materials (2012) 22**
   2285–2294
2. Naderer, M.; Schütz, D.; Kainz, T.; Mittermayr, F.; Reichmann, K.:
   The formation of secondary phases in Bi0.5Na0.375K0.125TiO3 ceramics. - in: **Journal**
   of the European Ceramic Society 32 (2012) , S. 2399 - 2404
3. Krauss, W.; Schütz, D.; Naderer, M.; Orosel, D.; Reichmann, K.:
   BNT-based multilayer device with large and temperature independent strain made by a
   water-based preparation process. - in: **Journal of the European Ceramic Society 31**
   (2011), S. 1857 - 1860
4. Krauss, W.; Schütz, D.; Mautner, F.-A.; Feteira, A.; Reichmann, K.:
   Piezoelectric properties and phase transition temperatures of the solid solution of (1-
   x)(Bi0,5Na0,5)TiO3 - xSrTiO3. - in: **Journal of the European Ceramic Society 30**
   (2010) , S. 1827 - 1832
5. Schütz, D.; Krauss, W.; Albering, J.; Kurta, C.; Reichmann, K.:
   The Chemical Interaction of Silver–Palladium Alloy Electrodes with Bismuth-Based
   Piezomaterials. - in: **Journal of the American Ceramic Society 93 (2010) 4, S. 1142 -**
   1147

www.MaterialsViews.com

ADVANCED
FUNCTIONAL
MATERIALS
www.afm-journal.de

FULL PAPER

Lone-Pair-Induced Covalency as the Cause of Temperature- and Field-Induced Instabilities in Bismuth Sodium Titanate

Denis Schütz,* Marco Deluca, Werner Krauss, Antonio Feteira, Tim Jackson, and Klaus Reichmann

Bismuth sodium titanate (BNT)-derived materials have seen a flurry of research interest in recent years because of the existence of extended strain under applied electric fields, surpassing that of lead zirconate titanate (PZT), the most commonly used piezoelectric. The underlying physical and chemical mechanisms responsible for such extraordinary strain levels in BNT are still poorly understood, as is the nature of the successive phase transitions. A comprehensive explanation is proposed here, combining the short-range chemical and structural sensitivity of in situ Raman spectroscopy (under an applied electric field and temperature) with macroscopic electrical measurements. The results presented clarify the causes for the extended strain, as well as the peculiar temperature-dependent properties encountered in this system. The underlying cause is determined to be mediated by the complex-like bonding of the octahedra at the center of the perovskite: a loss of hybridization of the $6s^2$ bismuth lone pair interacting with the oxygen p-orbitals occurs, which triggers both the field-induced phase transition and the loss of macroscopic ferroelectric order at the depolarization temperature.

1. Introduction

Contemporary high-precision micropositioning systems and sensors rely on the outstanding electromechanical properties exhibited by lead zirconate titanate (PZT)-based solid solutions. The ability to control the electromechanical performance of PZT via chemical doping is certainly one of its most attractive features. Hence, PZT can be employed either in the fabrication of actuators (such as fuel-injection valves or micropositioning systems) or in sensors (such as pressure and acceleration sensors). Indeed, PZT owes its tremendous commercial success to this unique versatility. Nevertheless, from a health perspective, the manipulation of toxic lead oxide during the fabrication of PZT-based components and their later disposal partially overshadows its technological merits. A ban of lead in electronic components is expected to be enforced as soon as some alternative materials are made available. Obviously, this poses restrictions on the further applicability of PZT and motivates the search for valid lead-free alternatives that are capable of reproducing its behavior at least partly. However, the substitution of PZT by lead-free materials has emerged to be more challenging than expected. Possible candidates are potassium sodium niobate (KNN) solid solutions for "hard"[1] applications where low losses and high coupling factors are necessary and bismuth sodium titanate (BNT) solid solutions for "soft" applications, like actuators, where the ability to extend under an applied electric field is of paramount importance. This latter material has been the focus of a plethora of structure- and application-related studies recently. Although initially characterized in the 1960s,[2] BNT solid solutions have seen a revival of research interest in recent years[3] due to the discovery of extended strains under high fields that surpass those reached by PZT.[4,5] This property makes BNT an excellent candidate for the replacement of PZT in actuators, despite its piezoelectric coefficient (d_{33}) being considerably lower than that of PZT under low field intensities.[6] The mechanism of the extended strain and especially its structural and chemical origins is, however, poorly understood. In addition, the high field intensities necessary to drive this effect still constitute a technological obstacle that needs to be overcome.

The crystal structure of BNT and its solid solutions has been extensively studied. At room temperature, all binary solid solutions replacing the univalent A-site cation (with the notable exception of Li substitution[6]) exhibit a phase transition from rhombohedral ($R3c$) (in recent studies, monoclinic Cc[8]) to

D. Schütz, Dr. W. Krauss, Prof. K. Reichmann
Christian Doppler Laboratory for Advanced Ferroic Oxides
Institute for Chemistry and Technology of Materials
Graz University of Technology
Stremayrgasse 9/3, A-8010 Graz, Austria
E-mail: denis.schuetz@tugraz.at

Dr. M. Deluca
Institut für Struktur- und Funktionskeramik
Montanuniversitaet Leoben
Peter Tunner Straße 5, A-8700 Leoben, Austria

Dr. M. Deluca
Materials Center Leoben Forschung GmbH
Roseggerstraße 12, A-8700 Leoben, Austria

Dr. A. Feteira
Christian Doppler Laboratory for Advanced Ferroic Oxides
School of Chemistry
University of Birmingham
Edgbaston, B15 2TT, Birmingham, UK

Dr. T. Jackson
School of Electronic, Electrical and Computer Engineering
University of Birmingham
Edgbaston, B15 2TT, Birmingham, UK

tetragonal (*P4bm*)[3], forming a morphotropic phase boundary (MPB) in between. In contrast to PZT, this MPB is not temperature invariant but is bent over a wide temperature range, leading to strong temperature dependences of the desired properties. This has been confirmed by high-resolution techniques,[7,8] utilizing both X-ray[9] and neutron scattering.[10] However, due to the inclusive nature of any bulk-scattering technique, this description should be considered only as the average long-range symmetry of the material.[10] Transmission-electron-microscopy (TEM) measurements of the material have indicated a stronger unstable nature of BNT with respect to PZT: different researchers have found different symmetries for the same nominal compositions,[11] both within the same sample,[8,12] and even within the same grain.[13] In other words, there is evidence that the room-temperature phase is, in fact, composed of three different symmetries (*Pm-3m*, *P4bm*, and *R3c*)[11,14] that coexist without macroscopic separation and that they are very close to each other with regard to the crystallographic cell constants, but not in symmetry.[11,14,15] These aspects have also been confirmed by means of Raman spectroscopy, both in pure BNT[16,17] and its solid solutions.[18–20] Room-temperature phase coexistence provides an explanation for the sensitivity of the material to processing parameters, or even to sample preparation before measurement.[11]

Another feature shared by all BNT solid solutions exhibiting an extended strain is the existence of an intermediate temperature-triggered phase transformation (in the range <100–250 °C, depending on the substituents) from the dominantly ferroelectric (FE) room-temperature phase to a (pseudo)-cubic phase. As increasing temperature above this point is accompanied by a loss of macroscopic ferroelectricity; this transition temperature is unanimously referred to as the depolarization temperature (T_d). The phase above T_d has been described as either anti-ferroelectric (AFE)[4] or nonpolar[21] (a term that includes anti-ferroelectric phases by definition) and is still subject to considerable debate in the literature. Its existence is, however, undisputed and can be easily verified from ε–T measurements, being visible as anomalies in both the relative permittivity and the loss factor (**Figure 1**). T_d can be shifted by the introduction of a low molar concentration of dopants, producing a downward (most prominently with Nd and Nb[6,22]) or upward shift (e.g., Fe). In this regard, two application-related approaches can be found in the literature. While some groups try to increase T_d and operate within the FE regime,[6] the other approach is to lower the T_d and operate within the nonpolar (AFE) regime, a safe distance from any phase transition, thus exploiting the field-driven extended strain. This latter choice is extremely advantageous for technological applications, since (together with avoiding the bent MPB) it allows the strain of the BNT solid solutions to be made temperature-independent within defined conditions.[23,24]

At the upper border of the nonpolar phase, the material presents relaxor ferroelectric behavior, which is signaled by the lack of a clear Curie–Weiss peak in ε–T measurements[25] and the frequency dispersion.[26] This is generally associated with the presence of polar nanoregions (directly observed at elevated temperatures[21]), which are credited to be the basis of such diffuse behaviour,[27] although other explanations are also being discussed.[28] The region of the diffuse T-dependent phase transition in relaxors where ergodic polar nanoregions fluctuate is
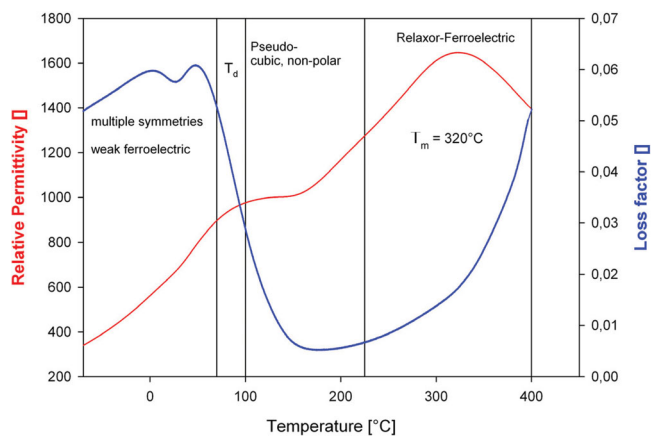

Figure 1. Temperature dependence of the relative permittivity and loss factor of BNT-BKT at 1 kHz. The temperature range in which the peculiar electromechanical behavior appears is indicated. T_d occurs at 70–100 °C, whereas the permittivity maximum in the region of the fluctuating nanoregions is assigned as T_m.

sometimes called the Burns region,[26] and the peak where they percolate is known as the Burns temperature (T_m).[25] This is physically different to the Curie temperature (T_C), which marks a sharp transition to a paraelectric phase.[29] The relaxor behavior is thought to be the result of the large lattice size and a valence mismatch at one of the cation sites, leading to the disorder-driven nucleation of polar nanoregions at high temperature and a subsequent frequency dispersion. In the most studied relaxor material, lead magnesium niobate (PMN), this criterion is satisfied by the B-site (Mg:Nb), whereas in BNT-solid solutions, it is fulfilled by the A-site (Bi:Na, Bi:K). Subsequent disorder phenomena stem from this occurrence.[25] Recently, evidence has been found that the covalent bond present in perovskites with A-site cations possessing lone pairs can cause additional disorder if the site occupancy is significantly less than 100%,[30–32] causing a superposition of short-range behavior on the long-range behavior.

The field-dependent behavior of BNT-derived materials is as peculiar as their temperature-dependent behavior. Interestingly, strain curves for materials exhibiting extended strain under a field show no occurrence of remnant strain[4,5,22,27] under a cyclic electric load (i.e., no characteristic "butterfly" hysteresis curves are found). Unlike the strain reported in conventional ferroelectric materials, the curve is not constantly linear, but can always be separated into: i) a low-strain part at low field ($d_{33} < 100$ pm V^{-1}); ii) an electrostrictive part exhibiting second-order curvature at intermediate fields; and iii) a ferroelectric part at high field showing a linear (first-order) curve[3,24,33] (cf. **Figure 2**).

Likewise, the polarization curves show a characteristic pinched loop under a cyclic electric field (similar to anti-ferroelectric materials) with little or no remnant polarization.

Comparing these datasets with the strain curves (Figure 2), the pinched region coincides with the low-strain part, the region from the opening, to the onset of saturation with the electrostrictive part, and the region of saturation, with the linear part, suggesting at least one additional phase transition under field.
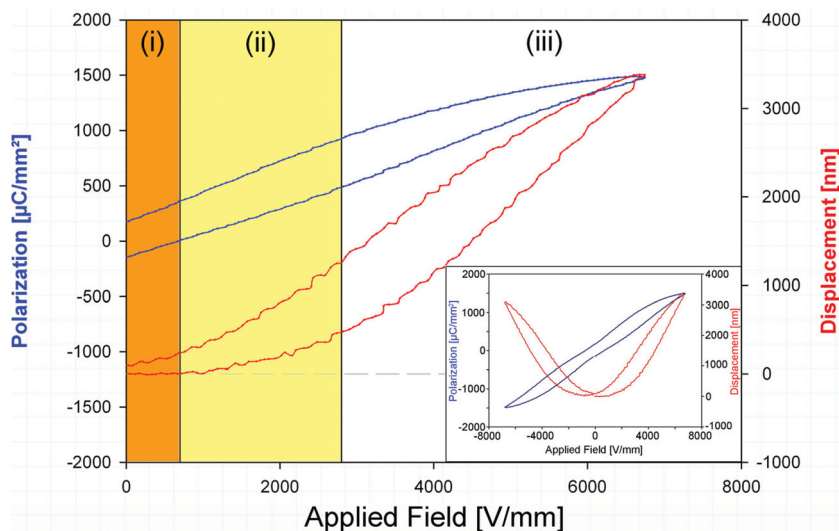
FULL PAPER

Figure 2. The positive part of the polarization- and strain versus applied electric field loops for BNT-BKT. The complete curves are shown in the inset. The regions indicated in the diagram are responsible for the peculiar electromechanical behavior and are related to a particular structure of the material: i) low-strain region, weak ferroelectric; ii) electrostrictive region, nonpolar (AFE); and iii) ferroelectric linear region, presence of polar nanodomains.

The structural mechanisms at the basis of this behavior are not clear, and in order to elucidate them, in situ field-dependent measurements capable of detecting symmetry changes or the development of ferroelectric ordering are necessary.

Daniels et al.[34] found a phase transition from pseudocubic to tetragonal above 3 kV mm^{-1}, confirming one phase transition under field. However, due to the initial field strength being too high, the first suggested phase transition from zero-field ferroelectric to nonpolar (AFE), which typically occurs from 0.5–1 kV mm^{-1}, would not have been visible in this experimental setup. The field intensity, however, coincides with the transition from nonpolar (electrostrictive) to ferroelectric relaxor (the beginning of the linear strain curve (Figure 2) behavior.

Similar results were reported in a recent study by Simons et al.[14] for a nominally rhombohedral composition. Again, the initial applied field was too large to expose any potential structural change occurring between the low strain and the electrostrictive regimes. Field-dependent TEM experiments performed by Kling et al.[11,35] showed a ferroelectric ordering (domains) developing under applied electric field, but, correspondingly, they were unable to reveal a possible phase transition under low fields.

The main open questions on BNT-based materials thus involve the field-dependent phase transitions (especially at low fields) and the structural mechanisms of transitions, measured in dependence of both the electric field and the temperature.

Recently, we manufactured a prototype stack featuring 50 active, 35 μm-sized layers of a neodymium-doped BNT-BKT (bismuth potassium titanate) ceramic,[23] which exhibits less than 10% variation of strain between 20 °C and 150 °C. In eschewing the MPB region of the BNT-BKT material in favor of more-temperature-stable properties, we chose to exploit the high-field-driven strain of the AFE phase. Nd was thus added to depress the T_d, and Li to improve the sintering characteristics.

The low thickness of the active layers allowed the stack to be handled safely under the needed high fields. Applying 200 V to the stack resulted, in fact, in a field intensity of 7 kV mm^{-1}, more than enough to trigger field-dependent effects, unlike in bulk samples (usually 1 mm in thickness), which would need 7000 V of applied electric tension to reach the same field intensities.

In this work, we combine strain and polarization measurements under high electric fields with in situ temperature- and field-dependent micro-Raman spectroscopic investigations of BNT-BKT stacks. The aim of our study was to clarify the nature of the above-mentioned phase transitions under temperature and field changes, supporting our reasoning with the results of the chemical- and structure-sensitive Raman technique.

Raman spectroscopy has already been used to detect phase changes in BNT-based solid solutions in dependence of temperature[9,16,18–20] and pressure.[36] Due to the intrinsic static disorder of BNT, and to the splitting of simultaneously Raman and IR-active bands into longitudinal-optical (LO) and transverse optical (TO) components, the Raman spectrum of BNT appears very broad; thus, a thorough assignment of the Raman modes is challenging. Consequently, detection of symmetry changes in dependence of temperature has seldom been reported.[17] This notwithstanding, previous Raman studies have confirmed the presence of the diffuse phase transition at T_d and linked it with the presence of polar nanodomains.[20,37] In this work, we build upon these findings, and provide, for the first time, a comprehensive study of BNT-BKT in dependence of both temperature and applied field. Special attention is given here to the A-site modes, since their behavior gives insight to the chemical peculiarities of the A–O bonds. Raman spectroscopy allows us to detect changes occurring at the short-range; the small interaction volume of this technique has the further advantage that, unlike in scattering experiments, the (Ag/Pd) electrode layer does not influence the measurements, making the stack-shaped samples ideal for this combined temperature- and field-dependent in situ approach.

2. Results

2.1. Electromechanical Behavior of BNT-BKT

The multilayer-stack object of our study was a modified BNT-BKT solid solution, with a low molar concentration of dopants introduced to improve performance. This composition shows all of the typical hallmarks of this class of materials, including a T_d, a relaxor transition and extended strain under high fields. The displacement and polarization curves show characteristics common to all solid solutions of BNT exhibiting extended strain. The only difference is a shift of T_d to lower values due to

Nd addition.[6] Consequently, this composition can be taken as a typical example, and the phase transition phenomena highlighted here can be applied to any non-MPB composition.

The temperature-dependent electrical measurements are summarized in Figure 1. We assigned the T_d, signified by the sudden drop in loss factor and relative permittivity, to be within the region between 70 °C and 100 °C. The beginning of the region of fluctuating nanoregions was found to be at approximately 220 °C, extending to 400 °C with a peak, the Burns temperature being 320 °C. The uncertainties of the heating-stage arrangement, as well as the diffuse nature of both phase transitions[3,11,26] make a more-accurate assignment difficult.

The electromechanical measurements of the stack can be seen in Figure 2. By visual inspection according to Rödel et al.[24,33] the first transition point was found to be at ≈0.7 kV mm^{-1}, signifying a transition from the low-strain regime to electrostrictive characteristics, whereas the transition to linear strain coinciding with the nonpolar to FE phase transition was assigned at ≈2.8 kV mm^{-1}.

2.2. The Raman Spectrum of BNT-BKT

The room-temperature crystal structure of the end members of the BNT-BKT solid solution has been reported as being rhombohedral $R3c$ for BNT and tetragonal $P4bm$ for BKT.[9] For compositions in the neighborhood of the MPB, generally a mixture of both phases has been reported.[11] Factor-group analysis leads to 13 simultaneously IR and Raman active modes for the $R3c$ structure[16]: $\Gamma_{R3c, \text{ Raman}} = 4A_1 + 9E$. For the tetragonal $P4bm$ structure of BKT, a total of 16 Raman-active modes are predicted, of which only 12 (of A_1 and E symmetry) are simultaneously infrared active[9,16]: $\Gamma_{P4bm, \text{ Raman}} = 4A_1 + 1B_1 + 3B_2 + 8E$. The Raman modes of A1 symmetry are associated with lattice displacements parallel to the c-axis of the unit cell, whereas the twofold-degenerate E modes represent phonons propagating perpendicular to the c-axis.[38] The simultaneous IR and Raman activity produces additional splitting of each A1 and E mode into their longitudinal-optical (LO) and transverse-optical (TO) components, so that, in principle, up to 24 and 28 modes should be visible for the $R3c$ and $P4bm$ unit cells, respectively. However, the scattering efficiency of some of these modes may be weak,[9] and, generally in BNT-based materials, they contribute (together with the additional Raman activity caused by short-range disorder[20]) only by increasing the width of neighboring modes with a higher intensity. Similar considerations apply in the case of a monoclinic Cc structure.[38] For the above reasons, all of the Raman modes in BNT-based materials are convoluted into three main observable peaks, and a complete assignment of the underlying phonon modes has never been reported.

Depolarized Raman spectra of (Li, Nd)-doped BNT-BKT in dependence of temperature and applied electric field are displayed in **Figure 3**a and 3b, respectively. The spectra have been corrected for the Bose–Einstein population factor. Spectral deconvolution was performed according to 13 Gaussian–Lorentzian peak functions by means of a best-fitting algorithm. The spectrum is consistent with previous reports,[9] and can be linked to a mixed rhombohedral-tetragonal crystal structure. The three main regions can be distinguished in the spectrum;
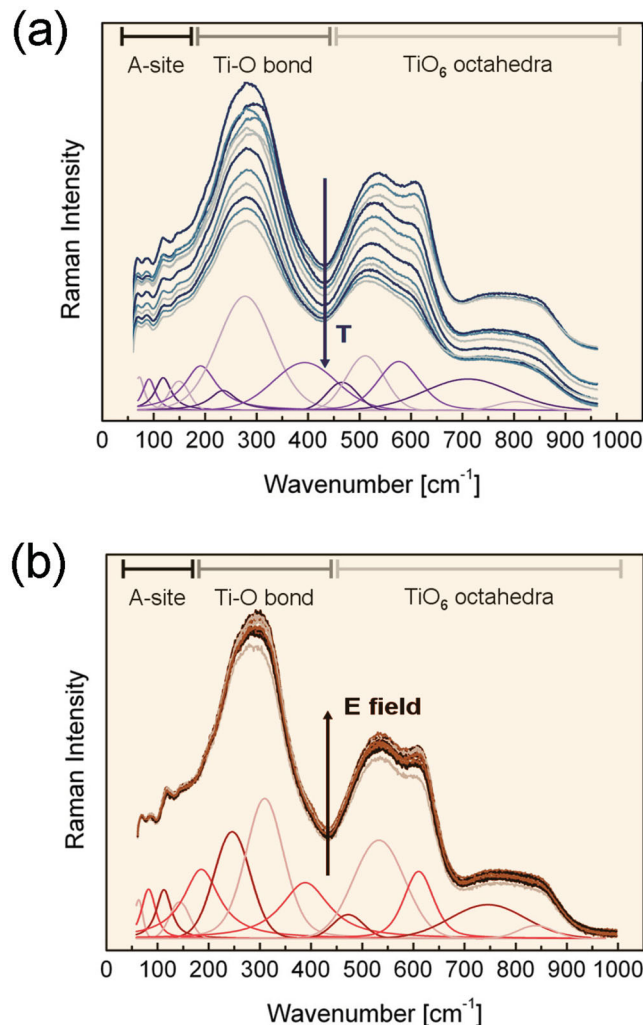

Figure 3. a,b) Depolarized Raman spectrum of Li/Nd-doped BNT-BKT as a function of temperature (a) and applied electric field (b). The spectra were deconvoluted according to 13 Gaussian–Lorentzian peak functions, and the fitting is displayed for high values of both temperature and field. The assignment of the spectral modes to particular lattice vibrations is also indicated.

each of them has a relationship with different kinds of vibration in the lattice:

- Wavenumbers $< \approx 150$ cm^{-1}: these modes can be associated with vibrations of the perovskite A-site, thus involving Bi, Na, K and Li cations. The presence of such distinct modes in this frequency range suggests possible cation ordering at the A-site. In order to provide sufficient Raman scattering to result in an observable mode, the size of the ordered clusters must, in fact, encompass at least ≈20 unit cells.[9] The mode at ≈135 cm^{-1} has previously been assigned as belonging to A_1 symmetry[39] and, more recently, associated with Na–O/K–O vibrations.[9] By means of considerations purely referring to the cation mass on the A-site, we can thus assign the two modes at ≈145 cm^{-1} and ≈115 cm^{-1} to Na–O/K–O vibrations, and the other modes to vibrations involving the Bi–O bond (85 cm^{-1} and 65 cm^{-1}).[9,40] The Li content was very low, so supposedly should not give rise to a visible peak.

www.MaterialsViews.com

ADVANCED
FUNCTIONAL
MATERIALS
www.afm-journal.de

FULL PAPER

- Wavenumber range 150–450 cm^{-1}: modes in this region can be associated with Ti–O vibrations. Especially, the mode with the highest intensity, at 305 cm^{-1}, has been assigned as an A$_1$ mode closely related to the strength of the Ti–O bond.[9] Soft-mode behavior in dependence of temperature has been reported previously for this peak.[18]

- The high-frequency bands above 450 cm^{-1} have all been associated with TiO$_6$ vibrations, namely the breathing and stretching modes of the oxygen octahedra. In the range 450–700 cm^{-1} (i.e., the second "hump" in the spectrum), three modes are observed, which have been previously assigned as A$_1$(TO) (at 485 cm^{-1}), A$_1$(LO) (at 540 cm^{-1}) and overlapping E(LO) and E(TO) modes (at 620 cm^{-1}).[9,36] However, the angular dependence of the intensity of the mode at 620 cm^{-1}, together with the temperature-dependent behavior similar to the mode at 305 cm^{-1}, suggest that this mode belongs to A$_1$ symmetry.[18,41] The broad, higher-frequency bands (the third "hump") are understood to be an A$_1$(LO) and E(LO) overlap.[9,18]

The fitting reported in Figure 3a,b refers to high values of temperature and applied field, respectively. For increasing temperature, the spectrum undergoes broadening and some of the modes (the ones at ≈245 cm^{-1} and ≈620 cm^{-1}, for instance) decrease their intensity. This is associated with the material becoming more BNT-like. In other words, there is a loss of polarity of the unit cell – the material resembles the pseudocubic structure. On the other hand, for high values of applied field (Figure 3b), the splitting of the Ti–O modes is preserved, and the material becomes more BKT-like. This signifies an increase in the polar character of the unit cell (i.e., more tetragonality).

2.3. Interpretation of Temperature Effects

The temperature dependence of the position, intensity and full width at half maximum (FWHM) of both the A-site-related and B-site-related modes are shown in **Figure 4**. In the absence of any phase transition, one would expect a steady phonon softening and an increase in mode FWHM with temperature. However, in the case of BNT-BKT, two clear anomalies are visible at ≈100 °C and ≈225 °C.

The first anomaly is an abrupt change in the phonon wavenumber (softening of the phonon modes) that takes place in the A-site-related modes at 100 °C. We caution the reader that the mode at ≈65 cm^{-1}, being located close to the cut-off of the filter, should be considered only for qualitative comparisons. Nevertheless, changes in this mode are reflected in all neighboring A-site modes, which demonstrates the reliability of our fitting procedure.

For higher temperatures, the modes steadily harden, up to ≈225 °C, above which they become nearly temperature-independent. This anomaly is also reflected in a change in the FWHM of the Ti–O and octahedra-related modes (cf. Figure 4f); namely, above 100 °C the FWHM values of the modes at ≈305 cm^{-1}, ≈485 cm^{-1} and ≈620 cm^{-1} increase. The softening of the A-site modes is due to a weakening of the bonding between the A-site cations and oxygen. Considering the presence of a lone-pair in Bi^{3+}, we suggest that this anomaly

is related to the loss of orbital hybridization between the 6s^2 orbitals of the Bi^{3+} and the oxygen p orbitals. Hybridization of the A-site lone pairs with oxygen was postulated as early as the 1950,[25,42–44] and is credited as being the reason for the high Curie temperature of lead titanate and PZT.[43] This high T_C cannot be explained otherwise, and the effect is called either covalency[45] or the "lone-pair effect"[46] in the literature. Warren et al.[47] credited the hybridization of the lead 6s$^{[2]}$ orbitals with oxygen, together with the resulting displacement, as the deciding factors for the enhanced ferroelectric properties of lead (zirconium) titanate.

Mechanistically speaking, this occurrence is possible through the hybridization of orbitals in the octahedral [Ti(Zr)O$_6$]$^{2-}$ structure found at the center of most perovskite ferroelectrics.[48,49] The empty d-shell of the central atom leads to a hybridization and shift in electron density from oxygen towards Ti^{4+}, a process that has been described to be very similar or identical to d^0 transition-metal-ligand systems found in complex chemistry.[49,50] This, in turn, depletes the bonded oxygen atoms of electron density in the direction of the A-site, allowing the lone pair (6s^2) of Bi^{3+} to hybridize with the oxygen's depleted p-orbitals, allowing a metal-oxygen-metal (B-O-A site, respectively) bond to form, thus distorting the octahedron.[50] This point can be illustrated by the contour plots of electron density found within Zhurova and Tsirelson's[51] treatment of SrTiO$_3$, and, even more clearly, in the theoretical treatments of BNT by Zeng et al.[52] and Gröting et al.,[53] who stated that "the strong hybridization effects of Ti–O and Bi–O states are obvious".

The "lone-pair effect" is also evident in the case of doping barium titanate with Pb^{2+}, Bi^{3+} or Tl$^{+[45]}$ cations, which share a common electronic structure ([Xe] 4f^{14}5d^{10}6s^2) in their preferred oxidation states, thus exhibit lone pairs and, together with the octahedral [Ti(Zr)O$_6$]$^{2-}$ structure, a lone-pair effect.[54]

Structurally, perovskites without a lone-pair-carrying A-site behave reliably according to Goldschmidt's tolerance factor,[55] their symmetry being exclusively governed by their ionic radii. Goldschmidt discovered a relationship between the ionic radii of A- and B-site cations in perovskites and their long-range crystal structure (Equation 1):

$$\tau = \frac{R_A - R_0}{\sqrt{2(R_B + R_0)}} \tag{1}$$

where τ is the Goldschmidt (or tolerance) factor, and R_A, R_B and R_O denote the Shannon radii of the A, B and oxygen sites, respectively.

A crystal system with a Goldschmidt factor above 1 means that the material is unable to form a non-hexagonal perovskite due to the A-site cations being too large to fit within the interstitial sites. A tolerance factor above 0.9 signifies an ideal cubic perovskite, while factors from 0.9 to 0.71 force rhombohedral, tetragonal or even monoclinic symmetries, at which point Glazer's octahedral tilt system[9,15] comes into play.

Materials with a lone-pair effect, like PZT, do not behave this way because their structure is constrained by the additional factor of A-site lone pairs bonding with the electron-depleted side of the oxygen, instead of the 12 nearly equidistant ionic bonds that are encountered in perovskites like barium titanate, whose A-site ions carry no lone pair.
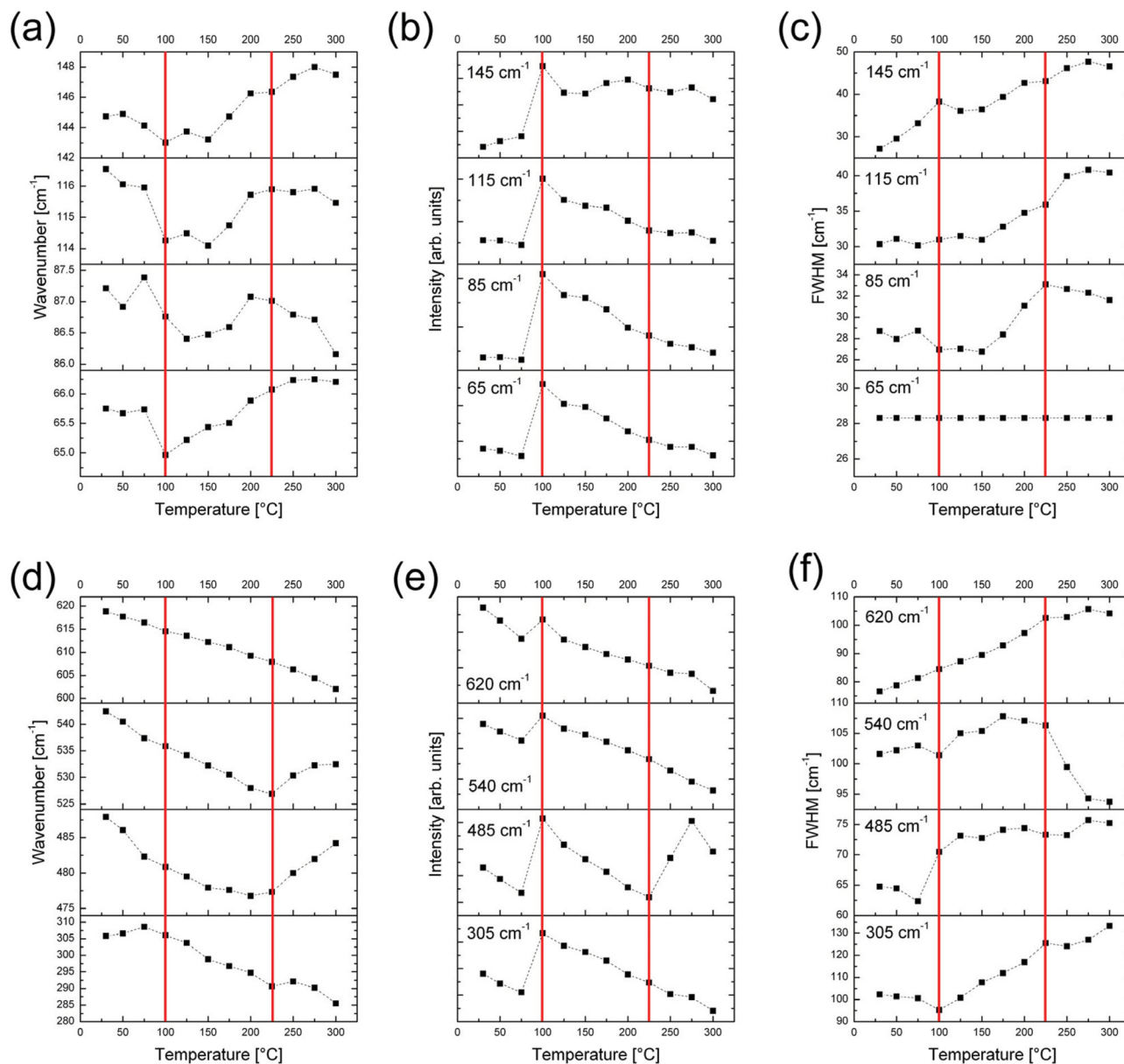
FULL PAPER

Figure 4. Temperature dependence of selected modes of the BNT-BKT spectrum. a–c) The peak position, intensity and FWHM of the A-site-related modes, respectively. d–f) The peak position, intensity and FWHM for the B-site modes. The FWHM of the 65 cm⁻¹ mode was kept fixed during fitting. The dashed lines connecting the experimental points are merely guides to the eye. The locations of the anomaly points (100 °C and 225 °C) are indicated by the red vertical lines.

All BNT solid solutions of research interest have a tolerance factor between 0.98 and 1, putting them firmly within the range of an ideal cubic perovskite.[56] However, at room temperature, they show average long-range symmetries from tetragonal to rhombohedral, reaching a (pseudo-)cubic state at T_d. This type of distortion of the underlying octahedra has been documented in numerous non-perovskite oxides (as well as in PZT and its end members) with an octahedrally co-ordinated d⁰ transition metal at the center of the complex.[50] The resulting distortion from a lone-pair-carrying atom at either: the edge (C_2), point (C_4) or face (C_3) of the octahedra, would produce

tetragonal (C_4), rhombohedral (C_3) or orthorhombic (C_2) distortions, respectively, in a perovskite lattice. This hybridization has been shown to be breakable by thermal vibration (see report by Halasyamani[50] and references therein). Also, Ti^{4+} in combination with Bi^{3+} has been noted to have a clear preference for the (C_4) distortion.

From the Raman results and the aforementioned theory, one can conclude that the mechanism at T_d is neither displacive nor order-disorder, but is rather mediated by the loss of hybridization of Bi^{3+} and oxygen through thermal vibrations along the polar axis. The sudden drop in the wavenumber of the A-site

modes at the transition point, T_d, can, in fact, be interpreted as a weakening of the A–O bonds. The consequent hardening of the modes can be then associated with the influence of the residual electrostatic forces at play between the Bi-ion lone pair and the oxygen atoms. This exact mechanism happens in PZT as well, but, due to the uniform A-site occupancy, coincides with the Curie temperature.

As a result of this change in the bond situation, a higher polarizability of the unit cells, resulting in the possible formation of nanodomains, is conceivable. This seems indeed in accordance with the behavior of the mode FWHM above 100 °C for the A-site, B-site and octahedral modes. In fact, we observed an increase in mode FWHM (cf. Figure 4c and 4f), signifying a higher degree of disorder in the lattice. Apart from the possible presence of nanodomains, this result confirms that the transition at 100 °C changed the symmetry of the complete unit cell from its constrained room-temperature state to the (pseudo-) cubic state (with tetragonal nanodomains in the case of this composition) predicted by the ionic radii. This is strong evidence that the mechanism of the depolarization phase transition is in fact mediated by the loss of constraint put upon the crystal system through the lone-pair effect of the Bi–O bond facilitated by thermal vibration. It is usually sufficient to postulate a change in bonding within a molecule if a change in the interatomic spring constant (A-site modes, specifically Bi–O modes) is accompanied by a change in symmetry of the whole molecule. Both criteria were satisfied with regard to the T_d. Additionally, the changes visible by Raman spectroscopy were corroborated by macroscopic T-dependent electrical measurements.

Why the Bi–O bond is more fragile than the Pb–O bond in PZT (where the polar phase is stabilized) is unknown; most likely, it is related to the site occupancy of the bismuth, which is usually at or less than 50% of an A-site. In addition, steric effects from the other members of the shared A-site would also have an influence. The shared site occupancy of bismuth, taken in connection with the fragile Bi–O bond and the random nature of the site occupancy[53,57] between bismuth and the univalent counterion, can also serve to explain the fragile nature of the room-temperature state, where a mixture of competing symmetries is found.[11] The bent MPB can, in turn, be described by a combination of the steric effects of larger or smaller univalent A″ ions being incorporated into the lattice. The Bi–O bonds, being weakened by the increased thermal vibrations, will, in fact, lose their constraining effect upon a temperature gradient, thus easing mixed A-site substitution and eventually producing the bent MPB. The straight MPB of PZT is, in turn, produced by the homogeneous A-site occupancy of lead[29,43,50] without compositional steric effects.

The second anomaly at 225 °C is related to the transition to the region of fluctuating nanoregions, as proven by the temperature dependence of the B-site and the octahedral modes. The Ti–O mode at ≈305 cm^{-1} (Figure 4d) initially undergoes softening, which demonstrates a smooth decrease of the unit-cell anisotropy with increasing temperature. The smooth shrinkage of the unit cell is then interrupted at 225 °C. The same temperature marks an anomaly in both octahedra-related modes, at 485 and 540 cm^{-1}: both modes harden for $T > 225$ °C. These two modes likely belong to E symmetry, whereas the mode at

620 cm^{-1}, showing a similar behavior (Figure 4d) to the one at 305 cm^{-1}, is confirmed to possess A$_1$ symmetry. These considerations suggest that the ongoing structural change occurs mainly in one crystallographic direction. Since the Ti–O bonds and the octahedral vibrations are influenced by the dynamics of the nanodomain phase,[58] this behavior is compatible with a diffuse phase transition marking the beginning of the region of fluctuating nanoregions (Figure 1), in which the material presents a macroscopic relaxor behavior. This was also confirmed by the ε–T measurements. In a word, the Raman spectroscopy results confirm that, with increasing temperature, a more disordered lattice is obtained, and this is mediated by a weakening of the Bi–O hybrid orbitals, which promotes an enhanced polarizability of the unit cell.

2.4. Influence of an Applied Field

The electric-field dependence of the Raman spectra of BNT-BKT is reported in **Figure 5**: the peak position, intensity and FWHM of the A-site modes are shown in Figure 5a–c, respectively. Figure 5d–f illustrate the same for the B-site modes. Two main anomalies, seen as an increase in the wavenumber of the Bi–O related peaks, are visible for increasing applied field, at ≈0.7 kV mm^{-1} and at ≈2.8 kV mm^{-1}. In addition, a sharpening of the octahedra-related mode at ≈620 cm^{-1} occurs in the low-field regime. Please note that this mode underwent broadening upon increasing temperature (Figure 4f). Regarding the B-site modes, it is noticeable that, during the whole range of applied field, the Ti–O mode at ≈305 cm^{-1} hardens constantly. This is the same mode that showed a steady softening with the anomaly at ≈225 °C, in the temperature dependence. The effect of the applied field is thus the opposite of that of temperature: applied field reduces disorder in the lattice (i.e., sharpening of modes) and increases the polarity of the unit cell (i.e., mode hardening and the spectrum resembling the BKT material). This appears to be mediated by a change occurring on the A-site at ≈0.7 kV, which is reflected in the oxygen octahedra as well (i.e., an anomaly in the A-site- and B-site-mode positions). This could be similar to the supposed loss of hybridization that occurs at 100 °C, with the only difference being that, by increasing the temperature, a more-disordered lattice was obtained due to the presence of nanodomains produced by bond weakening (i.e., a more-cubic lattice), while these nanodomains will orient themselves under increasing field into the field direction and thus produce a more-polar (i.e., more-tetragonal) lattice. This can indeed be connected to the field-induced giant strain that is observed in this material. In other words, the low-strain regime of the material (0–0.7 kV mm^{-1}) is governed by the small intrinsic converse piezoelectric effect, whereas the electrostrictive regime (0.7–2.8 kV mm^{-1}) can be linked to the metastable state introduced through the weakening of the Bi–O bond. This gives rise to a more-cubic regime, whereas the final linear part could be related to the nucleation of tetragonal (in other compositions rhombohedral), polar nanodomains within the (pseudo)-cubic matrix. This aspect can be pointed out considering the anomalies in the peak positions of the A-site and B-site modes at ≈2.8 kV mm^{-1} and, especially, the mode FWHM increase for the Ti–O peak (at ≈305 cm^{-1}) above 2.8 kV mm^{-1} (i.e., higher disorder in the

ADVANCED
FUNCTIONAL
MATERIALS
www.afm-journal.de
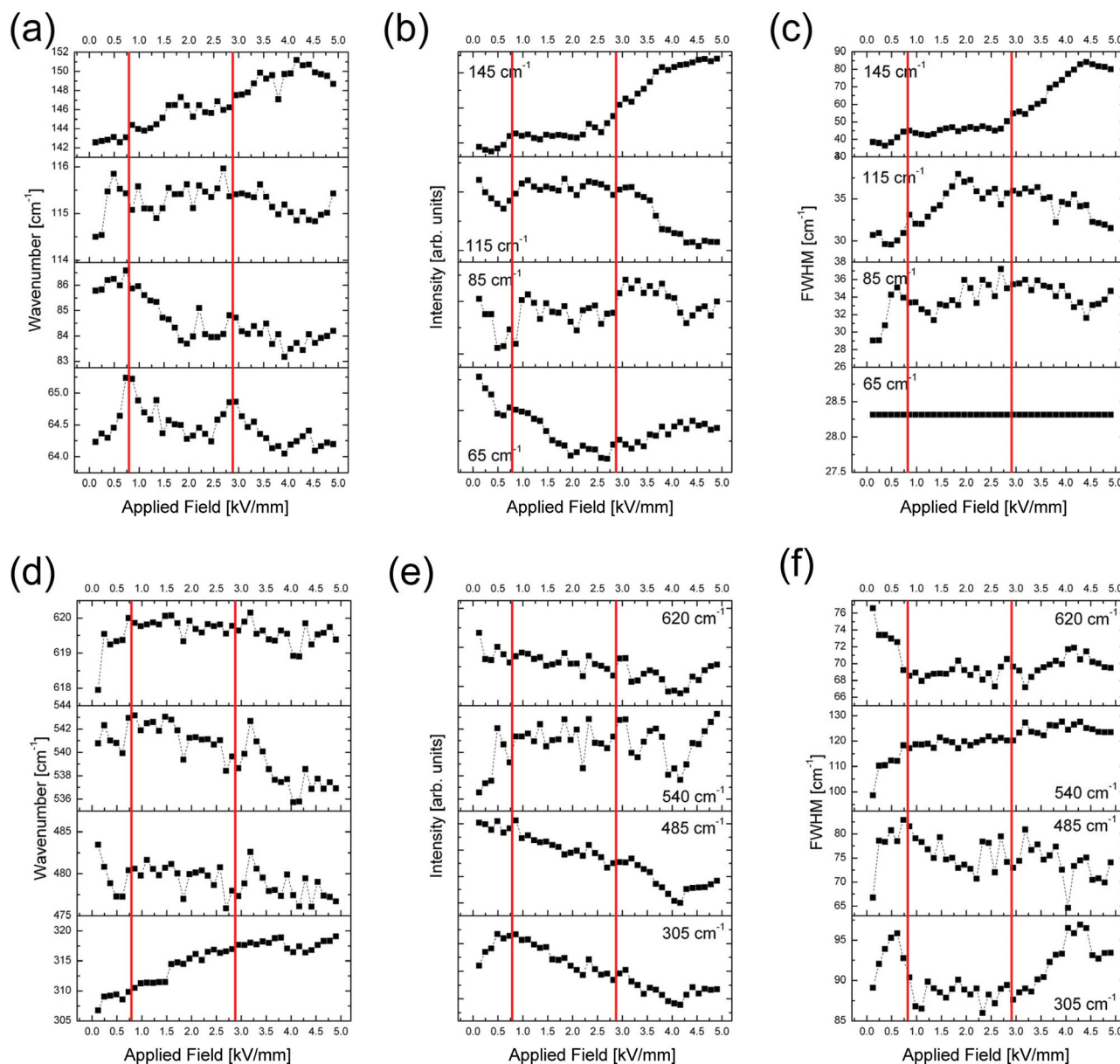
Materials
Views
www.MaterialsViews.com

Figure 5. Electric-field dependence of selected modes of the BNT-BKT spectrum. a–c) The peak position, intensity and FWHM of the A-site-related modes. d–f) The peak position, intensity and FWHM of the B-site modes. The FWHM of the 65 cm^{-1} mode was kept fixed during fitting. The dashed lines connecting the experimental points are merely guides to the eye. The locations of the anomaly points (0.7 kV mm^{-1} and 2.8 kVmm^{-1}) are indicated by the red vertical lines.

lattice above this point). Conveniently, electrostrictive effects tend to be more pronounced in perovskites with a structure close to cubic (PMN etc.),[59,60] thus explaining the behavior of the material during the electrostrictive part of the strain curve. Consequently, if this is the cause for the extended strain, any electromechanical measurement of the material above or approaching T_d should show an immediate electrostrictive curve from low fields as well as a more pinched polarization loop. This exact behavior is widely seen within different solid solutions of BNT[23,24,54,61] (and also within our stack), confirming this aspect of our analysis. The gradual transition into ferroelectric relaxor behavior is, in essence, a field-forced nonpolar

(AFE)-to-ferroelectric phase transition, which has been documented in numerous anti-ferroelectrics.[62] This is the phase transition observed by Daniels[34] and Simons[14] in their in situ scattering experiments under a field. The behavior, especially in the electrostrictive regime and above, can therefore be understood as a metastable state with multiple states accessible with a minimal change in intrinsic energy → a flat free-energy surface (see report by Damjanovic[63] and references therein). Unlike conventional ferroelectrics, this region is not compositional, but field- and temperature-dependent, and occurs through a wide compositional range. In summary, the field-dependency results, in correlation with the temperature-dependency results,

show that the phase transition at higher fields and the gradual loss of Bi–O covalence are, in fact, interrelated. These findings are in accordance with previously published in situ data[64] and also with recent modeling work on this system.[53] In addition, a recent paper using the same experimental method has shown polar nanoregions developing in Bi^{3+}-doped $KNbO_3$ as a consequence of the lone pairs interacting with the oxygen octahedra,[65] which further strengthens our conclusions.

3. Conclusions

We have shown that the depolarization temperature is a result of the breaking of Bi–O hybridization and the subsequent release of the constraint it puts upon the crystal system. This allows the structure to reset itself to the symmetry dictated by its ionic radii. This observation is linked to the potential instability of the room-temperature state of this type of ceramic material, as well as the bent nature of the MPB. As expected, the relaxor ferroelectric nature of the material above the nonpolar AFE phase region was substantiated and an order/disorder-driven effect based upon the A-site was confirmed. This also confirms previous field-dependent measurements. Thus, the mechanism of the extended-field-induced strain in BNT solid solutions is a succession of different effects that are linked by a common cause. The Bi–O bond breaking leads to the introduction of a more cubic regime (or a mixture of nanodomains in a pseudocubic matrix) favoring the electrostrictive response in the second regime. The subsequent field-induced nonpolar (AFE)-to-FE phase transition under high field is also a direct consequence of this symmetry change and the applied field, accounting for the linear part of the electromechanical curve at high fields. There is still a lot to be understood about the system, especially regarding the role of vacancies, processing routes and their influence on the switching behavior, as well as the exact nature of the phase above T_d, but a further step in understanding this complex system has been taken.

4. Experimental Section

The ceramic powder for the multilayer-stack had a composition of $[Bi_{0.49}Nd_{0.01}Na_{0.335}K_{0.125}Li_{0.04}]TiO_3$, and was made by a modified mixed oxide process. The reagent-grade raw materials were Bi_2O_3 (HEK-Oxides), Na_2CO_3 (Merck), K_2CO_3 (Merck), Li_2CO_3 (Merck), TiO_2 (Tronox) and Nd_2O_3 (Treibacher). The raw materials were ball-milled for 5 h in a laboratory ball-mill (Dyna–Mill Multi Lab) with water as a solvent, and were subsequently dried using a laboratory spray-dryer. After calcination at 900 °C for 2 h, additionally 1 mol% of Nd_2O_3 was added and a second milling for 5 h and drying took place with the same equipment. From this powder, a water-based slurry was made with a binder, and tape casting was performed on laboratory equipment. 50 layers were printed with Ag/Pd-metal paste (70/30), stacked in a format of 10×10 cm, with additional covering layers, and they were pressed under a uniaxial load of 100 tons. After dicing and binder burnout, sintering took place in air at a temperature of 1100 °C for 5 h. The final dimensions were $7 \times 7 \times 2$ mm with an active-layer thickness of approximately 35 μm. The sintered multilayer stacks were contacted with silver paste (burn-in temperature: 750 °C) for the electric measurements. Before any measurement, the stack was poled at 7 kV mm^{-1}.

Depolarized Raman spectra were obtained in back-scattering geometry using a micro-Raman spectrometer (Model InVia, Renishaw,

New Mills, UK), equipped with a Rayleigh line-rejection edge filter that was set for the 532 nm excitation of an Ar$^+$ ion laser, which allowed ripple-free measurements down to 50 cm^{-1} from the laser line. Spectra were acquired using a 50× microscope objective and a laser power of 10 mW focused on a spot of ≈ 2 μm. The Raman spectra were obtained at 20 K intervals in the temperature range 300 –570 K using a temperature stage (THM600 Linkam, Tadworth, UK). The electrical-field-dependent spectra were acquired at 2 V intervals up to 200 V, using a high-voltage power supply.

The temperature dependence of the permittivity was measured using a Novocontrol Concept 40 impedance analyzer. Measurements were performed from −100 °C to 400 °C at a heating rate of 2 K min^{-1}. The polarization and displacement curves were measured using an aixPES Piezoelectric Evaluation System from aixACCT, from room temperature to 150 °C.

[1] S. Zhang, J. B. Lim, H. J. Lee, T. R. Shrout, *IEEE Trans. Ultrason., Ferroelect. Freq. Control* **2009**, *56*, 1523.
[2] G. Smolenskii, V. Isupov, A. Agranivyskaya, N. Krainik, *Sov. Phys. –Solid State IV* **1960**, *2*, 2651.
[3] J. Rödel, W. Jo, K. T. P. Seifert, E.-M. Anton, T. Granzow, *J. Am. Ceram. Soc.* **2009**, *92*, 1153.
[4] S.-T. Zhang, A. B. Kounga, E. Aulbach, T. Granzow, W. Jo, H.-J. Kleebe, J. Rödel, *J. Appl. Phys.* **2008**, *103*, 034107.
[5] S.-T. Zhang, A. B. Kounga, E. Aulbach, W. Jo, T. Granzow, H. Ehrenberg, J. Rödel, *J. Appl. Phys.* **2008**, *103*, 034108.
[6] T. Takenaka, H. Nagata, *J. Eur. Ceram. Soc.* **2005**, *25*, 2693.
[7] E. Aksel, J. S. Forrester, J. L. Jones, P. A. Thomas, K. Page, M. R. Suchomel, *Appl. Phys. Lett.* **2011**, *98*, 152901.
[8] C. Ma, X. Tan, E. Dul'kin, M. Roth, *J. Appl. Phys.* **2010**, *108*, 104105.
[9] J. Kreisel, A. M. Glazer, G. Jones, P. A. Thomas, L. Abello, G. Lucazeau, *J. Phys.: Condens. Matter* **2000**, *12*, 3267.
[10] S. Gorfman, P. A. Thomas, *J. Appl. Crystallogr.43*, **2010**, 1409.
[11] L. A. Schmitt, J. Kling, M. Hinterstein, M. Hoelzel, W. Jo, H.-J. Kleebe, H. Fuess, *J. Mater. Sci.* **2011**, *46*, 4368.
[12] X. Tan, E. Aulbach, W. Jo, T. Granzow, J. Kling, M. Marsilius, H.-J. Kleebe, J. Rödel, *J. Appl. Phys.* **2009**, *106*, 044107.
[13] L. A. Schmitt, H.-J. Kleebe, *Funct. Mater. Lett.* **2010**, *03*, 55.
[14] H. Simons, J. Daniels, W. Jo, R. Dittmer, A. Studer, M. Avdeev, J. Rödel, M. Hoffman, *Appl. Phys. Lett.* **2011**, *98*, 082901.

FULL PAPER

[15] M. Troccaz, P. Gonnard, Y. Fetiveau, L. Eyraud, G. Grange, *Ferro-electrics* **1976**, *14*, 679.

[16] J. Petzelt, S. Kamba, J. Fábry, D. Noujni, V. Porokhonskyy, A. Pashkin, I. Franke, K. Roleder, J. Suchanicz, R. Klein, G. E. Kugel, *J. Phys.: Condens. Matter* **2004**, *16*, 2719.

[17] L. Luo, W. Ge, J. Li, D. Viehland, C. Farley, R. Bodnar, Q. Zhang, H. Luo, *J. Appl. Phys.* **2011**, *109*, 113507.

[18] D. Rout, K. S. Moon, V. S. Rao, S. J. L. Kang, *J. Ceram. Soc. Jpn.* **2009**, *117*, 797.

[19] D. Rout, K. S. Moon, S. J. L. Kang, I. W. Kim, *J. Appl. Phys.* **2010**, *108*, 084102.

[20] B. Wylie-van Eerd, D. Damjanovic, N. Klein, N. Setter, J. Trodahl, **2010**, *Phys. Rev. B: Condens. Matter 82*, 104112.

[21] C. W. Tai, S. H. Choy, H. L. W. Chan, *J. Am. Ceram. Soc.* **2008**, *91*, 3335.

[22] Z. Shujun, T. R. Shrout, H. Nagata, Y. Hiruma, T. Takenaka, *IEEE Trans. Ultrason. Ferroelect. Freq. Control* **2007**, *54*, 910.

[23] W. Krauss, D. Schütz, M. Naderer, D. Orosel, K. Reichmann, *J. Eur. Ceram. Soc.* **2011**, *31*, 1857.

[24] K. T. P. Seifert, W. Jo, J. Rödel, *J. Am. Ceram. Soc.* **2010**, *1396*, 1392.

[25] R. E. Newnham, *Properties of Materials: Anisotropy, Symmetry, Structure*, Vol. *1*, Oxford University Press, Oxford **2005**.

[26] A. A. Bokov, Z. G. Ye, *J. Mater. Sci.* **2007**, *1*, 31.

[27] T. R. Shrout, S. J. Zhang, *J. Electroceramics* **2007**, *19*, 113.

[28] R. Blinc, *J. Phys. Chem. Solids* **2000**, *61*, 177.

[29] B. Jaffe, W. R. Cook, H. L. C. Jaffe, *Piezoelectric Ceramics*, Academic Press, London **1971**.

[30] A. Feteira, D. C. Sinclair, J. Kreisel, *J. Am. Ceram. Soc.* **2010**, *93*, 4174.

[31] V. Shuvaeva, D. Zekria, A. M. Glazer, Q. Jiang, S. M. Weber, P. Bhattacharya, P. A. Thomas, *Phys. Rev. B: Condens. Matter* **2005**, *71*, 174114.

[32] W. Dmowski, S. B. Vakhrushev, I.-K. Jeong, M. P. Hehlen, F. Trouw, T. Egami, *Phys. Rev. Lett.* **2008**, *100*, 137602.

[33] W. Jo, T. Granzow, E. Aulbach, J. Rödel, *J. Appl. Phys.* **2009**, *105*, 094102.

[34] J. E. Daniels, W. Jo, J. Rödel, J. L. Jones, *Appl. Phys. Lett.* **2009**, *95*, 032904.

[35] J. Kling, X. Tan, W. Jo, H.-J. Kleebe, H. Fuess, J. Rödel, *J. Am. Ceram. Soc.* **2010**, *93*, 2452.

[36] J. Kreisel, A. M. Glazer, P. Bouvier, G. Lucazeau, *Phys. Rev. B: Condens. Matter* **2001**, *63*, 1.

[37] E. Aksel, J. Forrester, B. Kowalski, M. Deluca, D. Damjanovic, J. L. Jones, *Phys. Rev. B: Condens. Matter* **2012**, *B 85*, 024121.

[38] R. Loudon, *Adv. Phys.* **1964**, *13*, 423.

[39] M. S. Zhang, J. F. Scott, J. A. Zvirgzds, *Ferroelect. Lett. Section* **1986**, *6*, 147.

[40] V. N. Denisov, A. N. Ivlev, A. S. Lipin, B. N. Mavrin, V. G. Orlov, *J. Phys.: Condens. Matter* **1997**, *9*, 4967.

[41] I. Gregora, P. Ondrejkovic, E. Simon, M. Berta, M. Savinov, J. Hlinka, H. Luo, Q. Zhang, *Ferroelectrics* **2010**, *404*, 220.

[42] J. B. Goodenough, *Phys. Rev.* **1955**, *100*, 564.

[43] G. Shirane, R. Pepinsky, B. C. Frazer, *Acta Crystallogr.* **1956**, *9*, 131.

[44] A. Villesuzanne, C. Elissalde, M. Pouchard, J. Ravez, *Eur. Phys. J. B* **1998**, *6*, 307.

[45] H. Kawanishi, K. Ishizumi, I. Takahashi, H. Terauchi, Y. Hayafuji, *Jpn. J. Appl. Phys.* **2006**, *46*, 1067.

[46] J. Ravez, *C. R. Acad. Sci., Ser. IIC: Chem.* **2000**, *3*, 267.

[47] W. Warren, J. Robertson, D. Dimos, B. A. Tuttle, G. E. Pike, D. A. Payne, *Phys. Rev. B: Condens. Matter* **1996**, *53*, 3080.

[48] M. Ahart, M. Somayazulu, R. E. Cohen, P. Ganesh, P. Dera, H.-K. Mao, R. J. Hemley, Y. Ren, P. Liermann, Z. Wu, *Nature* **2008**, *451*, 545.

[49] P. Garcia-Fernandez, J. A. Aramburu, M. T. Barriuso, M. Moreno, *J. Phys. Chem. Lett.* **2010**, *1*, 647.

[50] P. S. Halasyamani, *Chem. Mater.* **2004**, *16*, 3586.

[51] E. A. Zhurova, V. G. Tsirelson, *Acta Crystallogr. B* **2002**, *B58*, 567.

[52] M. Zeng, S. W. Or, H. L. W. Chan, *J. Appl. Phys.* **2010**, *107*, 043513.

[53] M. Gröting, S. Hayn, K. Albe, *J. Solid State Chem.* **2011**, *184*, 2041.

[54] W. Krauss, D. Schütz, F. A. Mautner, A. Feteira, K. Reichmann, *J. Euro. Ceram. Soc.* **2010**, *30*, 1827.

[55] V. M. Goldschmidt, *Naturwissenschaften* **1926**, *14*, 477.

[56] W.-C. Lee, C.-Y. Huang, L.-K. Tsao, Y.-C. Wu, *J. Eur. Ceram. Soc.* **2009**, *29*, 1443.

[57] J. Kling, S. Hayn, L. A. Schmitt, M. Gröting, H.-J. Kleebe, K. Albe, *J. Appl. Phys.* **2010**, *107*, 114113.

[58] A. Slodczyk, P. Colomban, M. Pham-Thi, *J. Phys. Chem. Solids* **2008**, *69*, 2503.

[59] A. V. Turik, A. A. Yesis, L. A. Reznitchenko, *J. Phys.: Condens. Matter* **2006**, *18*, 4839.

[60] H. Uršič, M. Škarabot, M. Hrovat, J. Holc, M. Skalar, V. Bobnar, M. Kosec, I. Muševič, *J. Appl. Phys.* **2008**, *103*, 124101.

[61] J. Shi, H. Fan, Z. Li, *Ferroelectrics* **2011**, *404*, 93.

[62] X. Tan, J. C. Frederick, C. Ma, W. Jo, J. Rödel, *Phys. Rev. Lett.* **2011**, *105*, 2.

[63] D. Damjanovic, *IEEE Trans. Ultrason. Ferroelect. Freq. Control* **2009**, *56*, 1574.

[64] M. Hinterstein, M. Knapp, M. Hölzel, W. Jo, A. H. Cervellino, H. Ehrenberg, H. Fuess, *J. Appl. Crystallogr.* **2010**, *43*, 1314.

[65] L. Luisman, A. Feteira, A. K. Reichmann, *Appl. Phys. Lett.* **2011**, *99*, 192901.

The formation of secondary phases in $Bi_{0.5}Na_{0.375}K_{0.125}TiO_3$ ceramics

Michael Naderer [a], Denis Schütz [a], Theresa Kainz [a], Klaus Reichmann [a,*], Florian Mittermayr [b]

[a] Graz University of Technology, Christian Doppler Laboratory for Advanced Ferroic Oxides, Stremayrgasse 9, 8010 Graz, Austria
[b] Graz University of Technology, Institute of Applied Geosciences, Rechbauerstraße 12, 8010 Graz, Austria

Abstract

The synthesis of $Bi_{0.5}Na_{0.375}K_{0.125}TiO_3$ (BNT–BKT or NBT-KBT) by the mixed oxide route was investigated using thermogravimetry, X-ray diffraction, scanning electron microscopy and electron microprobe analysis. The results show the formation of a paraelectric secondary phase with the composition $(K,Na)_2Ti_6O_{13}$ during sintering. Thermogravimetric measurements indicate that the main loss of volatile components mainly occurs during the calcinations step, exceeding the theoretical loss by more than 2%. These losses, most likely caused by evaporation of K_2O induce a high number of Schottky-vacancies. These vacancies highly affect the electrical properties of the material. The formation of the secondary phase leads to a shifted composition of the ceramic to approximately $Bi_{0.5}Na_{0.4}K_{0.1}TiO_3$.
© 2012 Elsevier Ltd. All rights reserved.

Keywords: BNT; Lead-free; Inclusions; Electron microscopy; Dielectric properties

1. Introduction

$Bi_{0.5}Na_{(0.5-x)}K_xTiO_3$ (short BNT–xBKT) is a promising candidate to replace lead-based materials in ferroelectric applications.[1–3] According to the RoHS-guideline, the use of materials with serious health risks is prohibited as soon as alternative materials are technically available. Structurally, BNT–xBKT forms a complex perovskite with a mixed A-site occupation (bismuth, potassium and sodium) and titanium as single ion on the B-site. BNT and BKT form solid solutions of various crystal symmetries in dependence of the ratio BNT:BKT. High amounts of BNT form a rhombohedral phase, while BKT-rich compositions are tetragonal. Pure BNT is also reported to be monoclinic.[4] The morphotropic phase boundary (MPB), where piezoelectric parameters are maximized is located between ratios of 16 and 20% BKT.[5–7]

Bismuth-alkali titanates (e.g. bismuth–sodium–titanate BNT or bismuth–potassium–titanate BKT) are known to form secondary phases during thermal processing. In literature different compositions for this phase are given, but the general trend is to higher amounts of Ti compared to BNT–xBKT. The difference in composition of the secondary phase can be explained with the diverse fabrication techniques of the ceramic, especially the highest temperature during calcination and sintering and of course the method of measurement. Proposed compositions are $K_2Ti_8O_{17}$ in BNT–BKT,[8] $NaBiTi_6O_{14}$ in BNT,[9] $K_2Ti_6O_{13}$ in BKT[10] or $K_2Na_4(TiO_3)_3$ in BNT–BT–KNN (BT: barium–titanate, KNN: potassium–sodium–niobate).[11]

The composition of the secondary phase found in this work can be written as $(Na, K)_2Ti_6O_{13} + xBi_2O_3$ with a strongly temperature dependent stoichiometric factor x for Bi_2O_3. Samples sintered at temperatures below 1050 °C show relatively high amounts of Bi_2O_3 in the secondary phase, at higher temperatures only traces of Bi_2O_3 can be found. A mechanism for this behavior will be presented. The secondary phase itself seems to have no influence on the electrical properties, the formation reaction and the resulting compositional shift therefore have an high impact for compositions close to the MPB.

2. Experimental

The compound was synthesized using a conventional mixed-oxide route. Stoichiometric quantities of reagent grade K_2CO_3 (99.99, Ferro GmbH), Na_2CO_3 (99.99, Merck), Bi_2O_3 (99.9, MCP-HEK GmbH) and TiO_2 (99.8%, Tronox) were mixed together and ball-milled in a planetary mill (Fritsch PULVERISETTE4). Since the alkali carbonates are soluble in water,

ethanol was used for this step. The ball milling was carried out in 5 cycles of 10 min milling and 10 min break to let the suspension cool down and prevent the evaporation of ethanol. In this milling step, yttrium-stabilized ZrO_2 balls with 5 mm diameter were used. Since K_2CO_3 and Na_2CO_3 are hygroscopic, these materials were dried at 250 °C and cooled in a desiccator over silica gel before weighing. After milling ethanol was removed from the suspension using a rotary evaporator and a drying oven at 120 °C.

The dry mixture was grinded and sieved to an agglomerate size less than 180 μm and put in an alumina crucible. The calcination step took place in a box furnace (Carbolite CWF 1300) with a first stage of 650 °C and a final stage of 950 °C to ensure the completion of the reaction. Heating rates for the calcination were 5 K/min, dwell time at both temperatures 120 min. The completion of this reaction was checked by X-ray diffraction (XRD) (Bruker AXS D5005 y-y, Cu Kα emitter, graphite secondary monochromator). Further analysis of the calcination reaction was done with a thermogravimetrical analysis coupled with differential scanning calorimetry (TGA-DSC) (Netzsch STA 409 CD with Aeolus masspectrometer) to measure the weight loss, the emanating gases and to determine the temperature levels for the reaction.

Subsequently, the material was ball-milled in ethanol using the planetary mill to reduce particle size. To ease this process, a dispersant (Dispex A40, Ciba Spezialitaetenchemie) was added. To ensure a small particle size, applied energy was higher compared to the first milling due the use of 2 mm yttrium-stabilized ZrO_2 balls and higher rotational speeds. The drying step was equivalent to the one after the first milling step. The agglomerate size was then reduced to 180 μm using test sieves. Before pressing the powder into discs with a diameter of 13 mm, 5 wt% of a binding aid (PEG20000, Alfa Aesar) were added.

The discs were pressed with 150 MPa for 5 min. To remove the binder before sintering, the samples were heated up to 450 °C in an open crucible, causing the thermal decomposition of the binding agent to CO_2 and H_2O. After that, the crucible was covered to reduce material losses due to evaporation of volatile components during sintering. Experiments with discs lying in powder of the same composition during sintering were also carried out; the effect on growth of the secondary phases was negligible.

Sintering temperatures were varied between 1000 °C and 1150 °C for duration of 5 h in oxidising atmosphere. After sintering, the density of the discs was measured. Preferred is Archimedes' method (Mettler Toledo XS204 DeltaRange), because geometric dimensions have no influence here. However, for samples below 1100 °C sintering temperature this method was not applicable because of the poor density. In this case, the geometric density was calculated using the thickness, diameter measured with a calliper rule (Mitutoyo CD-15DCX) and weight of the discs (Acculab ALC210.4). Due to shape irregularities of the samples, this method cannot deliver results as exact as the Archimedes' method.

For further XRD analysis, the sintered samples were ground in an agate mortar to a fine powder. For scanning electron microscopy (SEM) investigations (Zeiss Ultra 55), the discs
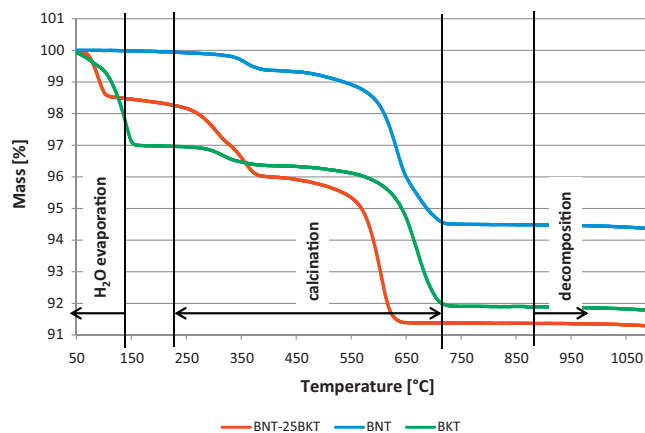
Fig. 1. TGA of BKT, BNT and BNT–25BKT raw materials mixtures. All compositions were milled in ethanol prior to measuring. Potassium containing mixtures take up water during processing.

were cut, grinded and polished with silica gel and coated with a carbon layer. This preparation was also used for the analysis with the electron microprobe (EMPA) with wavelength dispersive X-ray spectroscopy (JEOL JXA 8200).

For permittivity measurement (HP 4192A LF Analyzer) the samples were coated with silver-paste and measured at 1 kHz with 1 V. Polarization and strain measurements were performed on an aixACCT aixPES system. Samples were lapped and sputtered with a gold layer. The electric field was applied with a frequency of 0.1 Hz (triangle shape).

3. Results and discussion

Fig. 1 shows the progress of the weight loss measured with TGA. The emanation of H_2O and CO_2 was monitored with MS. Below 150 °C water evaporates, the following weight losses between 250 °C and 750 °C were assigned to the elimination of CO_2. At temperatures >1050 °C, the ceramic starts to decompose, the losses here are assumed to be mostly caused by evaporation of Bi_2O_3 and, to a smaller fraction, M_2O (M = Na, K).

The calculated weight losses caused by CO_2 are shown in Table 1; the measured values are considerably higher for BNT–25BKT. Pure BNT and BKT show almost no excess losses. The measured losses correspond to the difference between the mass after the heat treatment and the mass after the evaporation of water.

Fig. 1 also shows that the powder mixture takes up a lot of water during processing when containing potassium (see weight loss below 150 °C). The used K_2CO_3 is very hygroscopic and therefore takes up humidity of the air, as well as water from the

Table 1
Weight losses of raw materials mixtures during TGA experiment.

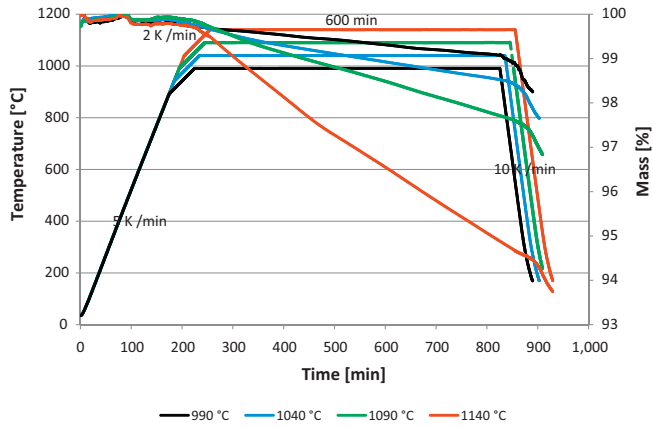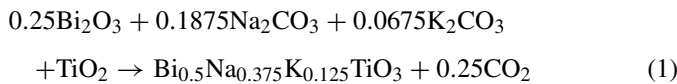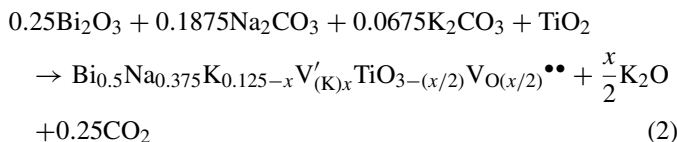|	Calculated [%]	Measured [%]	Difference [%]
BKT	4.76	5.04	0.28
BNT	4.94	5.23	0.29
BNT–25BKT	4.89	7.15	2.26

Fig. 2. TGA diagrams at constant temperature for 10 h duration at different temperatures. The used samples were made of calcined powder, pressed to pellets with 150 MPa without binding agent. The dashed lines show the used temperature profile, and the solid lines show the weight loss of the sample.
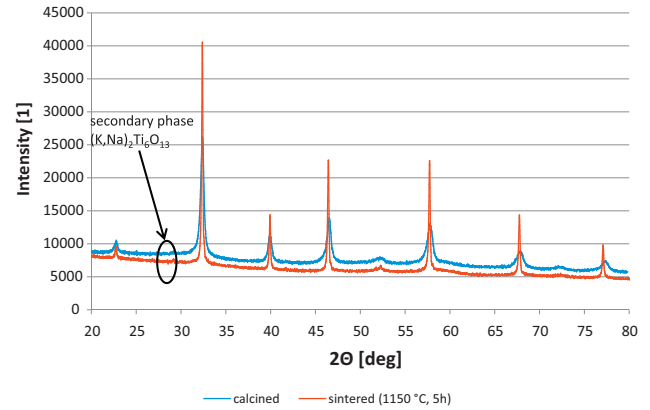

Fig. 3. XRD pattern of calcined (upper spectrum) and sintered (lower spectrum) sample. The secondary phase is visible at 29°; the sintered sample shows improved crystallinity than calcined powder.

used ethanol. Since Na_2CO_3 is not as hygroscopic as K_2CO_3, this effect is far less pronounced in pure BNT.

The complete calcination reaction, carried out in 2 steps at 650 °C and 900 °C can be formulated with Eq. (1):

$$0.25Bi_2O_3 + 0.1875Na_2CO_3 + 0.0675K_2CO_3$$

$$+TiO_2 \rightarrow Bi_{0.5}Na_{0.375}K_{0.125}TiO_3 + 0.25CO_2 \qquad (1)$$

The additional weight loss in BNT–25BKT during calcination, assumed to be caused by evaporation of K_2O, which decomposes at 350 °C[12] would lead to the formation of a high concentration of vacancies in the material as described in Eq. (2).

$$0.25Bi_2O_3 + 0.1875Na_2CO_3 + 0.0675K_2CO_3 + TiO_2$$

$$\rightarrow Bi_{0.5}Na_{0.375}K_{0.125-x}V'_{(K)x}TiO_{3-(x/2)}V_{O(x/2)}{}^{\bullet\bullet} + \frac{x}{2}K_2O$$

$$+0.25CO_2 \qquad (2)$$

This high amount of vacancies, both on the monovalent A-site and the oxygen site of the perovskite is prone to destabilize the lattice. Further the evaporation of K_2O causes a shift in A/B-ratio. Eq. (3) shows the formation of a secondary phase of alkali-polytitanate from the starting compounds, which would reduce the number of vacancies in the perovskite phase and reduces the deviation of the A/B-ratio. The formation of the secondary phase also starts at temperatures below 1000 °C. M refers to Na^+ and K^+ since these elements are chemically very much alike.

$$M_2O + 6TiO_2 \rightarrow M_2TiO_6O_{13} \qquad (3)$$
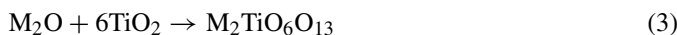
Under sintering conditions, the material starts to decompose and again shows weight loss. This reaction already starts at a temperature of 990 °C as seen in Fig. 2 and is caused by the vacancies introduced during calcination. Sintering in air reduces the amount of oxygen vacancies and leads to decomposition of the material in order to keep charge neutrality. This reaction can be observed with TGA because of the occurring loss of bismuth and alkali metals.[11] The decomposition is obviously a continuous process, since the weight loss is linear over duration of 10 h.

The XRD patterns (Fig. 3) of both the calcined powder and a sample sintered at 1150 °C for a duration of 5 h show small peaks at 29°, caused by the secondary phase. Due to the loss of K_2O during the calcination, the matrix is now close to the morphotropic phase boundary and the symmetry of the matrix cannot be described as purely tetragonal or rhomboedric.

The secondary phase was investigated using SEM and electron microprobe analysis. Because it contains low amounts of bismuth compared to the matrix, it is clearly visible as dark inclusions when imaging backscattered electrons with SEM. This difference is also shown in the mapping image received from the electron microprobe analysis.

Fig. 4 shows SEM images of samples sintered at temperatures between 1000 °C and 1150 °C for 5 h. All samples show secondary phase inclusions, the lower density at low sintering temperatures is also clearly visible. In the following mappings the distribution of the metal ions around such an inclusion of a secondary phase is shown. We also found traces of zirconium in the sample, which contaminates the material during the second milling. The amount of zirconium in the matrix is low with 0.65 mol% compared to the secondary phase, where it reaches 1.96 mol%. The matrix material and the secondary phases appear to be very homogenous. The apparent diffusion zone is an artifact introduced through the interaction volume of the electron beam during excitation of the material, as with any beam based method.[13]

The mapping in Fig. 5 clearly shows the different compositions of matrix an secondary phase. As reference materials the mineral sanidine, Bi_2O_3, TiO_2 and ZrO_2 were used. All elements were quantified using WDS, acceleration voltage was set to 15 kV at a working distance of 11.0250 mm. The elemental composition of the ceramic and the secondary phase is summarized in Table 2.

Table 2 shows, that at 1100 °C sintering temperature, the composition is no longer BNT–25BKT (0.75BNT–0.25BKT) but 0.78BNT–0.22BKT. At 1150 °C the shift is even larger to BNT–17BKT (0.83BNT–0.17BKT). This shift is caused by the loss of K_2O during the calcination and the decomposition according to Eq. (4) during sintering. The loss of monovalent
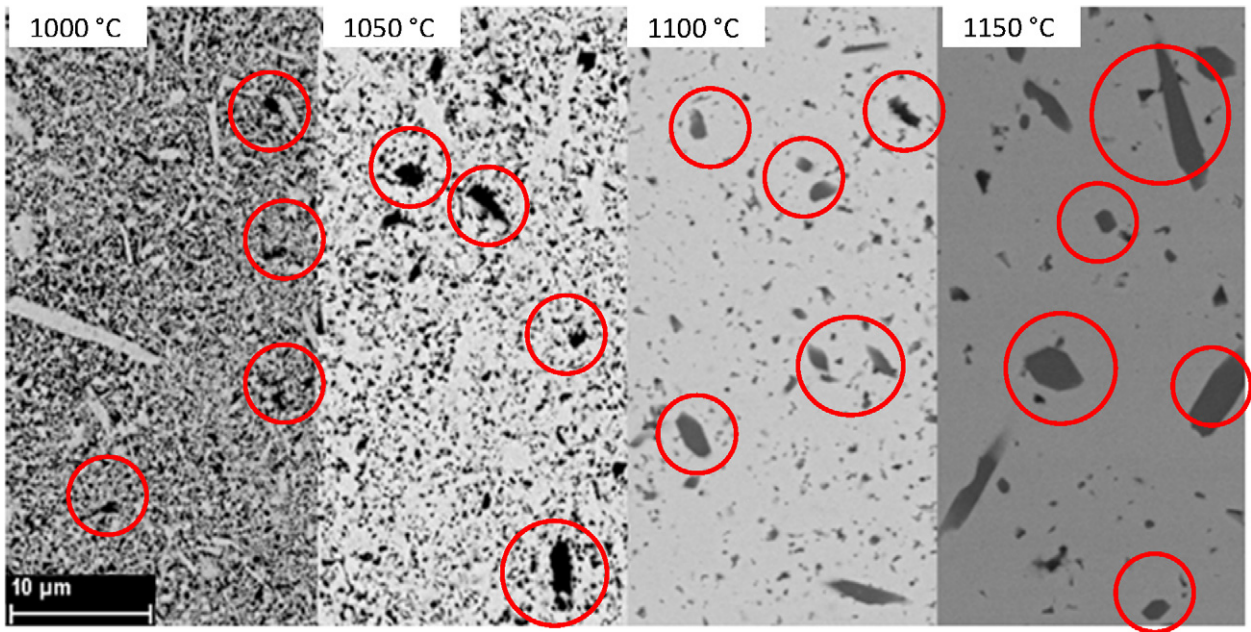
Fig. 4. SEM image of matrix and secondary phase (red circles, dark inclusions). The density visibly rises at higher sintering temperatures. (For interpretation of the references to color in this figure legend, the reader is referred to the web version of this article.)

A-site ions leads to instability of the system at higher temperatures.

The secondary phase consists of a polytitanate with a constant ratio of alkali ion:titanium of 1:3. At sintering temperatures below 1100 °C, Bi is also present in this phase. The data also confirm that the formation of the secondary phase occurs during calcination and again above 1050 °C as a result of the decomposition of the material. The higher the sintering temperature, the lower the Bi-content of the secondary phase, which indicates that the source of the weight loss at temperatures >1050 °C
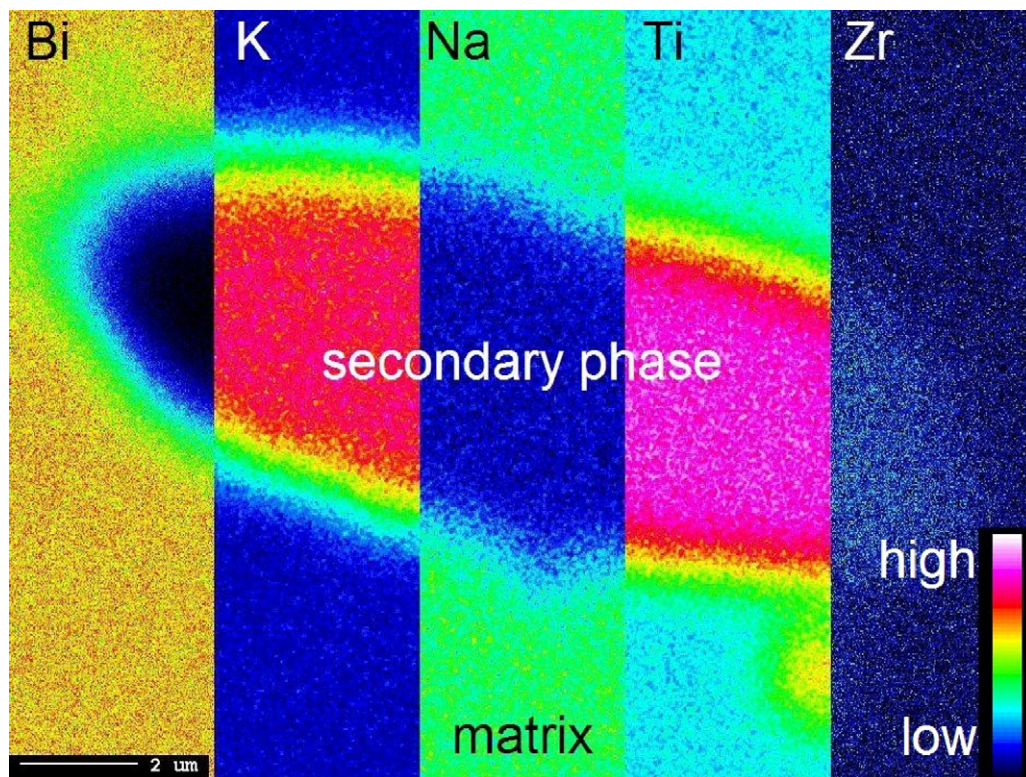
Fig. 5. Elemental distribution in matrix and secondary phase measured with EMPA using WDS detectors. Apparent zoning is caused by the interaction of the electron beam with the material.

Table 2

Composition of matrix and secondary phase determined by EMPA (standard deviation 0.84%, calculated from 43 measurements). Data is normalized to Ti = 1 for perovskite and (Ti + Zr) = 6 for secondary phase. The values in the table show the stoichiometric coefficients.

Sintering temperature	Matrix				Secondary phase				
	Bi	Na	K	Ti	Bi	Na	K	Ti	Zr
Target	0.5	0.375	0.125	1	sum = 2			sum = 6	
1000 °C	0.505	0.410	0.117	1	1.028	0.664	1.416	5.873	0.127
1050 °C	0.509	0.406	0.113	1	0.370	0.348	1.562	5.819	0.181
1100 °C	0.502	0.410	0.112	1	0.046	0.254	1.699	5.897	0.103
1150 °C	0.508	0.414	0.087	1	0.027	0.427	1.574	5.889	0.111
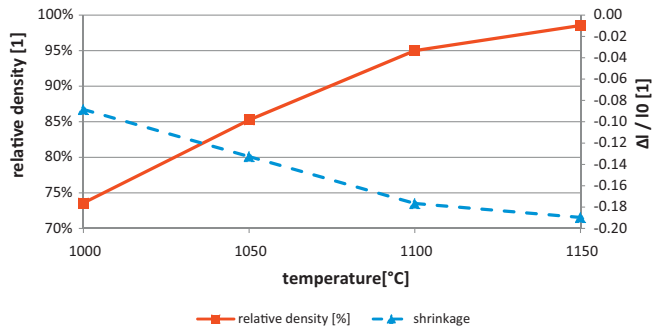
Fig. 6. Density and shrinkage of BNT–25BKT over sintering temperature (sintering duration 5 h).

is Bi_2O_3 evaporating from the secondary phase. The reaction during calcination inflicts the defect and vacancy situation in the material, leading to decomposition during sintering. Both formation reactions of the secondary phase lead to the same compound $M_2Ti_6O_{13}$. The main difference is that the decomposition reaction does not affect the A/B-ratio, nor does it lead to vacancies.

We suggest that the decomposition of the material and the growth of the secondary phase follow Eq. (4). Since BNT and BKT show the same decomposition behaviour[9,10] and Na as well as K form the same compounds with Ti and Zr,[14,15] both are referred to as M:

$$16Bi_{0.5}M_{0.5}TiO_3 \rightarrow M_2Ti_6O_{13} + 10Bi_{0.5}M_{0.5}TiO_3$$
$$+ \frac{3}{2}Bi_2O_3 + \frac{1}{2}M_2O \qquad (4)$$
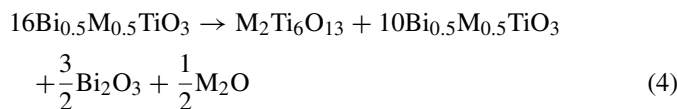
The most important conclusion from Eq. (4) is that the decomposition does not change the A/B-ratio of the matrix. The formation of the secondary phase creates $M_2Ti_6O_{13}$ and, due to the high sintering temperatures, releases volatile oxides.

Density increases with higher sintering temperatures as expected (Fig. 6).

The low relative density of samples sintered below 1100 °C renders electrical measurements meaningless. The dielectric

values for the samples at higher temperatures are presented in Table 3. The polarization curve is also heavily pinched, compared to the ferroelectric loops published (Fig. 7).

The characteristic values of the hysteresis loop differs from published data of the BNT–BKT system.[16] Solid solutions of BNT and BKT usually are reported as ferroelectric with standard shaped open hysteresis loops at room temperature. Pinched loops like such presented in this work, are measured at elevated temperatures.[17] Due to different measurement parameters, the values for dielectric properties in the literature are hardly comparable.

4. Summary

It is shown that the critical step in manufacturing BNT–xBKT is the calcination. The formation of BNT–xBKT and $M_2Ti_6O_{13}$ are competing reactions, especially regarding K. The formation of the secondary phase during the calcination reaction leads to a perovskite with a high defect concentration, according to Eq. (2). Those defects destabilize the system at the high sintering temperatures and lead to further formation of the secondary phase. The formation of a secondary phase in sodium deficient BNT has been reported before,[9] this work proposes a mechanism of the generation and growth of these inclusions. Both works indicate that the loss of monovalent ions leads to the decomposition of the ceramic.

According to TGA data (Fig. 2), the material is prone to further decomposition above 1100 °C. The decomposition reaction (Eq. (4)) forms a similar compound, but does not change
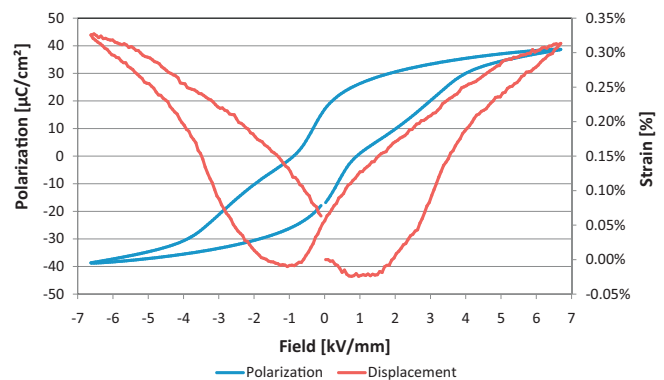
Table 3

Dielectric parameters measured at room temperature; f = 1 kHz, V_{rms} = 1 V.

	ε_r [1]	tan δ [1]	E_C [kV/mm]	P_r [μC/cm^2]
BNT–25BKT 1100 °C	1144	0.0726	1.52	16.8
BNT–25BKT 1150 °C	1332	0.0716	0.79	15.8

Fig. 7. Hysteresis loop of BNT–25BKT showing pronounced pinching and very low values for E_C and P_R. The saturated polarization is comparable to published values.[16,17] The hysteresis loop was measured with 0.1 Hz at room temperature.

the A/B-ratio of the ceramic since BNT–xBKT decomposes to BNT–xBKT, $M_2Ti_6O_{13}$, Bi_2O_3 and M_2O. Still, the formation of the secondary phase prefers K as the alkali ion, so the decomposition leads to BNT-rich systems. This is the reason for a change of the stoichiometric factor x in BNT–xBKT before and after sintering. The piezoelectric parameters highly differ from published data of comparable compositions. The behaviour of $M_2Ti_6O_{13}$ in electric field is unknown, but its formation influences the stoichiometry and the defect situation in the ceramic.

Acknowledgments

References

1. Haertling GH. Ferroelectric ceramics: history and technology. *Journal of the American Ceramic Society* 1999;**82**(4):797–818.
2. Rödel J, Jo W, Seifert KTP, Anton E, Granzow T, Damjanovic D, et al. Perspective on the development of lead-free piezoceramics. *Journal of the American Ceramic Society* 2009;**92**(6):1153–77.
3. Takenaka T, Nagata H, Hiruma Y. Current developments and prospective of lead-free piezoelectric ceramics. *Japanese Journal of Applied Physics* 2008;**47**(5):3787–801.
4. Aksel E, Forrester JS, Jones JL, Thomas PA, Page K, Suchomel MR, et al. Monoclinic crystal structure of polycrystalline $Na_{0.5}Bi_{0.5}TiO_3$. *Applied Physics Letters* 2011;**98**(15):152901.
5. Hiruma Y, Yoshii K, Nagata HT, Takenaka T. Phase transition temperature and electrical properties of $Bi_{0.5}Na_{0.5}TiO_3$–$Bi_{0.5}A_{0.5}TiO_3$ (A = Li and K) lead-free ferroelectric ceramics. *Journal of Applied Physics* 2008;**103**(8):084121.
6. Isupov VA. Ferroelectric $Na_{0.5}Bi_{0.5}TiO_3$ and $K_{0.5}Bi_{0.5}TiO_3$ perovskites and their solid solutions. *Ferroelectrics* 2005;**315**:123–47.
7. Schmitt LA, Kling J, Hinterstein M, Hoelzel M, Jo W, Kleebe HJ, et al. Structural investigations on lead-free $Bi_{0.5}Na_{0.5}TiO_3$-based piezoceramics. *Journal of Materials Science* 2011;**46**(12):4368–76.
8. Chen P-Y, Chou C-C, Tseng T-Y, Chen H. Second phase and defect formation in $Bi_{0.5}Na_{0.5−x}K_xTiO_3$ ceramics. *Japanese Journal of Applied Physics* 2010;**49**:061506.
9. Spreitzer M, Valant M, Suvorov D. Sodium deficiency in $Na_{0.5}Bi_{0.5}TiO_3$. *Journal of Materials Chemistry* 2007;**17**(2):185–92.
10. König J, Spreitzer M, Jancar B, Suvorov D, Samrdzija Z, Popovic A, et al. The thermal decomposition of $K_{0.5}Bi_{0.5}TiO_3$ ceramics. *Journal of the European Ceramic Society* 2009;**29**:1695–701.
11. Schuetz D, Krauss W, Albering J, Kurta C, Reichmann K. The chemical interaction of silver–palladium alloy electrodes with bismuth-based piezomaterials. *Journal of the American Ceramic Society* 2010;**93**(4):1142–7.
12. Holleman AF, Wiberg E. *Inorganic Chemistry*. 101st ed. New York: De Gruyter; 1995.
13. Hornbogen E, Skrotzki B. *Mikro- und Nanoskopie der Werkstoffe*; 2009.
14. Dash S, Sood DD, Prasad R. Phase diagram and thermodynamic calculations of alkali and alkaline earth metal zirconates. *Journal of Nuclear Materials* 1996;**228**(1):83–116.
15. Eriksson G, Pelton AD. Critical evaluation and optimization of the thermodynamic properties and phase diagrams of the MnO–TiO_2, MgO–TiO_2, FeO–TiO_2, Ti_2O_3–TiO_2, Na_2O–TiO_2, and K_2O–TiO_2 systems. *Metallurgical and Materials Transactions B* 1993;**24B**(5):795–805.
16. Otoničar M, Škapin SD, Spreitzer M, Suvorov D. Compositional range and electrical properties of the morphotropic phase boundary in the $Na_{0.5}Bi_{0.5}TiO_3$–$K_{0.5}Bi_{0.5}TiO_3$ system. *Journal of the European Ceramic Society* 2010;**30**(4):971–9.
17. Takenaka T, Nagata H, Hiruma Y. Phase transition temperatures and piezoelectric properties of $(Bi_{0.5}Na_{0.5})TiO_3$- and $(Bi_{0.5}K_{0.5})TiO_3$-based bismuth perovskite lead-free ferroelectric ceramics. *IEEE Transaction on Ultrasonics, Ferroelectrics, and Frequency Control* 2009;**56**(8):1595–612.

Short communication

BNT-based multilayer device with large and temperature independent strain made by a water-based preparation process

Werner Krauss, Denis Schütz, Michael Naderer, Denis Orosel, Klaus Reichmann *

Graz University of Technology, Christian Doppler Laboratory for Advanced Ferroic Oxides, Stremayrgasse 9, 8010 Graz, Austria

Abstract

A piezoelectric multilayer device based on bismuth–sodium–titanate ceramics (BNT) co-fired with Ag/Pd inner electrodes is described and its dielectric and piezoelectric properties are measured. The ceramic powder and tape was made by a water-based preparation process. After printing with Ag/Pd paste for inner electrodes these tapes were stacked to a multilayer device with 50 active layers. This device exhibited a large and temperature independent strain around 0.19% between 25 °C and 150 °C. The large strain is due to a field-induced phase transition. The low temperature dependence results from the broadening of the nonpolar phase by doping.
© 2011 Elsevier Ltd. All rights reserved.

Keywords: BNT; Lead-free; Multilayer; Piezoelectricity; Actuators

1. Introduction

For decades researchers work in the field of lead-free piezoelectric ceramics to find a material that could replace lead–zirconate–titanate in piezoelectric devices. Excellent reviews on that topic are given by Rödel et al.[1] or Takenaka et al.[2]

$Bi_{0.5}Na_{0.5}TiO_3$ (BNT) is one of the most promising lead free materials for actuator applications, which was first reported by Smolenskii et al.[3] It has a perovskite type structure with rhombohedral symmetry at room temperature. The depolarization temperature (T_d) is at 186 °C and the temperature at the maximum of the permittivity (T_m) at 335 °C.[3,4] Both temperatures can be shifted by doping. It exhibits a morphotropic phase boundary with tetragonal compounds, such as barium titanate[5] and bismuth–potassium–titanate.[6,7] Zhang et al.[8] found a large strain in the system $Bi_{0.5}Na_{0.5}TiO_3$–$BaTiO_3$–$K_{0.5}Na_{0.5}NbO_3$ (BNT–BT–KNN) which is due to a field-induced nonpolar/ferroelectric phase transition. In literature the nonpolar phase is sometimes termed as antiferroelectric which is supported by the shape of the polarization curves. Structural changes at T_d, which were suggested by Hiruma et al.[7] were not confirmed by

Jones et al.,[9] who performed Rietveld neutron powder profile analysis of the compound $Na_{0.5}Bi_{0.5}TiO_3$ over the temperature range from 5 to 873 K.

Key for a device fabrication is the multilayer technology, which requires co-firing of ceramics and metal electrodes, preferentially Ag/Pd-alloys. The first BNT-based multilayer actuator was presented by Takenaka et al.,[10] who used Pt-electrodes because of the concern of a bismuth–palladium reaction.[11,12] Schütz et al.[13] showed that BNT based ceramics do not interact with palladium during the sintering process as long as free bismuth oxide is not present. Hence the use of Ag/Pd-alloys for the co-fired inner-electrodes should be possible.

Other drawbacks for the use as material for piezoelectric devices are the huge intrinsic losses due to the large hysteresis and a pronounced temperature dependence of the piezoelectric properties due to the phase transition at the depolarization temperature.

To become temperature independent in dielectric and piezoelectric properties in an extended temperature range it is necessary to broaden the nonpolar phase, i.e. to lower the depolarization temperature T_d and to increase the temperature at the maximum of the permittivity T_m. This can be done in different ways. The major point is to increase the volume on the A-site of the perovskite to facilitate nonpolar ordering. This can be achieved by doping with smaller ions on the A-site[14] or larger ions on the B-site[15] of the perovskite, by the formation of vacan-

---

* Corresponding author. Tel.: +43 316 873 8285; fax: +43 316 873 8272.
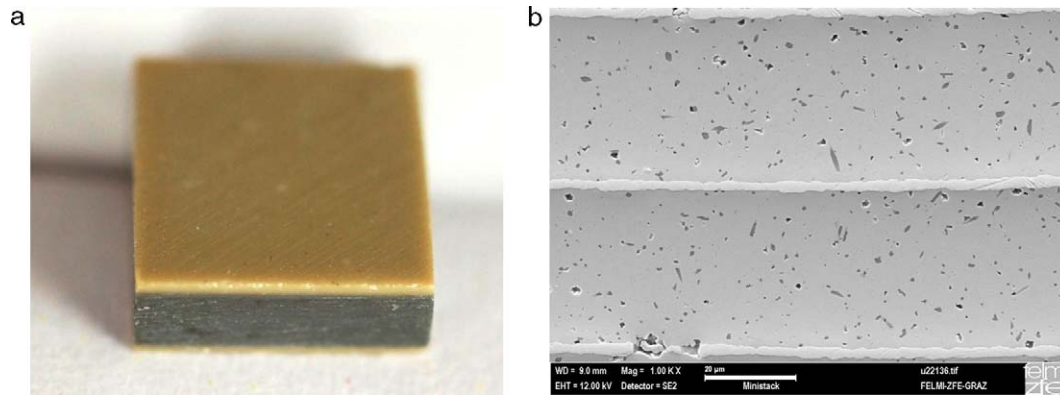 *E-mail address:* k.reichmann@tugraz.at (K. Reichmann).

Fig. 1. Photograph of the multilayer device (a) and SEM image of the active layers with Ag/Pd inner electrodes (b). The scale bar in the SEM image indicates the length of 20 μm.

cies and the reduction of the rhombohedral distortion by adding tetragonal compounds like $BaTiO_3$ (BT)[5,16] or $Bi_{0.5}K_{0.5}TiO_3$ (BKT).[6,17]

Desirable for the replacement of PZT is a cost effective production process. PZT is made by a mixed oxide process with water as a solvent, which is comparably cheap and safe. BNT-based ceramics are usually made in ethanol because of the solubility of the alkaline raw-materials. But ethanol is very expensive in comparison with water and one has to install an explosion protection in the powder and tape production line.

In this work, we present a method to produce a cost effective lead-free ceramic multilayer device with large strain and reduced temperature dependence. Therefore we designed a ceramic material based on BNT that was prepared by using water as a solvent.

2. Experimental

The powder for the multilayer-stack is $[Bi_{0.50}Na_{0.335}K_{0.125}Li_{0.04}]TiO_3$ doped with 2 mol% Nd which was made by a modified mixed oxide process. The reagent grade raw materials were Bi_2O_3 (HEK-Oxides), Na_2CO_3 (Merck), K_2CO_3 (Merck), Li_2CO_3 (Merck), TiO_2 (Tronox) and Nd_2O_3 (Treibacher). The raw materials were ball milled for 5 h in a laboratory ball mill (Dyna-Mill Multi Lab) with water as a solvent and subsequently dried with a laboratory spray dryer. After calcination at 900 °C for 2 h a second milling for 5 h and drying took place with the same equipment. From this powder a water-based slurry was made with a binder and tape casting was done on a laboratory equipment. 50 layers were printed with Ag/Pd-metal paste (70/30), stacked in a format of 10 cm × 10 cm with additional covering layers and were pressed under uniaxial pressure of 100 tons. After dicing and binder burn out sintering took place in air at a sintering temperature of 1100 °C for 5 h. The final dimensions were 7 mm × 7 mm × 2 mm with an active layer thickness of approximately 35 μm. The sintered multilayer-stacks were contacted with silver paste (burn-in temperature 750 °C) for electric measurements. In Fig. 1 one can see the sintered multilayer-stack and the SEM-image of the active layers.

The temperature dependence of the permittivity was measured using a Novocontrol Concept 40 impedance analyzer. Measurements were performed from −100 °C to 400 °C with a heating rate of 2 K/min. The polarization and displacement curves were measured with aixPES Piezoelectric Evaluation System from aixACCT from room temperature to 150 °C. The curves of polarization and displacement shown in Fig. 3 were measured at room temperature as the last cycle of three. SEM images were taken on a FEI Quanta 600 scanning electron microscope.

3. Results and discussion

With the choice of material we considered the phase diagram published by Hiruma et al.,[18] who found for the composition $[Bi_{0.50}Na_{0.335}K_{0.125}Li_{0.04}]TiO_3$ a depolarization temperature (T_d) of 160 °C and temperature at the maximum of the permittivity (T_m) of 290 °C. The concept of broadening the nonpolar phase was achieved by doping with 2 mol% Nd. As one can see in Fig. 2 this amount of Nd has enlarged the nonpolar phase from approximately 50 °C (T_d) to 320 °C (T_m).

In Fig. 3 one can see a narrow nonpolar polarization curve with low remnant polarization and a displacement curve with no remnant displacement and a maximum strain of about 0.19%.
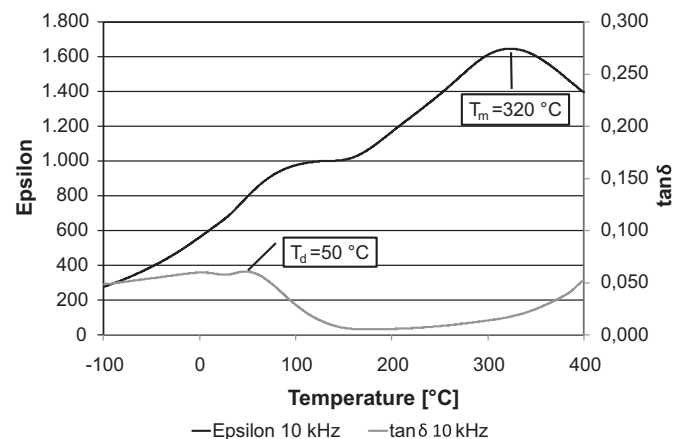
Fig. 2. Temperature dependence of permittivity (epsilon) and loss factor (tan δ) for $[Bi_{0.50}Na_{0.335}K_{0.125}Li_{0.04}]TiO_3$ doped with 2 mol% Nd.
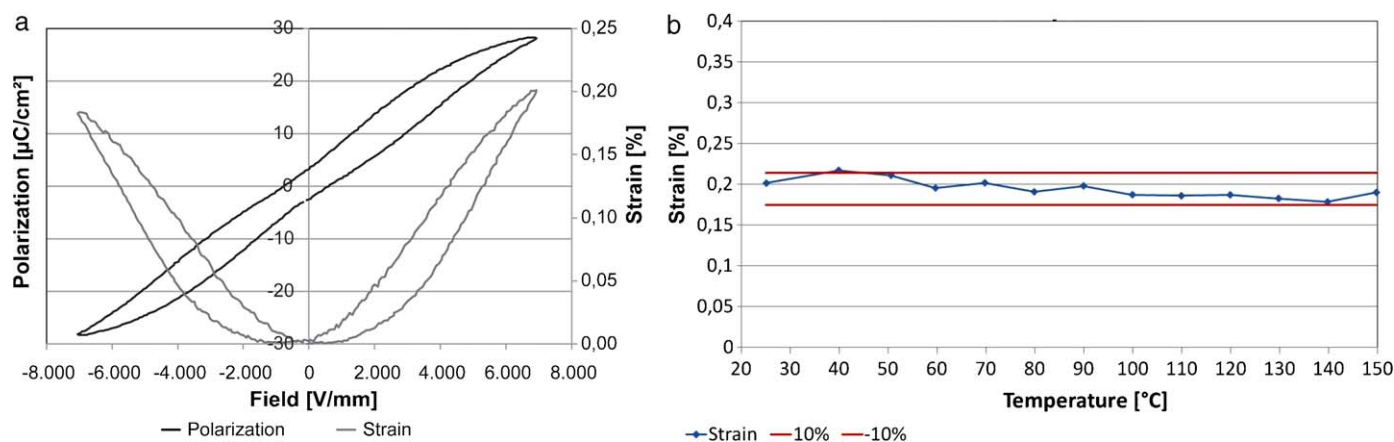
Fig. 3. Field dependence of polarization and displacement of the multilayer stack at room temperature, third cycle of three (a) as well as strain at 7 kV/mm vs. temperature measured with a frequency of 0.1 Hz (b).

Due to the dependence of T_d on frequency (which accounts only for a minor part of the shift) and electric field the above mentioned phase transition can be shifted from 50 °C (under small signal conditions of 10 kHz and 1 V) to below room temperature under large signal conditions (0,1 Hz and 200 V), which is the reason for the observed shape of the polarization and strain curves at room temperature. As we have shown in a previous work on solid solutions of BNT with $SrTiO_3$[19] there is a shift of about 75 K to lower temperatures from the small signal data to the high signal data. Further this concept yields a nearly constant strain of about 0.19% at 7 kV/mm with a tolerance of about ±10% in a temperature interval ranging from 25 °C to 150 °C.

4. Summary

We have shown that by enlarging the nonpolar phase in BNT-based piezoelectric ceramics by doping with Nd we are able to obtain a ceramic material with low intrinsic losses, low remnant polarization and a temperature independent strain in the desired operating temperature range.

Furthermore we have demonstrated the processing of a multi-layer device with a water based route using Ag/Pd inner electrodes. SEM images prove that the inner electrodes do not exhibit any delaminating, and there is no indication of a bismuth–palladium reaction. The actuator dimensions were 7 mm × 7 mm × 2 mm containing 50 active layers with approximately 35 μm layer thickness. The obtained strain at a field of 7 kV/mm gained the value of 0.19% with a variation of ±10% in the temperature range between 25 °C and 150 °C.

References

1. Rödel J, Jo W, Seifert K, Anton E, Granzow T, Damjanovic D. Perspective on the development of lead-free piezoceramics. *Journal of the American Ceramic Society* 2009;**92**:1153–77.
2. Takenaka T, Nagata H, Hiruma Y. Current developments and prospective of lead-free piezoelectric ceramics. *Japanese Journal of Applied Physics* 2008;**47**:3787–801.
3. Smolenskii GA, Isupov VA, Agranivyskaya AI, Krainik NN. New ferroelectrics of complex composition. IV. *Soviet Physics Solid State* 1961;**2**:2651–4.
4. Nagata H, Shinya T, Hiruma Y, Takenaka T. Piezoelectric properties of bismuth sodium titanate ceramics. *Ceramic Transaction: Development in Dielectric Materials and Electronic Devices* 2004;**167**:213–21.
5. Takenaka T, Maruyama K, Sakata K. $(Bi_{1/2}Na_{1/2})TiO_3$–$BaTiO_3$ system for lead-free piezoelectric ceramics. *Japanese Journal of Applied Physics* 1991;**30**:2236–9.
6. Sasaki A, Chiba T, Mamiya Y, Otsuki E. Dielectric and piezoelectric properties of $(Bi_{0.5}Na_{0.5})TiO_3$–$(Bi_{0.5}K_{0.5})TiO_3$ systems. *Japanese Journal of Applied Physics* 1999;**38**:5564–7.
7. Hiruma Y, Yoshii K, Nagata H, Takenaka T. Investigation of phase transition temperatures on $(Bi_{1/2}Na_{1/2})TiO_3$–$(Bi_{1/2}K_{1/2})TiO_3$ and $(Bi_{1/2}Na_{1/2})TiO_3$–$BaTiO_3$ lead-free piezoelectric ceramics by electrical measurements. *Ferroelectrics* 2007;**346**:114–9.
8. Zhang S, Kounga AB, Aulbach E, Granzow T, Jo W, Kleebe HJ, Rödel J. Lead-free piezoceramics with giant strain in the system $Bi_{0.5}Na_{0.5}TiO_3$–$BaTiO_3$–$K_{0.5}Na_{0.5}NbO_3$. I. Structure and room temperature properties. *Journal of Applied Physics* 2008;**103**.
9. Jones GO, Thomas PA. Investigation of the structure and phase transitions in the novel A-site substituted distorted Perovskite compound $Na_{0.5}Bi_{0.5}TiO_3$. *Acta Crystallographica Section B, Foundations of Crystallography* 2002;**58**:168–78.
10. Nagata H, Hiruma Y, Takenaka T. Electric-field-induced strain for $(Bi_{1/2}Na_{1/2})TiO_3$-based lead-free multilayer actuator. *Journal of the Ceramic Society of Japan* 2010;**118**:726.
11. Wang SF, Huebner W. Interaction of Ag Pd metallization with lead and bismuth oxide-based fluxes in multilayer ceramic capacitors. *Journal of the American Ceramic Society* 1992;**75**:2339–52.
12. Wang SF, Huebner W. Interaction of silver palladium electrodes with lead-based and bismuth-based electroceramics. *Journal of the American Ceramic Society* 1993;**76**:474–80.
13. Schuetz D, Krauss W, Albering J, Kurta C, Reichmann K, The chemical interaction of silver–palladium alloy electrodes with bismuth-based piezomaterials. Journal of the American Ceramic Society 93;1142–7.
14. Hiruma Y, Watanabe Y, Nagata H, Takenaka T. Phase transition temperatures of divalent and trivalent ions substituted $(Bi_{1/2}Na_{1/2})TiO_3$ ceramics. *Key Engineering Materials* 2007;**350**:93–6.

15. Zuo R, Ye C, Fang X, Li J. Tantalum doped $0.94Bi_{0.5}Na_{0.5}TiO_3$–$0.06BaTiO_3$ piezoelectric ceramics. *Journal of the European Ceramic Society* 2008;**28**:871–7.

16. Watanabe Y, Hiruma Y, Nagata H, Takenaka T. Phase transition temperature and electrical properties of divalent ions (Ca^{2+}, Sr^{2+} and Ba^{2+}) substituted ($Bi_{1/2}Na_{1/2}$)TiO_3 ceramics. *Ceramics International* 2008;**34**:761–4.

17. Yang Z, Liu B, Wei L, Hou Y. Structure and electrical properties of $(1–x)Bi_{0.5}Na_{0.5}TiO_3$–$xBi_{0.5}K_{0.5}TiO_3$ ceramics near morphotropic phase boundary. *Materials Research Bulletin* 2008;**43**:81–9.

18. Hiruma Y, Nagata H, Takenaka T. Phase-transition temperatures and piezoelectric properties of ($Bi_{1/2}Na_{1/2}$)TiO_3–($Bi_{1/2}Li_{1/2}$)TiO_3–($Bi_{1/2}K_{1/2}$)TiO_3 lead-free ferroelectric ceramics. *IEEE Transactions on Ultrasonics, Ferroelectrics, and Frequency Control* 2007;**54**(12).

19. Krauss W, Schütz D, Mautner FA, Feteira A, Reichmann K. Piezoelectric properties and phase transition temperatures of the solid solution of $(1 − x)$($Bi_{0.5}Na_{0.5}$)TiO_3–$xSrTiO_3$. *Journal of the European Ceramic Society* 2010:1827–32.

Piezoelectric properties and phase transition temperatures of the solid solution of $(1-x)(Bi_{0.5}Na_{0.5})TiO_3–xSrTiO_3$

Werner Krauss [a],[*], Denis Schütz [a], Franz Andreas Mautner [b], Antonio Feteira [c], Klaus Reichmann [a]

[a] *Graz University of Technology, Christian Doppler Laboratory for Advanced Ferroic Oxides, Stremayrgasse 16, 8010 Graz, Austria*
[b] *Graz University of Technology, Institute of Physical and Theoretical Chemistry, Rechbauerstraße 12, 8010 Graz, Austria*
[c] *The University of Birmingham, School of Chemistry, Edgbaston, Birmingham B15 2TT, United Kingdom*

Abstract

The phase diagram of $(1-x)(Bi_{0.5}Na_{0.5})TiO_3–xSrTiO_3$ was completed and investigations on polarization and strain in this system were carried out. $(1-x)(Bi_{0.5}Na_{0.5})TiO_3–xSrTiO_3$-ceramics were prepared by conventional mixed oxide processing. The depolarization temperature (T_d), the temperature of the rhombohedral–tetragonal phase transition (T_{r-t}) and the Curie temperature (T_m) were determined by measuring the temperature dependence of the relative permittivity. All solid solutions of $(1-x)(Bi_{0.5}Na_{0.5})TiO_3–xSrTiO_3$ show relaxor behavior (A-site relaxor). From XRD-measurements a broad maximum of the lattice parameter can be observed around $x=0.5$ but no structural evidence for a morphotropic phase boundary was found. SEM-analysis revealed a decrease of the grain size for increasing $SrTiO_3$-content. At room temperature a maximum of strain of about 0.29% was found at $x=0.25$ which coincides with a transition from a ferroelectric to an antiferroelectric phase. The temperature dependence of the displacement indicates an additional contribution from a structural transition (rhombohedral–tetragonal), which would be of certain relevance for the existence of a morphotropic phase boundary.
© 2010 Elsevier Ltd. All rights reserved.

Keywords: Dielectric properties; Piezoelectric properties; Perovskites; Actuators

1. Introduction

$(Bi_{0.5}Na_{0.5})TiO_3$ (BNT) is one of the most investigated lead-free piezoelectric materials.[1,2] It has a perovskite type structure with rhombohedral symmetry (R3C) at room temperature. The depolarization temperature (T_d) is at 186 °C and the Curie temperature (T_m) at 335 °C. T_d and T_m both can be shifted by doping[3] or by the formation of solid solutions with alkaline earth titanates.[3,4] $Bi_{0.5}Na_{0.5}TiO_3$ shows strong ferroelectricity ($P_r = 38 \mu C/cm^2$), but it also has drawbacks like a large coercive field of about 7 kV/mm, which leads to problems in the poling process. To overcome these problems and to optimize the properties of $Bi_{0.5}Na_{0.5}TiO_3$ solid solutions with other lead-free materials can be used. In combination with compounds of tetragonal symmetry (e.g. $BaTiO_3$ and $(Bi_{0.5}K_{0.5})TiO_3$)[5–11] the solid solution system with $Bi_{0.5}Na_{0.5}TiO_3$ exhibits a morphotropic phase boundary (MPB). It is known that morphotropic phase boundaries lead to higher values of d_{33} and k_{33}. For the solid solution $(1-x)(Bi_{0.5}Na_{0.5})TiO_3–xBaTiO_3$ the morphotropic phase boundary is found at $x=0.06$ with a minimum in T_d at about 100 °C.

$SrTiO_3$ has a perovskite type structure and a cubic symmetry at room temperature. Below −168 °C a transition to tetragonal symmetry is reported by Jauch and Palmer.[12] Hypothetically there is the possibility to observe a phase transition from a rhombohedral to tetragonal phase in solid solutions with $Bi_{0.5}Na_{0.5}TiO_3$. In all known cases of a morphotropic phase boundary in solid solutions of $Bi_{0.5}Na_{0.5}TiO_3$ and a tetragonal phase the depolarization temperature as well as the Curie temperature exhibit a minimum. Out of this reason it is necessary in the system $(1-x)(Bi_{0.5}Na_{0.5})TiO_3–xSrTiO_3$ to measure at low temperatures to observe a phase transition from a rhombohedral to a tetragonal phase. A phase diagram (Fig. 1) of $(1-x)(Bi_{0.5}Na_{0.5})TiO_3–xSrTiO_3$ published by Watanabe et al.[4] exists up to $x=0.25$. Watanabe used the maxima in the permittivity vs. temperature curves measured at a frequency of 10 kHz. The first maximum at lowest temperature, called the depolarization temperature (T_d) is connected to the

* Corresponding author. Tel.: +43 316 873 8270; fax: +43 316 873 8272.
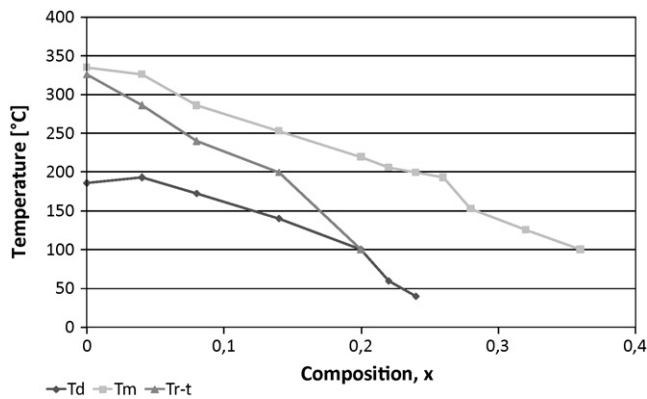*E-mail address:* werner.krauss@tugraz.at (W. Krauss).

Fig. 1. Dielectric transitions for $(1 - x)(Bi_{0.5}Na_{0.5})TiO_3–xSrTiO_3$ (data published by Watanabe et al.[4]) (depolarization temperature (T_d), rhombohedral–tetragonal phase transition temperature (T_{r-t}) and the temperature (T_m) of the maximum dielectric constant for x in $(1 - x)(Bi_{0.5}Na_{0.5})TiO_3–x$ $SrTiO_3$.

ferroelectric/antiferroelectric phase transition, the maximum at the highest temperature assigned to the Curie temperature (T_m) is associated with the transition from antiferroelectric to paraelectric. Between these two transition temperatures Watanabe identified a third transition temperature, which he called rhombohedral–tetragonal phase transition temperature (T_{r-t}). Just recently Hiruma et al.[13] verified a very small tetragonal distortion in pure BNT above this T_{r-t}, which supports Watanabes hypothesis.

Hiruma et al.[14] also found a strain maximum in the system $(1 - x)(Bi_{0.5}Na_{0.5})TiO_3–xSrTiO_3$ at $x = 0.26$ and they suggested that a morphotropic phase boundary is the reason for the large strain. Because of obvious differences to the characteristic features of the system BNT-BT we decided to complete the phase diagram over the whole composition range and look for structural and dielectric features that would support the existence of a morphotropic phase boundary.

2. Experimental procedure

The samples were prepared by a conventional mixed oxide process. In the first step a $Bi_{0.5}Na_{0.5}TiO_3$ master batch was made from bismuth oxide (reagent grade, HEK-Oxide GmbH), sodium carbonate (reagent grade, Merck) and titanium oxide (reagent grade, Bayer). After the first calcination at 850 °C the $Bi_{0.5}Na_{0.5}TiO_3$ was weighted together with strontium carbonate (reagent grade, Solvay) and titanium oxide in the chosen stoichiometry. After milling in a planetary mill (Fritsch Pulverisette 4) a second calcination took place at 850 °C. The powder was milled again and out of the dried powder a granulate was made by adding 5% polyethylene glycol 20 000 as a binder. The granulate was sieved and discs with a diameter of 13 mm were uniaxially cold pressed with a load of 2 tonnes. The discs were decarbonised at 450 °C and then sintered between 1200 and 1300 °C for 2 h. The proper sintering temperature was determined by dilatometry (*NETZSCH DIL 402 C*). Samples with a SrTiO_3-content up to $x = 0.5$ were sintered at 1200 °C, for higher SrTiO_3-content 1300 °C was used.

The sintered discs were gold sputtered for contacting. The X-ray powder data were collected in the reflection mode at room temperature and −243 °C with a Philips Expert diffractometer using Cu/Kα radiation. The cooling equipment was a closed cycle He cryostat (He-TTK Anton Paar) with cooling range between −263 and +27 °C. Data sets were collected from 20° to 80° (2-theta), step-width = 0.02° (2-theta) and step-time = 20 s/step. The lattice parameters were determined by Rietveld refinement using Philips Expert software. The temperature dependence of the relative permittivity was measured in the temperature range of −50 °C to 300 °C using Novocontrol Concept 40. The samples with $x = 0.8$ and 0.9 were measured from −243 °C to room temperature using an LCR bridge (Model E4980A, Agilent) coupled to a closed-circuit He-Cryocooler (Model CC 2.5 Oxford Instruments). For all samples the frequencies 1 kHz, 10 kHz and 100 kHz were used. The polarization and displacement curves were measured with aixPES (Piezoelectric Evaluation System from aixACCT) from room temperature to 150 °C.

3. Results and discussion

For identification of structural changes throughout the composition range we carried out low temperature XRD-measurements at −243 °C to identify an expected transition between rhombohedral and tetragonal phase. In our XRD-spectra of $(1 - x)(Bi_{0.5}Na_{0.5})TiO_3–xSrTiO_3$ (Fig. 2) we could not detect any tetragonal distortion, even not for pure SrTiO_3. We concluded, that the tetragonal distortion in the system $(1 - x)(Bi_{0.5}Na_{0.5})TiO_3–xSrTiO_3$ is too small to be detected within the resolution of the equipment available.

The calculated lattice parameters (for cubic indexing) are in good agreement with literature data. In Fig. 3 one can see that there is a broad maximum of the lattice parameter around $x = 0.5$. The decrease of the lattice parameter for $x > 0.5$ cannot be interpreted by Vegards law which would postulate a steady increase of the lattice parameter because the ionic radius of strontium is larger than either bismuth or sodium. The differences of the lattice parameters measured at −243 °C and at room temperature, which are in the range of the thermal expansion,
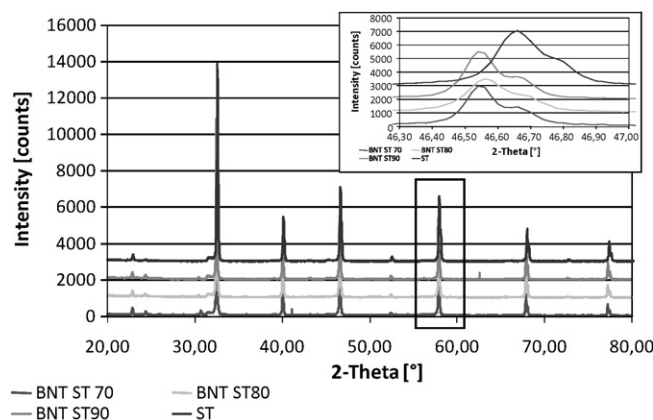

Fig. 2. XRD-spectra of $(1 - x)(Bi_{0.5}Na_{0.5})TiO_3–xSrTiO_3$ for $x = 0.7$ (BNT ST 70), $x = 0.8$ (BNT ST 80), $x = 0.9$ (BNT ST 90) and $x = 1.0$ (ST) at −243 °C.
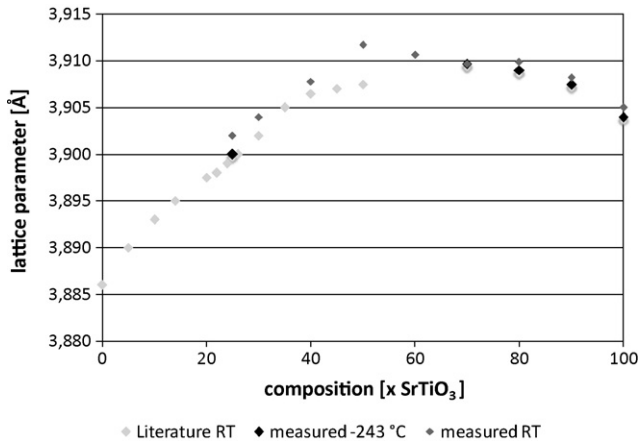
Fig. 3. Lattice parameters for $(1-x)(Bi_{0.5}Na_{0.5})TiO_3-xSrTiO_3$ (literature data from Park and Hong[15]).

Fig. 6. Microstructure of $0.60(Bi_{0.5}Na_{0.5})TiO_3-0.40SrTiO_3$ (SEM-image).

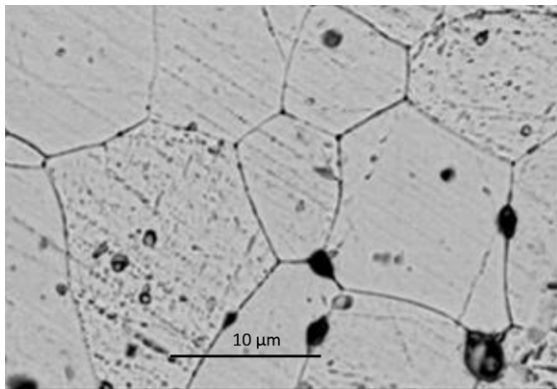

Fig. 4. Microstructure of $0.90(Bi_{0.5}Na_{0.5})TiO_3-0.10SrTiO_3$ (SEM-image).
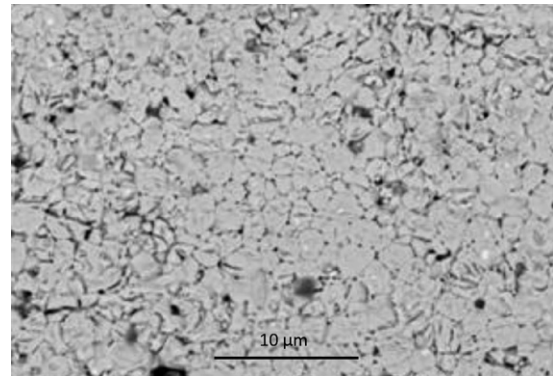
Fig. 7. Microstructure of $0.10(Bi_{0.5}Na_{0.5})TiO_3-0.90SrTiO_3$ (SEM-image).

do not support any significant structural changes, that would give evidence for a morphotropic phase boundary in the system $(1-x)(Bi_{0.5}Na_{0.5})TiO_3-xSrTiO_3$.

With the applied preparation conditions we achieved dense ceramics as one can see in micrographs of polished and etched samples (Figs. 4–7). The formation of a solid solution with $SrTiO_3$ strongly influences the microstructure of the $Bi_{0.5}Na_{0.5}TiO_3$-ceramic. The grain size of the system $(1-x)(Bi_{0.5}Na_{0.5})TiO_3-xSrTiO_3$ decreases from

approximately $10\,\mu m$ for $x=0.1$ to a grain size of around $3\,\mu m$ for $x=0.9$.

On the temperature dependence of the relative permittivity (Figs. 8–11) the maximum at the highest temperature was assigned to the Curie temperature T_m, the maximum at the lowest temperature to the depolarization temperature T_d. Maxima in between (T_{r-t}) were assigned to a rhombohedral/tetragonal phase transition according to the nomenclature used by Watanabe et al.[4] For $x>0.23$ T_{r-t} coincides with T_d, for $x>0.60$ only one maximum is observed, which is assigned to T_m. One can see that there is a frequency dependence of the

Fig. 5. Microstructure of $0.73(Bi_{0.5}Na_{0.5})TiO_3-0.27SrTiO_3$ (SEM-image).
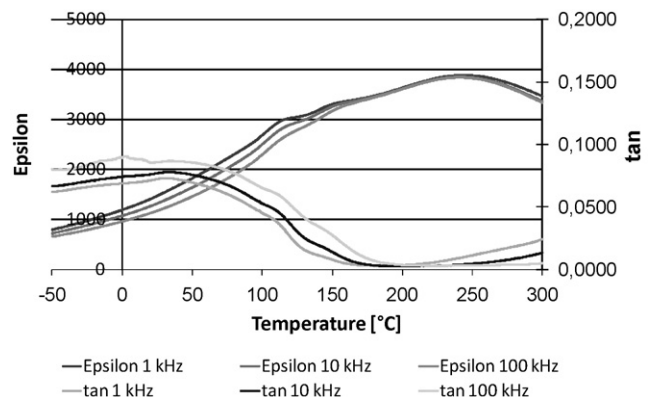
Fig. 8. Temperature dependence of the relative permittivity of $0.80(Bi_{0.5}Na_{0.5})TiO_3-0.20SrTiO_3$.
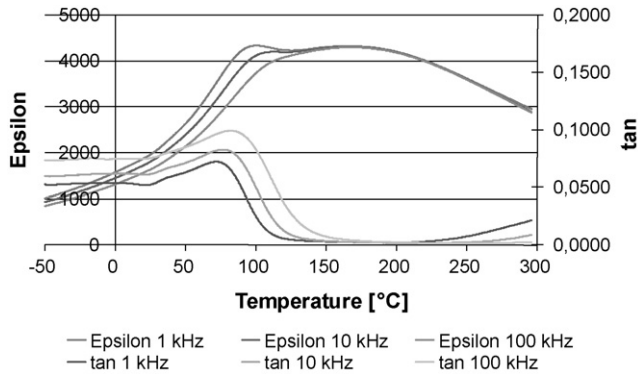
Fig. 9. Temperature dependence of the relative permittivity of $0.70(Bi_{0.5}Na_{0.5})TiO_3–0.30SrTiO_3$.
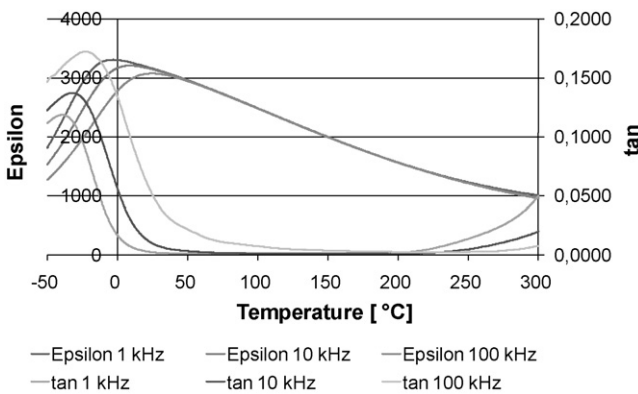
Fig. 10. Temperature dependence of the relative permittivity of $0.40(Bi_{0.5}Na_{0.5})TiO_3–0.60SrTiO_3$.

depolarization temperature T_d up to $x = 0.6$. On samples with $x > 0.6$ we find frequency dependence of the Curie temperature (T_m). From that we can state that all solid solutions of $(1 − x)(Bi_{0.5}Na_{0.5})TiO_3–xSrTiO_3$ exhibit relaxor behavior (A-site relaxor).

In accordance to Watanabe we used the permittivity data at 10 kHz to plot the phase diagram (Fig. 12). The phase diagram shows, that the Curie temperature T_m decreases almost linearly with increasing $SrTiO_3$-content to $−144\,°C$ at $x = 0.9$. Between
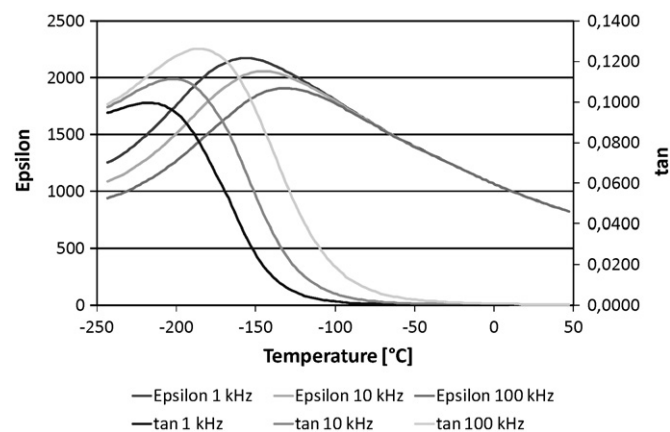
Fig. 11. Temperature dependence of the relative permittivity of $0.10(Bi_{0.5}Na_{0.5})TiO_3–0.90SrTiO_3$.
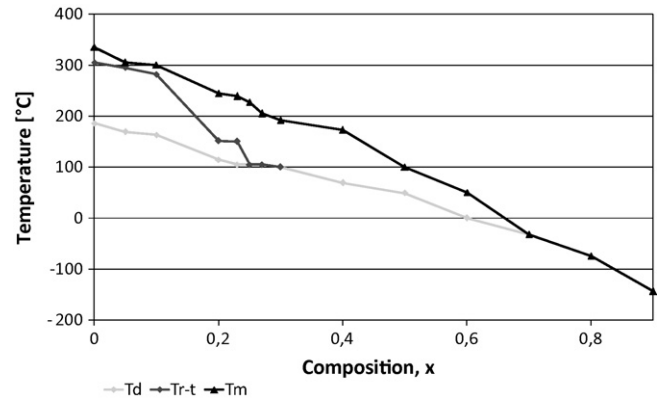
Fig. 12. Dielectric transitions for $(1 − x)(Bi_{0.5}Na_{0.5})TiO_3–xSrTiO_3$.

$x = 0.6$ and $x = 0.7$ the depolarization temperature T_d decreases to $0\,°C$. Up to $x = 0.7$ there is a non-polar phase between T_m and T_d. For higher strontium titanate content this non-polar phase disappears. In comparison to Watanabes phase diagram we observe T_d and $T_{r–t}$ in the range of $0.2 < x < 0.3$ to be approximately $70\,°C$ higher.

Polarization and displacement curves (Fig. 13) illustrate the varying ferroelectric behavior at room temperature. Starting from ferroelectric behavior up to $x = 0.1$ (Fig. 13a and d) the systems shifts more and more towards antiferroelectric behavior (Fig. 13b and e). This supports the assumption that the non-polar phase between T_d and T_m is in fact antiferroelectric. Samples with $x > 0.4$ become paraelectric (Fig. 13c and f). This indicates that under high electric field (up to 6 kV/mm) the transition temperature T_d is shifted to lower temperatures.

In Fig. 14 the remnant polarization and the maximum polarization is drawn over the whole composition range. It illustrates a strong decrease in the remnant polarization at about $x = 0.25$. For $x > 0.5$ the remnant polarization approaches zero.

If the strain at room temperature is plotted against composition a pronounced strain maximum of 0.29% at $x = 0.25$ is found (Fig. 15), where Watanabe et al.[4] suggested the existence of a morphotropic phase boundary. For a similar system – $(1–x–y)(Bi_{0.5}Na_{0.5})TiO_3–xBaTiO_3y(Na_{0.5}K_{0.5})NbO_3$ – Zhang et al. suggest, that such a large strain is due to a combination of the lattice volume change caused by a field-induced AFE-FE phase transition and ferroelectric domain reorientation.[16] In another publication Zhang et al.[17] suggest that the reason for the large strain could be due to electrostriction.

To discuss this question we plotted the temperature dependence of the strain under maximum electric field for the composition $x = 0.2$ (Fig. 16). We observed two maxima, marked with arrows, which could be attributed to phase transitions at T_d and $T_{r–t}$. The first maximum would indicate a contribution of a ferroelectric/antiferroelectric phase transition. The second maximum would indicate a contribution from a structural transition (rhombohedral–tetragonal), which would be of certain relevance for the existence of a morphotropic phase boundary.

One can see from Fig. 16, that under high electric field there is a shift of both the depolarization temperature and the rhombohedral–tetragonal transition temperature of about $70\,°C$ to lower temperatures in comparison to the
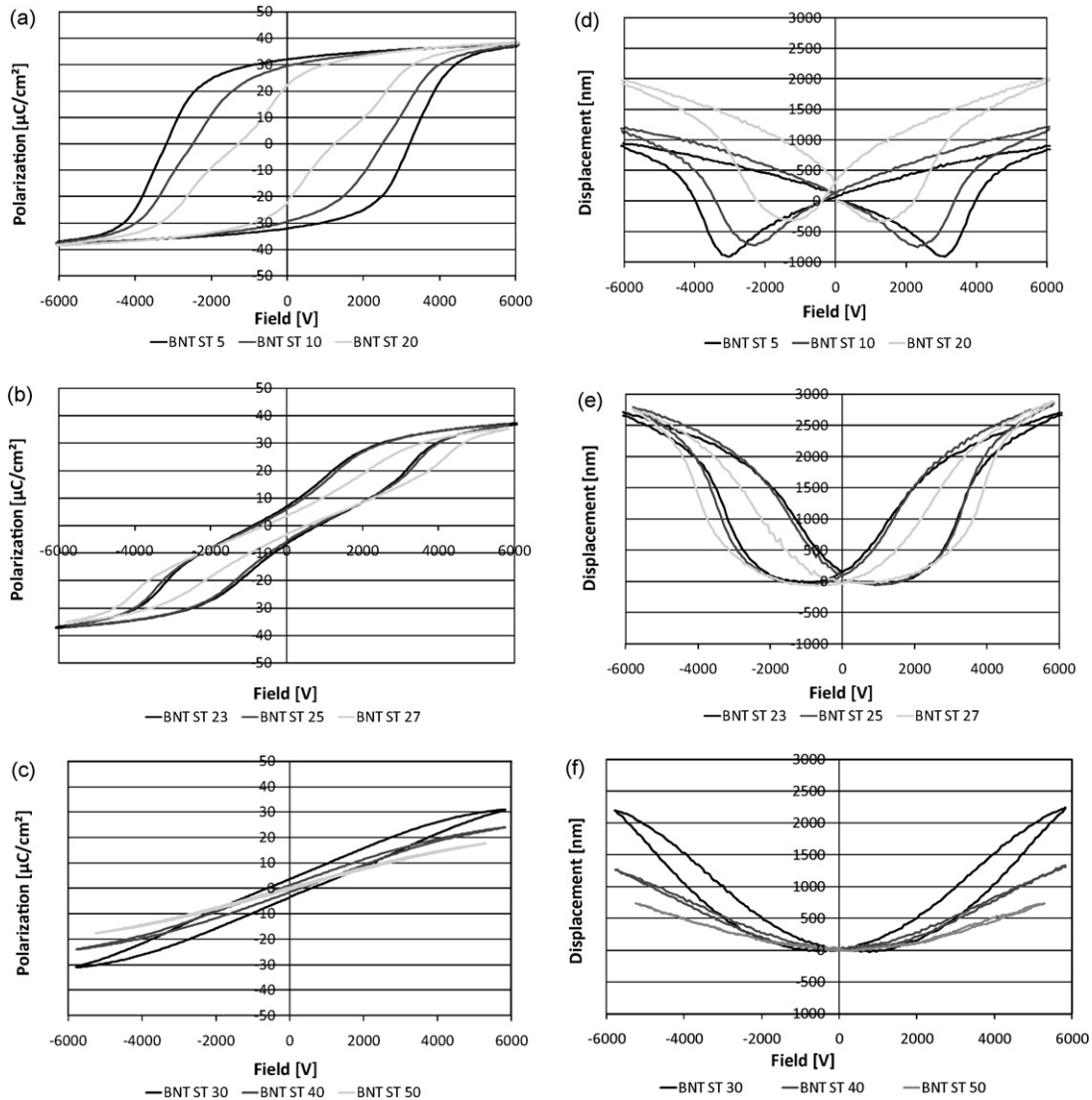
Fig. 13. Polarization and displacement curves for the system $(1-x)(Bi_{0.5}Na_{0.5})TiO_3-xSrTiO_3$.

phase diagram drawn from the dielectric transitions for $(1-x)(Bi_{0.5}Na_{0.5})TiO_3-xSrTiO_3$ (Fig. 12). This characteristics was observed also by Zhang et al.[16] in the system $(1-x-y)(Bi_{0.5}Na_{0.5})TiO_3-xBaTiO_3y(Na_{0.5}K_{0.5})NbO_3$. This gives strong evidence that both phase transitions are field

induced. The reason for the rhombohedral distortion of bismuth sodium titanate is most probably the formation of a covalent binding between the free electron pair of bismuth to a triple of the oxygen-atoms of the surrounding oxygen-dodecahedron being the reason for the A-site relaxor characteristics we observed
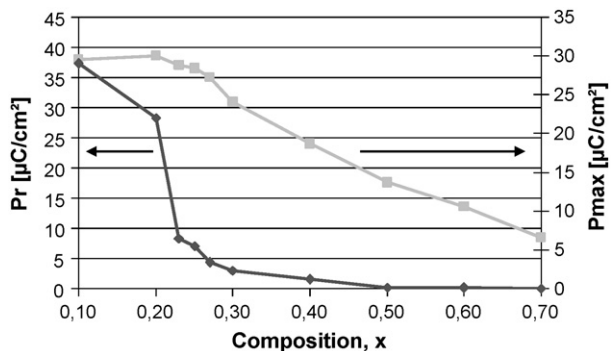
Fig. 14. Remnant polarization (P_r) and maximum polarization (P_{max}) of the system $(1-x)(Bi_{0.5}Na_{0.5})TiO_3-xSrTiO_3$.
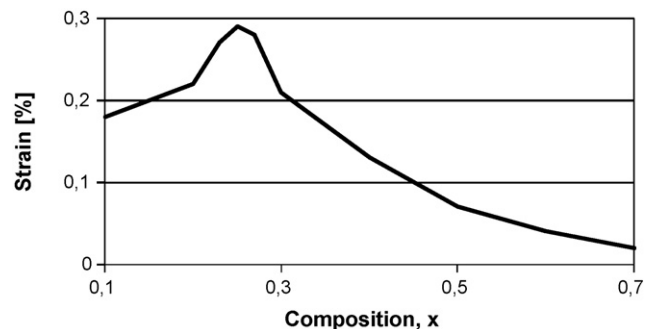
Fig. 15. Maximum strain at room temperature for the system $(1-x)(Bi_{0.5}Na_{0.5})TiO_3-xSrTiO_3$.
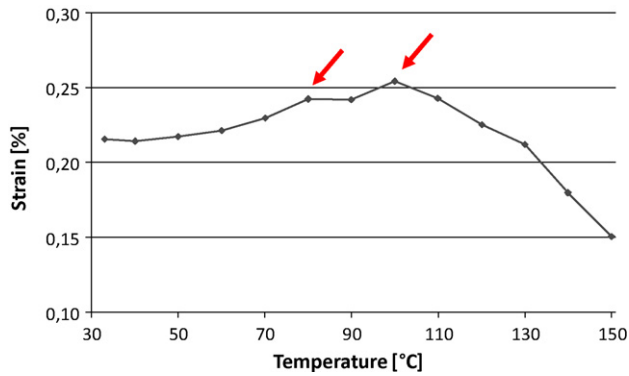
Fig. 16. Temperature dependence of the strain for $0.80(Bi_{0.5}Na_{0.5})TiO_3$–$0.20SrTiO_3$.

in this system (similar to lead containing relaxors, where an antiferroelectric ordering of the lead ions is observed[18]). Obviously the ordering induced by this covalent binding could be influenced either by an electrical field or temperature.

At the current status of our investigations we support the hypotheses stated by Zhang, since we did not find any structural features that hold up for a morphotropic phase boundary. In a very common sense the phase transition between ferroelectric and antiferroelectric phase at T_d or the supposed transition between a rhombohedral and a tetragonal phase at $T_{r–t}$ can be called a morphotropic phase boundary if only the maximum strain is considered a necessary attribute for it.

4. Conclusion

The phase diagram for $(1-x)(Bi_{0.5}Na_{0.5})TiO_3$–$xSrTiO_3$ was completed between $x=0$ and $x=1$. No tetragonal distortion could be detected in the whole composition range. The lattice parameter (for cubic indexing) has a broad maximum at $x=0.5$ contrary to the trend of ionic radii. Relaxor behavior was observed in all solid solutions (A-site relaxor). An antiferroelectric phase exists from pure $Bi_{0.5}Na_{0.5}TiO_3$ to a concentration of approximately $x=0.7$. We support the hypothesis that the reason for the maximum strain of 0.29% at $x=0.25$, which coincides with the transition from ferroelectric to antiferroelectric behavior, is a field-induced AFE-FE phase transition. A certain contribution of a structural transition (possibly rhombohedral–tetragonal) holds up for the existence of a morphotropic phase boundary.

Acknowledgements

References

1. Smolenskii GA, Isupov VA, Agranivyskaya AI, Krainik NN. New ferroelectrics of complex composition. IV. *Soviet Physics: Solid State* 1961;**2**:2651–4.
2. Rödel J, Jo W, Seifert K, Anton E, Granzow T, Damjanovic D. Perspective on the development of lead-free piezoceramics. *Journal of the American Ceramic Society* 2009;**92**:1153–77.
3. Hiruma Y, Watanabe Y, Nagata H, Takenaka T. Phase transition temperatures of divalent and trivalent ions substituted $(Bi_{1/2}Na_{1/2})TiO_3$ ceramics. *Key Engineering Materials* 2007;**350**:93–6.
4. Watanabe Y, Hiruma Y, Nagata H, Takenaka T. Phase transition temperature and electrical properties of divalent ions (Ca^{2+}, Sr^{2+} and Ba^{2+}) substituted $(Bi_{1/2}Na_{1/2})TiO_3$ ceramics. *Ceramics International* 2008;**34**:761–4.
5. Takenaka T, Maruyama K, Sakata K. $(Bi_{1/2}Na_{1/2})TiO_3$–$BaTiO_3$ system for lead-free piezoelectric ceramics. *Japanese Journal of Applied Physics* 1991;**30**:2236–9.
6. Zuo R, Ye C, Fang X, Li J. Tantalum doped $0.94Bi_{0.5}Na_{0.5}TiO_3$–$0.06BaTiO_3$ piezoelectric ceramics. *Journal of the European Ceramic Society* 2008;**28**:871–7.
7. Lin D, Xiao D, Zhu J, Yu P. Piezoelectric and ferroelectric properties of lead-free $[Bi_{1-y}(Na_{1-x-y}Li_x)]0.5Ba_yTiO_3$ ceramics. *Journal of the European Ceramic Society* 2006;**26**:3247–51.
8. Yang Z, Liu B, Wei L, Hou Y. Structure and electrical properties of $(1-x)Bi_{0.5}Na_{0.5}TiO_3$–$xBi_{0.5}K_{0.5}TiO_3$ ceramics near morphotropic phase boundary. *Materials Research Bulletin* 2008;**43**:81–9.
9. Xu C, Lin D, Kwok KW. Structure, electrical properties and depolarization temperature of $(Bi_{0.5}Na_{0.5})TiO_3$–$BaTiO_3$ lead-free piezoelectric ceramics. *Solid State Sciences* 2008;**10**:934–40.
10. Sasaki A, Chiba T, Mamiya Y, Otsuki E. Dielectric and piezoelectric properties of $(Bi_{0.5}Na_{0.5})TiO_3$–$(Bi_{0.5}K_{0.5})TiO_3$ systems. *Japanese Journal of Applied Physics* 1999;**38**:5564–7.
11. Shieh J, Wu KC, Chen CS. Switching characteristic of MPB compositions of $(Bi_{0.5}Na_{0.5})TiO_3$–$BaTiO_3$–$(Bi_{0.5}K_{0.5})TiO_3$ lead-free ferroelectric ceramics. *Acta Materialia* 2007;**55**:3081–7.
12. Jauch W, Palmer A. Anomalous zero-point motion in $SrTiO_3$: results from γ-ray diffraction. *Physical Review B* 1999:2961–3.
13. Hiruma Y, Nagata H, Takenaka T. Thermal depoling process and piezoelectric properties of bismuth sodium titanate ceramics. *Journal of Applied Physics* 2009;**105**.
14. Hiruma Y, Imai Y, Watanabe Y, Nagata H, Takenaka T. Large electrostrain near the phase transition temperature of $(Bi_{0.5}Na_{0.5})TiO_3$–$SrTiO_3$ ferroelectric ceramics. *Applied Physics Letters* 2008;**92**.
15. Park S-E, Hong KS. Variations of structure and dielectric properties on substituting A-site cations for Sr^{2+} in $(Na_{1/2}Bi_{1/2})TiO_3$. *Journal of Materials Research* 1997;**12**:2152–7.
16. Zhang S, Kounga AB, Aulbach E, Granzow T, Jo W, Kleebe HJ, et al. Lead-free piezoceramics with giant strain in the system $Bi_{0.5}Na_{0.5}TiO_3$–$BaTiO_3$–$K_{0.5}Na_{0.5}NbO_3$. I. Structure and room temperature properties. *Journal of Applied Physics* 2008;**103**.
17. Zhang S, Kounga AB, Jo W, Jamin C, Seifert K, Granzow T, et al. High-strain lead-free antiferroelectric electrostrictors. *Advanced Materials* 2009;**21**:1–5.
18. Chen IW, Li P, Wang Y. Structural origin of relaxor perovskites. *Journal of Physics and Chemistry of Solids* 1995;**57**:1525–36.

journal

The Chemical Interaction of Silver–Palladium Alloy Electrodes with Bismuth-Based Piezomaterials

Denis Schuetz,[†] Werner Krauss, Joerg Albering, Christoph Kurta, and Klaus Reichmann

Christian Doppler Laboratory for Advanced Ferroic Oxides, 8010 Graz, Austria

Multilayer technology relies heavily on the chemical compatibility of metal and ceramic. This work focuses on the ceramic–electrode interaction between $92Bi_{0.5}Na_{0.5}TiO_3$–6 Ba TiO_3–$2K_{0.5}Na_{0.5}NbO_3$ [$(Bi_{0.46}Na_{0.47}Ba_{0.06}K_{0.01})(Nb_{0.02}Ti_{0.98})O_3$], a promising actuator material and forerunner to an emerging class of lead-free actuator materials, and a silver–palladium alloy for inner electrodes, the only currently viable material for the firing temperatures necessary ($1100°C$). Of special concern was the high content of bismuth in the ceramic since prior investigations suggest that Bi_2O_3 (as well as various bismuth titanates) used as a fluxor in electroceramics are prone to forming the intermediate-phase bismuth palladate (Bi_2PdO_4), which can lead to poor contacting and delamination of multilayer stacks. Remarkably, no evidence of bismuth palladate formation could be found. However, the phase relations of the bulk ceramic have proven to be quite complex. Potassium was being drained out of the bulk ceramic either constituting the secondary phase $K_4Na_2(TiO_3)_3$ in unmodified experiments or evaporating and being replaced by silver in samples in contact with Ag. Mechanisms for the formation of these phases or the lack thereof are proposed. These findings were obtained by XRD, TG-DSC, and SEM with EDX, and LA-ICPMS.
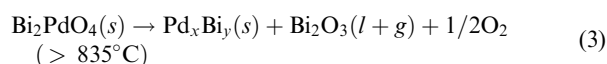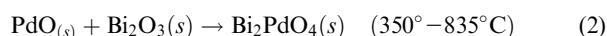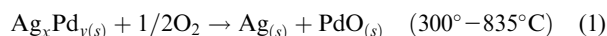
I. Introduction

L EAD zirconium titanate (PZT) has long been unchallenged in the field of piezoelectric actuator materials. Through half a century of process improvements and the introduction of dopants,[1,2] its properties remain uncontested. Even though it has been tried for at least a decade,[3–5] attempts to eliminate lead from piezomaterials have proven difficult. This has much to do with the properties of lead itself. The electronic structure of Pb^{2+} is ideal for implementation into a piezoelectric perovskite. A full set of $5d^{10}$ electrons as well as weak shielding from the $6s^2$ electrons above combined with its comparatively large ionic radius provide an atom with high polarizability and a lone pair to bind to the oxygen ion, which contributes to the overall polarization of a ferroelectric titanate.[6,7] Evidently, no other element has the necessary set of values to directly replace lead. Hence, it comes as no surprise that most systems of lead-free ceramics either perform poorly with regard to d_{33} or utilize a radically different mechanism of operation.[8,9] This is the case with the $(94-x)Bi_{0.5}Na_{0.5}TiO_3$–$6BaTiO_3$–$xK_{0.5}Na_{0.5}NbO_3$ [$(94-x)$BNT–6BT–xKNN] system first described by Zhang *et al.*[10–12] used in this work. The system itself shows great promise in the development of actuators, with two compositions showing the largest strain $x = 2$ ($\Delta l/l_0 = 0.45$ at% 8 kV/mm) and $x = 4$ ($\Delta l/l_0 = 0.43$ at% 11 kV/mm), the cause of which is still discussed in the literature. Zhang and colleagues[13,14] suggested a field-forced

antiferroelectric–ferroelectric phase transition observed in similar lead-based materials.

BNT as well as BNT–BT exhibit an antiferroelectric phase at elevated temperatures ($>200°C$);[15–17] the addition of KNN to the former seems to disrupt long-range ferroelectric order, giving rise to coexisting FE and AFE phases at room temperature in a narrow region of the phase diagram (around 2% KNN).[11] With increasing content of KNN, the antiferroelectric phase dominates and the large strain becomes more difficult to achieve. For reasons of practicality, the material chosen for this work is $92BNT–6BT–2KNN$ [$(Bi_{0.46}Na_{0.47}Ba_{0.06}K_{0.01})(Nb_{0.02}Ti_{0.98})O_3$] with a sintering temperature of $1100°C$ taken from prior research.

Cofiring ferroelectric materials with electrodes as multilayers have long been the method of choice for developing actuators. Naturally cofiring ceramics with its metallization has its own set of problems, namely the possibility of metallization material diffusing into the ceramic and constituting secondary phases, leading to delamination or changing the electrical properties of the ceramic.[18] This problem is recognized in silver–palladium alloys used widely in high-firing electroceramics. Palladium ($T_m = 1554.9°C$)[19] greatly decreases the volatility of silver ($T_m = 961.78°C$) as well as increases the melting point (T_m) of the alloy up to temperatures, which make it usable for high-firing electroceramics (e.g., $T_m = 1160°C$ for Ag/Pd = 70/30).[20] Even though the Ag/Pd is almost consolute, between $300°$ and $835°C$, palladium oxidizes to PdO (reaction (1)), constituting a secondary phase within the alloy, thereby increasing the silver content and making the alloy more heterogeneous and volatile. Dilatometric data also suggest that due to the partial oxidation of the alloy it can expand by 15% or more when using a slow heating process (Pd→PdO: $V_{oxide}/V_{metal} = 1.68$).[21,22] This can be avoided by increasing the rate of heating throughout the relevant temperature range, thereby taking advantage of the slow kinetics of the reaction to have a smaller fraction of the palladium to become oxidized. Even so, it is unlikely to prevent the formation of PdO and all the associated problems.

In contact with bismuth-containing materials, the reactions become more complex. In two separate studies, Wang and Huebner[23,24] have demonstrated the intermediary phase bismuth palladate (alternately dibismuth palladate; Bi_2PdO_4) forming between Bi_2O_3, widely used as a fluxor, as well as various bismuth titanates and PdO in the so-called "bismuth reaction" (reaction (2)). This reaction is reported to occur in Ag/Pd alloy electrodes as well, at temperatures between $350°$ and $835°C$

$$Ag_xPd_{y(s)} + 1/2 O_2 \rightarrow Ag_{(s)} + PdO_{(s)} \quad (300°-835°C) \quad (1)$$

$$PdO_{(s)} + Bi_2O_{3(s)} \rightarrow Bi_2PdO_{4(s)} \quad (350°-835°C) \quad (2)$$

$$Bi_2PdO_{4(s)} \rightarrow Pd_xBi_{y(s)} + Bi_2O_3(l+g) + 1/2 O_2 \quad (>835°C) \quad (3)$$

In addition to this when Bi_2PdO_4 decomposes over $835°C$, bismuth and palladium become alloyed to a limit of solubility of 16 mol% Bi (reaction (3)), which could lead to capacitance

problems in addition to delamination. So far, no bismuth-containing perovskites have been studied as to their chemical compatibility to electrode materials but the need for this is obvious as the majority of lead-free candidate materials are either based on BNT or incorporate bismuth in some form; see Shrout and colleagues[25,26] and references therein.

The objective of this study is to investigate the phase relation between BNT–BT–KNN and Ag/Pd alloys using a modified powder mixture technique. Because diffusion of electrode materials into ceramics up to 1 mm[27] is suggested, doping with silver and palladium was carried out to provide an insight into the chemical modification, phase relations, and microstructural development of the ceramics in the vicinity of the electrode.

II.   Experimental Procedure

(1)   Sample Preparation

Ceramic powders were prepared using the mixed metal oxide route. A stoichiometric mixture of the oxides and carbonates Bi_2O_3 (Reagent grade-HEK GmbH, Lübeck, Germany), Na_2CO_3 (Reagent grade-Merck), TiO_2 (Reagent grade-Tronox), $BaCO_3$ (Reagent grade-Solvay SA, Solvay SA Buxelles, Belgium), Nb_2O_5 (Reagent grade-H.C. Starck, Goslar, Germany), and K_2CO_3 (Reagent grade-Ferro GmbH, Ferro, Cleveland, OH) was dried in air at 300°C overnight, allowed to cool in a desiccator, and homogenized in a planetary mill (180 rpm; secondary ratio 1.8; 6 × 20 min) with yttria-stabilized zirconia balls (5 mm diameter) in absolute ethanol with 1 mL of Dispex A40 (Ciba Spezialitaetenchemie, Basel, Switzerland) detergent to prevent flocculation. The ethanol was evaporated under reduced pressure and the resulting powder was calcined at 900°C for 3 h in a closed Al_2O_3 container using a muffle kiln. No reaction with the container was observed. After calcination, the resulting ceramic was deagglomerated in ethanol, a planetary mill (200 rpm; secondary ratio (−2), 6 × 15 min), and 2 mm yttria-stabilized zirconia balls were utilized. The dried slurry was sieved and stored in a desiccator. For doped samples 1 mol% Ag (as Ag_2O reagent grade; Ferro GmbH) or 1 mol% Pd (as PdO; synthesized from $PdCl_2$ (Merck) by calcinating $PdCl_2$ at 570°C for 1 h) was added to the ceramic powder before deagglomeration.

This study utilized a commercially available inner electrode paste for screen-printing (Dupont chemicals, Wilmington, DE) with a defined Ag/Pd atomic ratio of 70/30 corresponding to a melting point of 1160°C. This should make it ideal for heat treatment of 1100°C maximum. Further, the paste contained an organic binder and solvents to facilitate screen printing but no glass fluxor or fillers like $BaTiO_3$. The data sheet, as well as the preliminary findings show the size range of particles in the paste to be very narrow and around 0.4 μm.

The powder mixtures were obtained by drying the electrode paste at 100°C overnight to obtain a material without a solvent but still containing the organic binders to avoid the metallic ductility, which would make further preparation difficult. The resulting material was still brittle enough to be ground using an agate mortar and pestle at room temperature. This enabled us to grind the material into aggregates 10–100 μm in size, which were then homogenized with the ceramic powder using a tumbler at ratios of volume of 10% (15.4 wt%), 20% (30.4 wt%), and 30% (45.8 wt%). A reference sample was added consisting of Bi_2O_3 with a 30% volume of Ag/Pd. All samples were then uniaxially cold pressed at 1.5 tons without a binder in a 13 mm die. Before heat treatment, the powder mixtures were debindered at 300°C for 1.5 h.

Heat treatment took place at two distinct temperatures of 750°C (3 h), to facilitate Bi_2PdO_4 development, and 1100°C (3 h) as the final sintering temperature, with a heating and cooling rate of 5 K/min. To take into account the formation of PdO and subsequent effects, a ramp of 10 K/min was introduced in the 1100°C experiments until 900°C was reached. A closed ceramic container was used when sintering the samples. To maintain a constant Bi_2O_3-vapor pressure within, BNT–BT powder was added to the boat to counter evaporation of Bi_2O_3 from the ceramic samples.

(2)   XRD

Samples were ground in an agate mortar and measured using a Bruker D5005 θ-θ with a copper $K\alpha$ emitter and a graphite secondary monochromator. All measurements were taken at room temperature with a range of 20°–90°, a step size of 0.02°, and a step time of 6 s. $K\alpha_2$ stripping and visualization was performed using the Diffrac+Basic suite (version 2006) and Rietveld refinement took place with Topaz (V 3.0).

(3)   SEM and EDX

All samples sintered at 1100°C were hard enough to be embedded in resin, cut, and polished. Samples sintered at 750°C were vacuum infiltrated by resin and subsequently cut and polished as they were too fragile to undergo a normal cutting or polishing process. All measurements were carried out using a LEO Gemini DSM982 (Zeiss, Jena, Germany) utilizing a 1–30 kV field emission gun at 15 kV and a Noran Voyager 3105A EDX detector (Noran Instruments Inc., Middleton, WI).

(4)   TG–DSC

Thermographic measurements were carried out on a Netzsch STA 409 (Selb, Germany) at a heating rate of 5 K/min under air. Undoped samples as well as a 30% powder mixture were measured.

(5)   LA–ICPMS

Experiments have been performed using laser ablation inductively coupled plasma mass spectroscopy (LA–ICPMS). Adjacent line scans with a length of 1500 μm each have been performed on undoped and doped (1% Ag and 1% Pd) disks using a UP-213 LA system (New Wave Research, Fremont, CA) with a Nd:YAG laser working at 213 nm wavelength coupled to an Agilent 7500ce ICPMS (Agilent Technologies, Waldbronn, Germany). Helium 5.0 was used as a carrier gas for the LA. Tuning of the system has been performed using a NIST (Gaithersburg, MD) SRM 612 glass standard. Laser and ICPMS settings have been optimized for a ceramic matrix (40 μm spot size, 8.6 J/cm^2 fluence, 10 Hz repetition rate, 10 μ/ms scan speed, 0.75 l/min carrier gas flow). Background correction was carried out with the undoped disk sample and ^{47}Ti was used as an internal standard for signal correction because it was the least volatile constituent in the matrix.

III.   Results

(1)   XRD

The pattern in Fig. 1 shows the ceramic after calcination and after sintering at 1100°C as well as the calculated reflexes for the ceramic taken from Zhang et al.[11]

Clearly, one can see that the actual solid-state reaction leading to the formation of the ceramic takes place during calcination and further heat treatment only increases the size of the crystallites. Furthermore, no other crystalline phase besides the perovskite was detected. Rietveld refinement results showed a cubic structure with a slight but undeterminable (0.2° maximum) rombohedral distortion (pseudocubic) with a unit cell size of 3.9049 Å ($\pm$0.0006 Å), which is in line with prior research.

With the exception of the reference sample composed of Bi_2O_3 and Ag/Pd, XRD measurements of powder mixtures fired at 750°C (Fig. 2) indicated no formation of bismuth palladate in any sample, showing that bismuth palladate does not originate from the bismuth-containing perovskite. PdO however, was clearly visible. Rietveld refinement showed no change in lattice constants or symmetry of the ceramic compared with the blank. This observation is compounded by the spectra taken of the
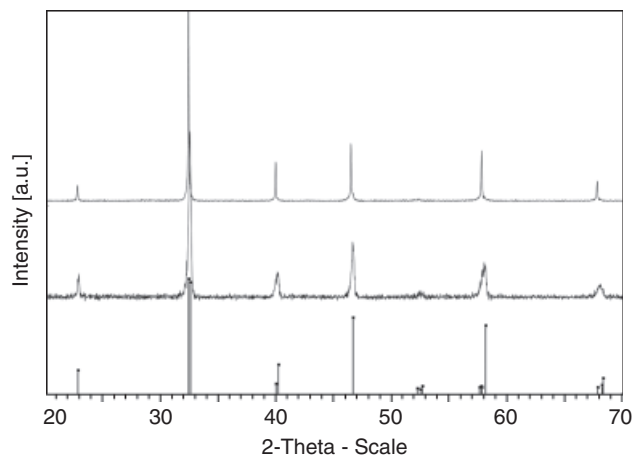
Fig. 1. XRD reflections of sintered (top) and calcined (middle) BNT–BT–KNN ceramic. The pattern below represents the calculated reflections, with cell constants taken from Zhang *et al.*[10]
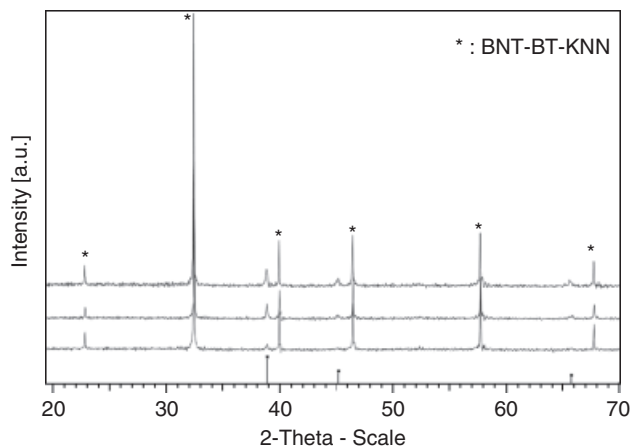

Fig. 3. Comparison of 1100°C powder mixtures 30% (top), 20% (middle), and 10% (bottom) the pattern below represents a calculated pattern for a 70/30 Ag/Pd alloy (FCC; $a = 4.0117$ Å).[20]

powder mixtures fired at 1100°C shown in Fig. 3. Naturally, neither PdO nor bismuth palladate was detected.

Ag/Pd peaks became subsequently broader with increased metal content, indicating inhomogeneity in the alloy. This can be attributed to the sample design because with a higher metal content, a correspondingly higher amount of Ag/Pd was at the surface of the sample, allowing for evaporation of silver and raising the compositions over the limit of detection. Also, there was no indication of Bi^{3+} alloying with Ag/Pd. This will be shown in greater detail in the SEM section.

Spectra of the doped samples showed only the perovskite. Rietveld refinement showed no change in lattice size or geometry. No Bi_2PdO_4 was detected in the Pd-doped sample.

(2) SEM and EDX

SEM micrographs of the unmodified ceramic sintered at 1100°C clearly showed a secondary phase (Figs. 4 and 5). From their lack of reflections in XRD, it can be considered amorphous, condensing out of a liquid phase with no long-range ordering. EDX spectra showed a high content of titanium, sodium, and potassium. No secondary phases were detected in the 750°C experiments. At both temperatures, no sinter skin was detected.

The doped ceramics have proven interesting with respect to the secondary phases. Inclusions failed to form in the Ag-doped ceramic. Ag was soluble in the ceramic. On the contrary, Pd seemed to be insoluble as it precipitated as metal throughout the doped ceramic (Fig. 5). The secondary phase was present in the Pd-doped ceramic in a distribution comparable to the unmodified samples. Figure 6 shows a comparison of the differently

doped ceramics at two different magnifications, which also provides an insight into the microstructural changes accompanying the doping.

The powder mixtures showed no reaction layer between the metal and the ceramic at both temperatures; EDX spectra indicated no bismuth present in the alloy, further confirming the nonformation of Bi_2PdO_4. No amorphous inclusions were detected in the powder mixtures and EDX spectra showed a silver concentration in the ceramic close to the limit of detection.

Micrographs of the Ag/Pd aggregates showed the segregation of the alloy whenever an evaporation of silver was possible, either through cracks in the material or whenever the aggregates were at the surface of the sample. Figure 7 shows two aggregates; one enclosed and homogenous, and one in contact with the atmosphere and segregated. This could be detected at both temperatures.

(3) TG–DSC

TG–DSC measurement confirmed the observations made through SEM and XRD. Figure 8 shows a TG–DSC measurement of a 30 vol% powder mixture. Clearly visible is the binder burnout starting at 180°C, peaking and finishing below 300°C. Also visible is the formation of PdO accompanied by an increase in mass as ambient oxygen was incorporated into the metal. No
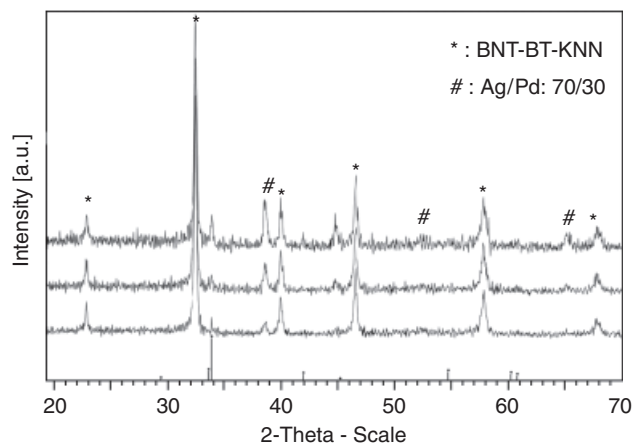

Fig. 2. Comparison of 750° powder mixtures 30% (top), 20% (middle), and 10% (bottom) the pattern below represents PdO (00-041-1107).
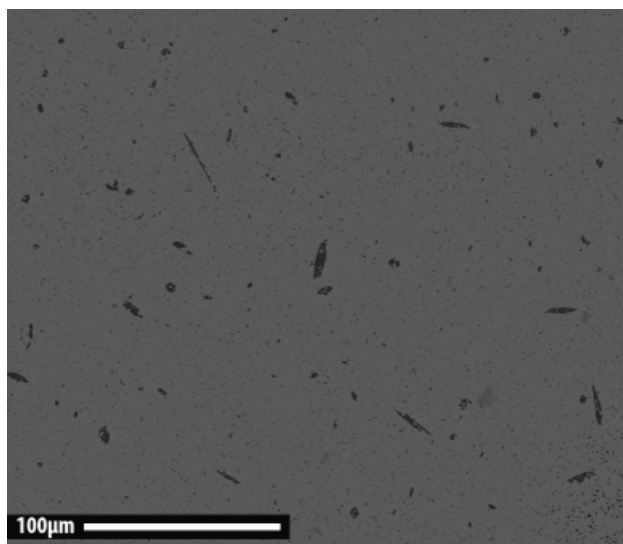

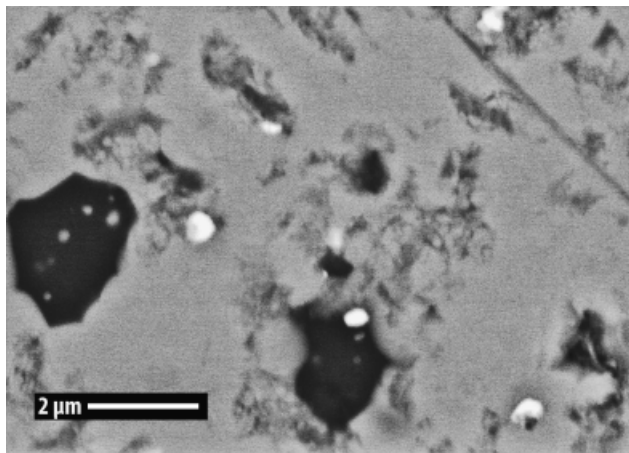**Fig. 4.** Secondary phase (dark) in the unmodified ceramic sintered at 1100°C.

Fig. 5. Pd-doped ceramic; clearly visible is the secondary phase (dark) and the precipitates of base Pd detected (bright).

indication of Bi_2PdO_4 formation was detected. The slight slope in TG above 800°C leads us to the assumption that Bi does indeed leave the perovskite (as a phase mixture of liquid and gaseous Bi_2O_3[28]) at elevated temperatures but as this occurs above the stability region of Bi_2PdO_4 formation, it does not lead to this intermediate phase developing. Apparently, the perovskite exhibits temperature stability greater than comparable bismuth oxides or titanates.

(4)   LA–ICPMS

Measurements using LA–ICPMS substantiated the earlier observations. The primary elements (Na, Ti, Bi) as well as Ba and Nb were detected uniformly. Zr and Y were found in traces and are thought to be contaminants introduced through the milling. Potassium quantification was difficult mainly due to the lack of a reliable matrix-matched standard. Additionally, the high content of sodium in the ceramic leads to polyatomic interference with the detector as $^{23}Na^{16}O^+$[29] increases the potassium count. Additional interference came from $^{38}Ar^1H^+$ forming out of the carrier gas, increasing the $^{39}K^+$ counts further.

However, a closer look at the line scans showed that the potassium-containing secondary phase was indeed detected through this method. Whenever the ablation beam was over one (or multiple in case of higher and broader peaks) potassium-rich inclusions (invisible to the light microscope used for targeting) the detector registered potassium intensities several times
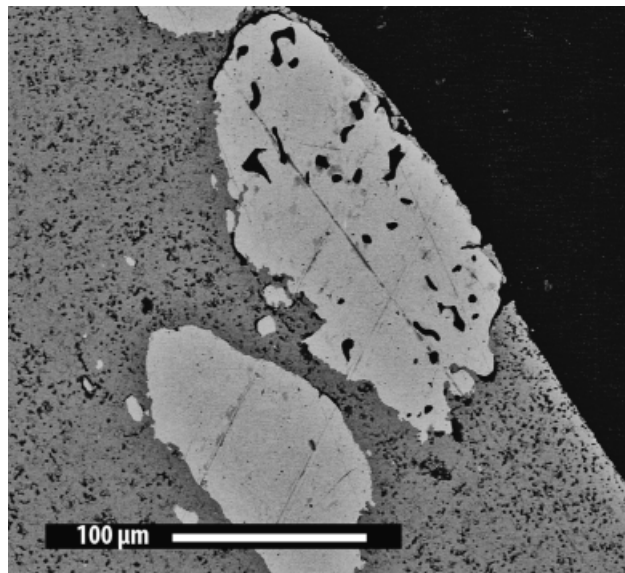

Fig. 7. Ag/Pd aggregates in 750°C sample (vacuum infiltrated). The exposed aggregate is showing clear signs of exsolution.

higher than the baseline; see Fig. 9 for an example. These "peaks" of K in the analysis were present in the undoped as well as the Pd-doped samples, confirming their inhomogeneity. The low lateral resolution of this method prevented a more exact comparison because the inclusions are much smaller ($\sim 5\ \mu m$) than the spotsize used (40 μm). Much the same was true for the observed Pd precipitates in the palladium-doped samples (see Fig. 10), which resulted in "peaks" whenever a precipitate was ablated, confirming the insolubility of Pd in the ceramic.

The silver-doped samples (Fig. 11) showed a uniform distribution of silver throughout the sample, confirming the solubility and incorporation of Ag^+ into the perovskite. The K content in the Ag-doped samples was uniform and comparable to the baseline of the Pd-doped or undoped samples. Even though exact quantification has proven elusive, we believe that most of the potassium was contained in the secondary phase in undoped and Pd-doped samples or had subsequently evaporated in the Ag-doped samples.

Lastly Fig. 12 presents a comparison of K content in the materials used; clearly, one can see the uniform distribution of the K in the Ag-doped samples, compared with the large inhomoge-
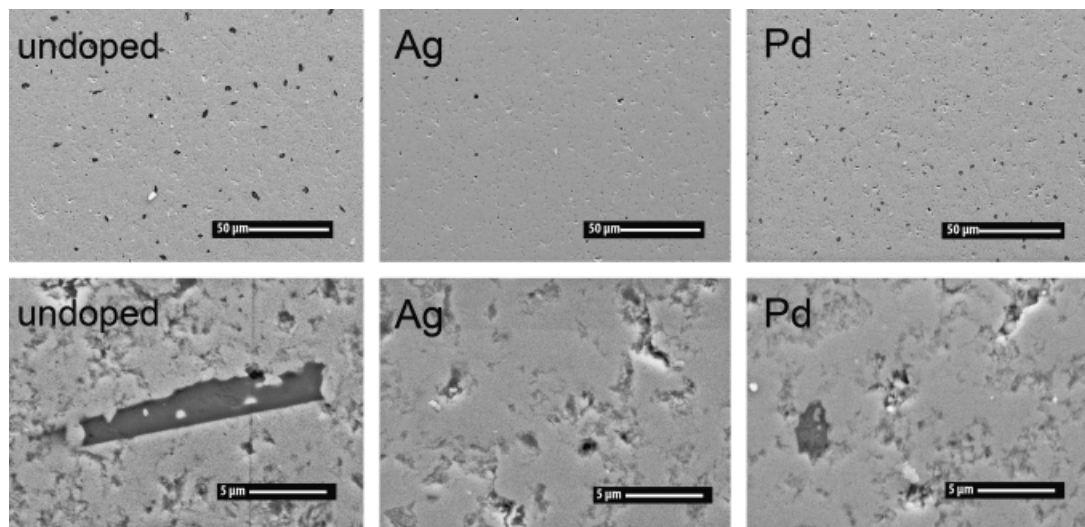

Fig. 6. SEM images of the differently doped ceramics at two magnifications. The secondary phase is clearly visible in both Pd-doped and undoped samples and notably absent in the Ag-doped samples. Pd precipitates are also visible in the Pd-doped sample.
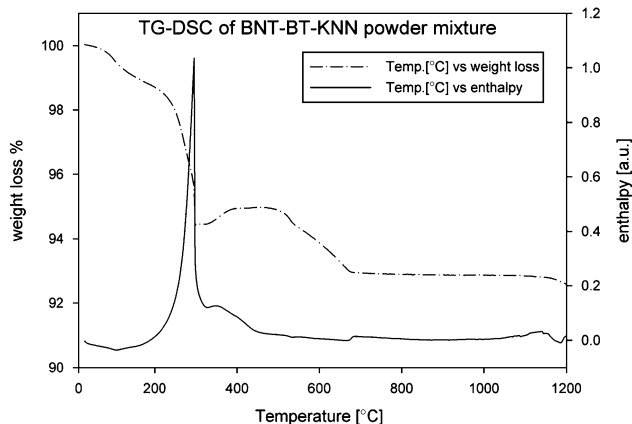
Fig. 8. TG–DSC of a 30% powder mixture with a heating rate of 10 K/min.

Fig. 10. Line scan of the Pd-doped ceramic clearly visible is the large inhomogenity of both K (secondary phase) and Pd (precipitates).

nity seen in undoped and less distinctive but clearly present in the Pd-doped samples.

IV. Discussion

All methods described have yielded consistent results. Apparently, Bi_2PdO_4 is unable to form out of the bismuth-containing perovskite. This can be attributed mostly to the greater thermal stability compared with Bi_2O_3 or similar oxides and titanates. In addition, BNT–BT–KNN was shown to exhibit an amorphous secondary phase when sintered at 1100°C. It can be assumed that most of the potassium contained in the ceramic can be found in this phase. Its composition of K, Na, Ti as well as the fact that it needs to have a liquid state between 750° and 1100°C to explain its amorphousness lead us to designate it as $K_4Na_2(TiO_3)_3$ first decribed by Belayev and Golovanova.[30] because no other compound in the ICSD database as well as the literature exhibits these characteristics. Multiple studies have found similar polytitanates in systems comparable to this, but they are thought to be distinct because of their clear long-range ordering[31] or the lack of potassium in the system.[32]

The formation of the secondary phase implies a change in chemical composition of the matrix phase. The proposed reaction of decomposition as well as the proposed final composition are shown below (reaction (4)) using the Kroeger–Vink notation assuming a 2-4-O^{2-} perovskite as the base. This does not account for the volatile constituents Bi and Na; the whole usual range of Schottky, Frenkel, and anti-Frenkel equilibria still applies. The calculation was carried out assuming that all the potassium left the perovskite, considering charge and mass balance
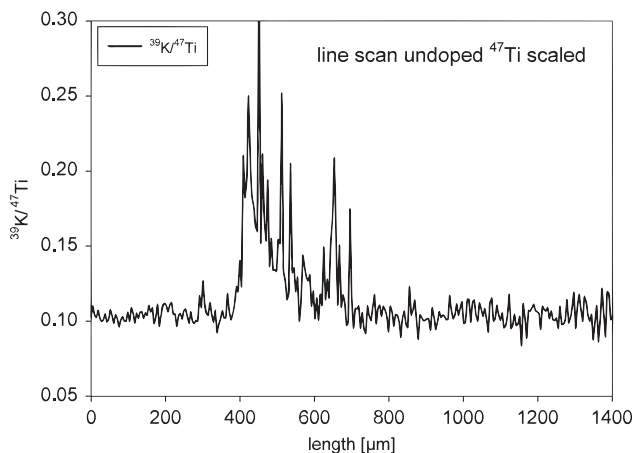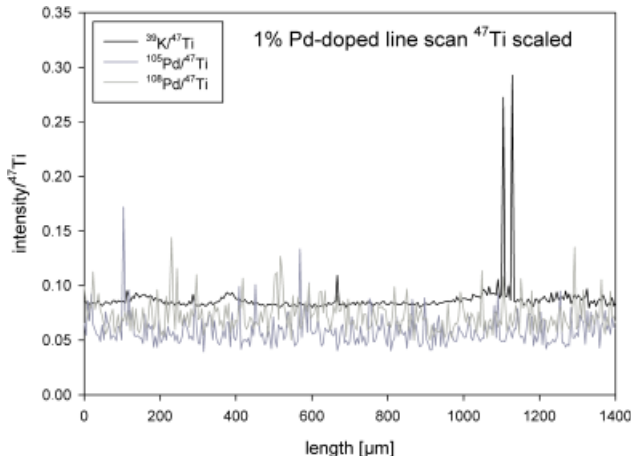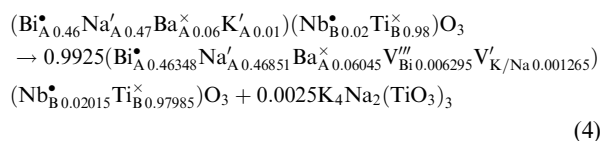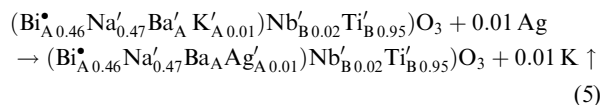
and rescaling to the more complete B site, which provides an insight into how the additional defects would look like in the bulk ceramic

$$(Bi^{\bullet}_{A\,0.46}Na'_{A\,0.47}Ba^{\times}_{A\,0.06}K'_{A\,0.01})(Nb^{\bullet}_{B\,0.02}Ti^{\times}_{B\,0.98})O_3$$
$$\rightarrow 0.9925(Bi^{\bullet}_{A\,0.46348}Na'_{A\,0.46851}Ba^{\times}_{A\,0.06045}V'''_{Bi\,0.006295}V'_{K/Na\,0.001265})$$
$$(Nb^{\bullet}_{B\,0.02015}Ti^{\times}_{B\,0.97985})O_3 + 0.0025K_4Na_2(TiO_3)_3$$

$$(4)$$

Because the secondary phase failed to show in any sample containing silver (powder mixtures, Ag doping) in addition to the uniformity of the signal of Ag^+ in LA–ICPMS, we assume solubility as well as incorporation into the perovskite lattice in this fashion (reaction (5)):

$$(Bi^{\bullet}_{A\,0.46}Na'_{A\,0.47}Ba'_A K'_{A\,0.01})Nb^{\bullet}_{B\,0.02}Ti'_{B\,0.95})O_3 + 0.01\,Ag$$
$$\rightarrow (Bi^{\bullet}_{A\,0.46}Na'_{A\,0.47}Ba_A Ag'_{A\,0.01})Nb^{\bullet}_{B\,0.02}Ti'_{B\,0.95})O_3 + 0.01\,K\uparrow$$

$$(5)$$

with potassium leaving the perovskite and evaporating in the following manner:

$$K_2O(s) \rightarrow 2K(g) + O_2(g)(>490°C)$$

$$(6)$$
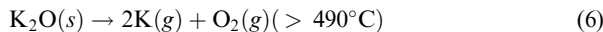
Silver solubility has been demonstrated in similar systems,[33,34] and so it is safe to assume silver to be able to consti-

Fig. 9. Line scan of K content in the undoped ceramic showing the inhomogenity caused by the secondary phase.
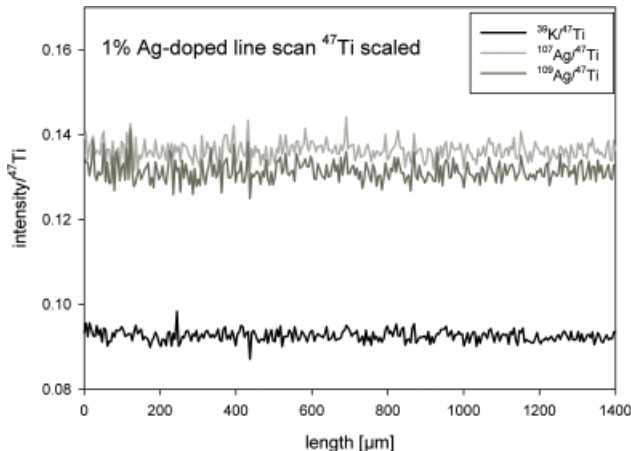

Fig. 11. Line scan of the Ag-doped ceramics; showing uniform Ag and K concentrations throughout the scanned area.
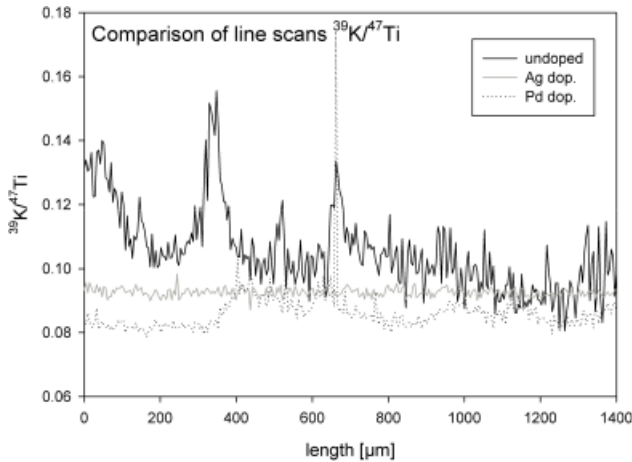
Fig. 12. Comparison of the K signal in three differently doped ceramics.

tute up to 10% of the A sites in such a perovskite lattice if the defects or composition allow for this.

V.   Conclusion

This study has shown the reactions of BNT–BT–KNN and silver palladium electrode material. Bi_2PdO_4 was not detected within any compositions owing to the greater thermal stability of the perovskite than comparable bismuth oxides or titanates. Because of the similarities between the material studied and other bismuth perovskite-based actuator materials, this should be relevant to all materials based on BNT. An amorphous secondary phase $(K_4Na_2(TiO_3)_3)$ was detected and identified within BNT–BT–KNN. Earlier studies on BNT–BT–KNN concentrated on XRD to assume a monophasic constitution of the material and so it is reasonable to assume this phase is not detrimental to piezoelectric performance. Furthermore, the potassium seems to be unnecessary to disturb the long-range ferroelectric ordering, this role falling to the niobium. In addition, we recommend that $K_{0.5}Na_{0.5}NbO_3$ (KNN) contained in this ceramic be replaced by $NaNbO_3$ (NN) in further studies to prevent the formation of the secondary phase.

It was shown that silver was soluble in the ceramic to at least 1% and was incorporated into the perovskite structure, replacing the potassium lost. Higher solubility is likely and is subject to further investigation. Pd has proven insoluble within the limits of detection. Any sample in contact with silver failed to register the secondary phase proposed to be $K_4Na_2(TiO_3)_3$ and registered low concentrations of potassium, giving credence to the potassium evaporating. The nonformation of Bi_2PdO_4 indicates the chemical compatibility of bismuth-containing perovskites with Ag/Pd electrode material and provides a further stepping stone on the quest for lead-free electronics.

References

[1]B. Jaffe and W. R. Cook, *Piezoelectric Ceramics*, Vol. 1, 1st edition, Academic Press, London, 1971.
[2]A. J. Moulson and M. J. Herbert, *Electroceramics*, Vol. 1, 2nd edition, Wiley, Chichester, U.K., 2003.
[3]T. Takenaka and H. Nagata, "Current Status and Prospects of Lead-Free Piezoelectric Ceramics," *J. Eur. Ceram. Soc.*, **25**, 2693–700 (2005).
[4]Y. Saito, H. Takao, T. Tani, T. Nonoyama, K. Takatori, T. Homma, T. Nagaya, and M. Nakamura, "Lead-Free Piezoceramics," *Nature*, **432**, 84–7 (2004).

[5]E. Cross, "Materials Science—Lead-Free at Last," *Nature*, **432**, 24–5 (2004).
[6]P. Baettig, C. F. Schelle, R. LeSar, U. V. Waghmare, and N. A. Spaldin, "Theoretical Prediction of New High-Performance Lead-Free Piezoelectrics," *Chem. Mater.*, **17**, 1376–80 (2005).
[7]R. E. Cohen, "Origin of Ferroelectricity in Perovskite Oxides," *Nature*, **358**, 136–8 (1992).
[8]J. G. Wu, G. Q. Kang, H. J. Liu, and J. Wang, "Ferromagnetic, Ferroelectric, and Fatigue Behavior of (111)-Oriented $BiFeO_3/(Bi_{1/2}Na_{1/2})TiO_3$ Lead-Free Bilayered Thin Films," *Appl. Phys. Lett.*, **94**, 172906 (2009).
[9]L. Wu, J. L. Zhang, C. L. Wang, and J. C. Li, "Influence of Compositional Ratio K/Na on Physical Properties in $(K_xNa_{1−x})NbO_3$ Ceramics," *J. Appl. Phys.*, **103**, 084116 (2008).
[10]S. T. Zhang, A. B. Kounga, E. Aulbach, H. Ehrenberg, and J. Rodel, "Giant Strain in Lead-Free Piezoceramics $Bi_{0.5}Na_{0.5}TiO_3$–$BaTiO_3$–$K_{0.5}Na_{0.5}NbO_3$ System," *Appl. Phys. Lett.*, **91**, 112906 (2007).
[11]S. T. Zhang, A. B. Kounga, E. Aulbach, T. Granzow, W. Jo, H. J. Kleebe, and J. Rodel, "Lead-Free Piezoceramics with Giant Strain in the System $Bi_{0.5}Na_{0.5}TiO_3$–$BaTiO_3$–$K_{0.5}Na_{0.5}NbO_3$. I. Structure and Room Temperature Properties," *J. Appl. Phys.*, **103**, 034107 (2008).
[12]S. T. Zhang, A. B. Kounga, E. Aulbach, W. Jo, T. Granzow, H. Ehrenberg, and J. Rodel, "Lead-Free Piezoceramics with Giant Strain in the System $Bi_{0.5}Na_{0.5}TiO_3$–$BaTiO_3$–$K_{0.5}Na_{0.5}NbO_3$. II. Temperature Dependent Properties," *J. Appl. Phys.*, **103**, 034108 (2008).
[13]S. E. Park, M. J. Pan, K. Markowski, S. Yoshikawa, and L. E. Cross, "Electric Field Induced Phase Transition of Antiferroelectric Lead Lanthanum Zirconate Titanate Stannate Ceramics," *J. Appl. Phys.*, **82**, 1798–803 (1997).
[14]L. Zhou, D. C. Lupascu, A. Zimmermann, and Y. Zhang, "Discontinuous Switching in Antiferroelectric Ceramics Monitored by Acoustic Emissions," *J. Appl. Phys.*, **97**, 124106, (2005).
[15]S. C. Zhao, G. R. Li, A. L. Ding, T. B. Wang, and Q. R. Yin, "Ferroelectric and Piezoelectric Properties of (Na, K)(0.5)Bi0.5TiO3 Lead Free Ceramics," *J. Phys. D: Appl. Phys.*, **39**, 2277–81 (2006).
[16]M. K. Zhu, H. C. Hu, N. Lei, Y. D. Hou, and H. Yan, "Dependence of Depolarization Temperature on Cation Vacancies and Lattice Distortion for Lead-Free $74(Bi_{1/2}Na_{1/2})TiO_3$–$20.8(Bi_{1/2}K_{1/2})TiO_3$–$5.2BaTiO_3$ Ferroelectric Ceramics," *Appl. Phys. Lett.*, **94**, 1–2 (2009).
[17]V. Dorcet, G. Trolliard, and P. Boullay, "The Structural Origin of the Antiferroelectric Properties and Relaxor Behavior of $Na_{0.5}Bi_{0.5}TiO_3$," *J. Magn. Magn. Mater.*, **321**, 1758–61 (2009).
[18]J. L. Cao, L. T. Li, and Z. L. Gui, "Interactions at the Cofired Interface of Ag/Pd Electrode and Lead-Based Ferroelectrics," *Mater. Sci. Eng. B*, **99**, 127–30 (2003).
[19]A. F. Holleman and N. Wiberg, *Inorganic Chemistry*, Vol. 1, 101st (German) edition, Walter de Gruyter, Berlin, 2001.
[20]J. G. Pepin, "Subsolidus Phase-Relations in the System Pd–Ag–O and Application to Multilayer Ceramic Composites," *Adv. Ceram. Mater.*, **3**, 517–9 (1988).
[21]C. A. Randall, A. Kelnberger, G. Y. Yang, R. E. Eitel, and T. R. Shrout, "High Strain Piezoelectric Multilayer Actuators—A Material Science and Engineering Challenge," *J. Electroceram.*, **14**, 177–91 (2005).
[22]R. Ueyama, K. Kamada, M. Harada, T. Ueyama, T. Yamamoto, and K. Kuribayashi, "Low Temperature Synthesis of Silver–Palladium Alloy Powders Internal Electrodes for Multilayer Ceramic Devices," *J. Mater. Sci.*, **36**, 371–9 (2001).
[23]S. F. Wang and W. Huebner, "Interaction of Ag Pd Metallization with Lead and Bismuth Oxide-BasedFluxes in Multilayer Ceramic Capacitors," *J. Am. Ceram. Soc.*, **75**, 2339–52 (1992).
[24]S. F. Wang and W. Huebner, "Interaction of Silver Palladium Electrodes with Lead-Based and Bismuth-Based Electroceramics," *J. Am. Ceram. Soc.*, **76**, 474–80 (1993).
[25]T. R. Shrout and S. J. Zhang, "Lead-Free Piezoelectric Ceramics: Alternatives for PZT," *J. Electroceram.*, **19**, 111–24 (2007).
[26]T. Takenaka, H. Nagata, and Y. Hiruma, "Current Developments and Prospective of Lead-Free Piezoelectric Ceramics," *Jpn. J. Appl. Phys., Part 1*, **47**, 3787–801 (2008).
[27]M. V. Slinkina, G. I. Dontsov, and V. M. Zhukovsky, "Diffusional Penetration of Silver From Electrodes Into PZT Ceramics," *J. Mater. Sci.*, **28**, 5189–92 (1993).
[28]D. Risold, B. Hallstedt, L. J. Gauckler, H. L. Lukas, and S. G. Fries, "The Bismuth–Oxygen System," *J. Phase Equilib.*, **16**, 223–34 (1995).
[29]K. E. Jarvis, A. L. Gray, and R. S. Houk, *Handbook of Inductively Coupled Plasma Mass Spectrometry*. Chapman and Hall, New York, 1992.
[30]I. N. Belyaev and T. G. Golovanova. In *Russ. J. Inorg. Chem* (*Engl. Transl.*); Engl. Transl. ed. 1965; Vol. 10, p. 1023–24.
[31]J. Konig, M. Spreitzer, B. Jancar, D. Suvorov, Z. Samardzija, and A. Popovic, "The Thermal Decomposition of $K_{0.5}Bi_{0.5}TiO_3$ Ceramics," *J. Eur. Ceram. Soc.*, **29**, 1695–701 (2009).
[32]M. Spreitzer, M. Valant, and D. Suvorov, "Sodium Deficiency in $Na_{0.5}Bi_{0.5}TiO_3$," *J. Mater. Chem.*, **17**, 185–92 (2007).
[33]Y. Lu, Y. Li, D. Wang, and Q. Yin, "Morphotropic Phase Boundary and Electrical Properties of $(Bi_{1/2}Na_{1/2})TiO_3$–$(Bi_{1/2}K_{1/2})TiO_3(Bi_{1/2}Ag_{1/2})TiO_3$ Ceramics," *Ferroelectrics*, **358**, 991–8 (2007).
[34]Y. Q. Lu, Y. X. Li, D. Wang, T. B. Wang, and Q. R. Yin, "Lead-Free Piezoelectric Ceramics of $(Bi_{1/2}Na_{1/2})TiO_3$–$(Bi_{1/2}K_{1/2})TiO_3$–$(Bi_{1/2}Ag_{1/2})TiO_3$ System," *J. Electroceram*, **21**, 309–13 (2008).   □